The Early Stages of Planet Formation in a Circumstellar Disc: a Theoretical and Numerical study

---

Dissertation

zur

Erlangung der naturwissenschaftlichen Doktorwürde
(Dr. sc. nat.)

vorgelegt der

Mathematisch-naturwissenschaftlichen Fakultät

der

Universität Zürich

von

Marina Galvagni

aus Italien

Promotionskomitee

Prof. Dr.	Ben Moore	(Vorsitz)
PD. Dr.	Prasenjit Saha	(Leiter)
Prof. Dr.	Lucio Mayer	
Dr.	Ravit Helled	

Zürich 2013

Ai miei genitori,
per avermi dato radici e ali

Acknowledgements

Four years have almost gone by since I first took a train to Zurich, without the slightest idea of what would happen, but full of hope. Now that this phase of my life is closing, it's time to thank those who made this incredible journey possible for me, and those who helped me enjoy it.

My first thanks go to my supervisors, Prasenjit Saha and Lucio Mayer. Thank for your support, your help and for the opportunity you gave me. Without both of you, I would not have been able to learn, experience, explore. My Doctorate has been full of science, adventures, encounters, lessons -and not only from a scientific point of view-, and I know I owe you this.

My thanks also to Fabian Heitsch and his group for hosting me, being patient with me and for all his good advice. I hope to be able to give something back to you.

I will never be able to thank enough my brothers and sister, who make me understand every day a little bit more that distances don't matter when it comes to family.

My times in Zurich have been enlightened by getting to know some great friends. So, thanks to Tristen Hayfield, not only for taking the time to teach me science, but most importantly for your advice on how to survive a Doctorate. At least, I knew since the beginning what I was going to walk in. Thanks to Raymond Anglil, for being the most *amazing* and caring deskmate someone could dream about. And thanks to Sraboni Ghose, for the special point of view that you have about everything. Every time we meet, your words and smile enlighten my day.

A special though goes to Pietro Alfarano, with whom I shared uncountable good food and wine, discussions, thoughts, hopes and fears. Your patience and your willingness to share are a precious treasure to me.

I am also grateful to the members of Dokholyan's lab, who add to my permanence in the USA an unique international-southern taste. You're too many to name you one by one, but I would like to give special thanks to Raymond Dokholyan, for trying to teach me Russian.

Last, I owe my deepest thanks to Marino Convertino, who chose to share every aspect of his and my life with me. Thanks for making with me the Convertino-Galvagni method work every day.

Summary

The aim of this thesis is to explore the early stages of planet formation, through analysis via analytical studies and simulating the physics of objects characterising young circumstellar discs. As a first step, in Chapter 2 we investigate the collapsing phase of a gaseous clump formed via Gravitational Instability in the outer part of young circumstellar discs. The novelty of our study resides in the realism of the simulations performed: high resolution 3D simulations, with a new equation of state derived from physical principles meant to accurately describe the regime under investigation. Moreover, the initial conditions for the clump are taken from previous global simulations; they are therefore the more realistic ones used in their kinds of studies to date. As a result of our study, the collapsing timescale for clumps is found to be comparable with the migration timescale of the object itself in the disc. Interestingly, this result is significantly slower then those presented in previous works, pointing towards a more central role for Gravitational Instability in the contest of planet formation.

This first result leads naturally to the following questions: what is the probability that a clump formed via Gravitational Instability survives the interactions with the environment, becoming a real protoplanet, and what would be the characteristics of this object? In order to answer these questions, in Chapter 3 we perform an investigation of the statistical outcome of a set of 2000 clumps which were formed in isolation by Gravitational Instability in a circumstellar disc and for which we follow their collapse coupled withd detailed interactions with the environment. Tidal disruption, migration and gap opening are taken into account at the same time as clump collapse. This study shows that more than half of the initial clumps are able to evolve and survive in the disc, becoming real protoplanets. Moreover, once a realistic description of the disc viscosity is taken into account, our study shows the formation of two populations of protoplanets: a populations of Hot Jupiters, orbiting inside 0.5 au from the star, with a typical mass in the range of 1-3 Jupiter masses, and a second population of massive gas giants (up to 15 Jupiter masses), orbiting at a few tens of au from the star. The results of this statistical study highlight the importance of Gravitational Instability in the formation of gas giant planets, and give some estimates that can be used for comparisons with observational results.

The young phase of the life of a circumstellar disc is characterized not only by the behaviour of its gas component, but also on the dust. Dust grains indeed come directly from the interstellar medium, and interact with one another once they are in the disc, colliding and forming larger objects with time. In Chapter 4 we present a study of this phenomena, focusing on the outcome of the collisions for grains with an initial size of a few μm, as expected for interstellar grains. Our study adds one new element in this analysis, which has been neglected in the past: the collisional velocity of grains is treated as a probability distribution function instead of a single fixed value. This simple modification of the model has a significant impact on the collisions' outcome, leading to the formation of objects of more then one order of magnitude larger size than the ones usually obtained. Our new model leads toward theoretical results which are more similar to the observational data.

Zusammenfassung

Das Thema dieser Doktorarbeit sind die Frühphasen der Planetenentstehung und die Physik der typischen Objekte in zirkumstellaren Scheiben. Diese Objekte werden mittels analytischer Modelle und numerischen Simulationen untersucht. Als erstes studieren wir (in Kapitel 1) die Kollapsphase von überdichten Gasgebieten, die durch Gravitationsinstabilitäten in den Aussenbereichen zirkumstellarer Scheiben entstehen. Die Innovation bei unseren Modellen besteht im Detailreichtum der Simulationen: hochauflösende dreidimensionale Simulationen mit einer neuen Zustandsgleichung , die aus einer möglichst genauen physikalischen Beschreibung der Umgebung abgeleitet wurde. Ausserdem stammen die Anfangsbedingungen für die Gasansammlungen aus grösserskaligen Simulationen der Scheiben und gehören damit zu den realistischsten, die bisher in dieser Art von Studien verwendet wurden. Ein Hauptergebnis unserer Modelle ist, dass die Zeitskala, auf der die überdichten Regionen kollabieren vergleichbar ist mit der Zeitskala, auf der die Regionen selbst durch die zirkumstellare Scheibe nach innen wandern. Dieses Ergebnis bedeutet interessanterweise einen wesentlich langsameren Kollaps als bisherige Studien ergeben haben, was auf eine zentralere Rolle von Gravitationsinstabilitäten bei der Entstehung von Planeten hindeutet.

Dieses erste Ergebnis wirft natürlich die Fragen auf: mit welcher Wahrscheinlichkeit überlebt eine solche Gasansammlung, die durch Gravitationsinstabilitäten entsteht, die Wechselwirkung mit der Umgebung in der Scheibe und wird tatsächlich zu einem Protoplaneten, und welche Eigenschaften würde ein solches Objekt haben? Um einer Antwort auf diese Fragen näher zu kommen, unternehmen wir in Kapitel 3 eine statistische Analyse der Ergebnisse von 2000 solcher Regionen, die durch Gravitationsinstabilitäten in zirkumstellaren Scheiben entstehen und für die wir ihren weiteren Kollaps in Wechselwirkung mit der Scheibe simulieren.

Dabei werden die Zerstörung der Objekte durch Gezeitenwechselwirkung, ihre Migration durch die zirkumstellare Scheibe und die Entstehung von ringartigen Lücken in der Scheibe genauso berücksichtigt, wie der gravitative Kollaps der Objekte. Wir stellen fest, dass mehr als die Hälfte der ursprünglichen Regionen es schaffen, sich in der Scheibe wirklich zu Protoplaneten zu entwickeln ohne dabei zerstört zu werden. Ausserdem zeigen wir, dass bei Berücksichtigung realistischer Modelle für die Viskosität der Scheiben sich zwei Populationen von Protoplaneten bilden: eine aus heissen Jupitern, die den Stern innerhalb von 0.5 AU umkreisen und typischerweise 1-3 Jupitermassen haben, sowie eine zweite Population gasreicher Riesenplaneten mit bis zu 15 Jupitermassen, die den Mutterstern innerhalb einiger 10 AU umkreisen. Die statistischen Ergebnisse unserer Analyse heben die Bedeutung der Gravitationsinstabilität für die Entstehung von Gasriesen hervor und resultieren in einigen Vorhersagen, die einen Vergleich mit Beobachtungsdaten ermöglichen.

Die Frühphase der Entwicklung zirkumstellarer Scheiben ist nicht nur durch die Eigenschaften des Gases charakterisiert, sondern auch durch die der Staubkomponente. Die Staubpartikel stammen aus dem interstellaren Medium, wechselwirken miteinander in der Scheibe durch Kollisionen und bilden mit der Zeit immer grössere Objekte. In Kapitel 4 präsentieren wir eine Untersuchung dieser Phänomene, wobei wir uns auf die Endprodukte von Kollisionen von Staubkörnern mit einer Anfangsgrösse von einigen μm konzentrieren, wie sie für interstellare Staubpartikel erwartet wird. Unsere Analyse enthält einen neuen Aspekt, der bisher vernachlässigt wurde: die Kollisionsgeschwindigkeit der Staubpartikel wird als Wahrscheinlichkeitsverteilung modelliert anstatt eines festen Wertes. Diese einfache Verbesserung des Modells hat weitreichende Folgen für die Endprodukte der Kollisionen und resultiert in der Entstehung von Objekten, die eine Grössenordnung grösser sind als die bisheriger Untersuchungen. Die Ergebnisse unseres neuen

Modells stimmen besser mit Beobachtungen überein.

Contents

1. Introduction

1.1. The discovery of extrasolar planets

Somewhere,

something incredible is waiting to be known.

[*C. Sagan*]

The existence of planets orbiting other stars than our Sun has always been postulated. Scientists, philosophers and especially science fiction writers of the past have been speculating about these objects and their formation history. Quite surprisingly, the detection of the first extrasolar planet dates not too far back in the past, only 20 years (Wolszczan and Frail, 1992). Since then, new detection techniques have been developed and a number of satellites have been performed. Today there are more then 800 confirmed extrasolar planets, and thousands of candidate objects. Their characteristics have been found to be quite different from those of the Solar System, which had been for the last centuries the only source of information which was available to create a planet formation theory. Therefore, the need of a new and more detailed theory of planet formation, which can explain the characteristics of the observed extrasolar planets, has introduced into the community, attracting the attention of a large number of scientists to this new field of astrophysics.

1.2. Extrasolar Planets: an observational prospective

The history of astronomy

is a story of receding horizons.

[*E. P. Hubble*]

1.2.1. Detection Techniques

There are currently four methods to detect extrasolar planets.

Radial velocity

Radial velocity is the most common techniques, used to detect more then 50 % of the confirmed planets. It is usually applied for nearby, Solar-type stars; the first extrasolar planet orbiting a Solar-type star has been detected through this method (Mayor and Queloz, 1995). This method

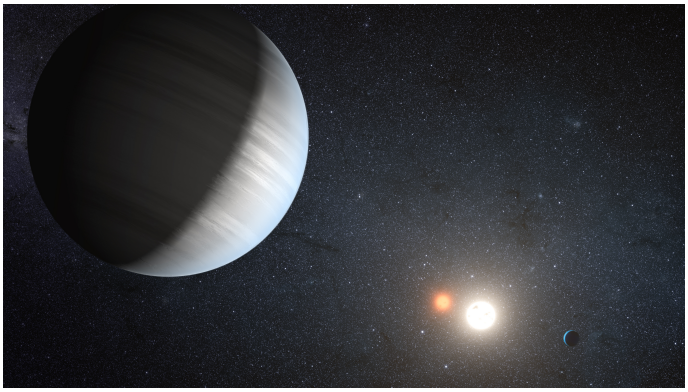

Figure 1.1.: Artist concept of extrasolar planet orbiting Kepler-47. Credits: `www.http://kepler.nasa.gov/`

is based on the idea that when one (or more) planet orbits a star, the star's motion is affected by the presence of this object. If the planet is on a circular orbit, indeed, the star orbits the center of mass with a velocity

$$v_* \sim \left(\frac{M_p}{M_*}\right)\sqrt{\frac{GM_*}{a}} \tag{1.1}$$

with M_p and M_* the planet and star masses and a semimajor axis. As the systems are usually observed not face-on, but with an inclination, what is really detected is the quantity K

$$K \propto M_p \sin(i)/a^{1/2} \tag{1.2}$$

with i inclination angle. Radial velocity measurements, therefore, detect only a lower limit for the planet mass. In order to break the degeneracy between planet mass and inclination, astrometric observations can be used (McArthur et al., 2010). The other quantities that are possible to measure via radial velocity are semi-major axis a, eccentricity e and the longitude of pericenter ϖ.

Radial velocity measurements require that the interference of the planet on the star motion is large enough to provide a correction to the star's velocity larger then the survey precision. This leads to a bias towards large and close-in planets.

One peculiar type of radial velocity measurement happens when the planet orbits a pulsar. A pulsar is a star which emits radio wave regularly as it rotates. Due to its stability in the emission frequency, the presence of a second body orbiting the star would lead to a detectable timing shift. This method is so sensitive that it is possible to detect extrasolar planets smaller than in any other case (down to a tenth of Earth masses). Moreover, it can provide information about the existence of a multiple planetary system. Pulsar timing is the technique which has been used for the first detection of an extrasolar planet (Wolszczan and Frail, 1992).

Transits

A transit search is a technique based on the idea that a planet passing in front of a star will decrease its observed luminosity. Since the first transit detection in 2000 (Charbonneau et al., 2000), there has been a large increase of these kinds of surveys, and today 35 % of the confirmed

extrasolar planets have been characterised using the transit method. The most famous and successful missions of this kind are the *COROT* (Auvergne, 2009) and *Kepler* (Borucki, 2010) missions. Both are space missions. Transit surveys can be completed by transit timing surveys, where the study of the differences between the luminosity absorption between different transits of the same extrasolar planet in front of the star can lead to the detection of a second orbiting object.

Transit surveys can be used to follow up the detections given by radial velocity; through this techniques it is possible to obtain information also in the planet radii. Moreover, transit surveys are less affected by the bias towards large planet size, leading to the first detections of *Super Earth* ($M_\oplus \lesssim M_P \lesssim M_N$ with M_N Neptune mass) extrasolar planets.

Gravitational lensing

Gravitational lensing (Beaulieu, 2006) is a ground-based technique. When light from a source encounters a star, it can get deflected by its gravitational field, leading to multiple images for the observer. If this star has a planet orbiting it, the gravitational field exerted by the planet can leave a signature on the light curve: the deflection of the source light from the planet leads to a magnification of the light curve that changes with time with the position of the planet. Therefore, although it is not possible to detect the multiple images formed by the lens of the planet, the change of magnification gives information on the presence of a body orbiting the star.

Although only 20 confirmed extrasolar planets have been detected through this technique, it is considered quite important because of its great sensitivity to low mass and close-in planets.

Direct imaging

Planets are fainter than their hosting stars, therefore direct imaging has a bias towards giant extrasolar planets at large distances, which is a range hard to explore with the most commonly used techniques (radial velocity and transit). Moreover, direct imaging detections are independent from the system inclination with respect to the observer.

Regardless of these nice observational features, pulsar timing is not a very used techniques (only 15 confirmed extrasolar planets have been studied with it). This is mainly due to two reasons: first, pulsars are quite rare stars, planets orbiting around a pulsar would hardly host life as we know it, making the search of those objects less appealing.

1.2.2. Extrasolar planet observed properties

Figure 1.2 shows the planet mass and semi-major axis for confirmed extrasolar planets. As it clearly appears, the solar system is a peculiar case and not the rule: large planets are common both at very large and very small distances, and Super-Earths and Earth-like planets are usually found packed close together, with multiple systems (up to 5 planets) inside 1 au from the hosting star. I refer the reader to the website `www.exoplanet.eu` for a collection of all the available data from detections. We list here some of the more prominent features from observations.

- Eccentric orbits are very common beyond the radius of tidal circularization. There seems to be no correlation between eccentricity and the planet mass.

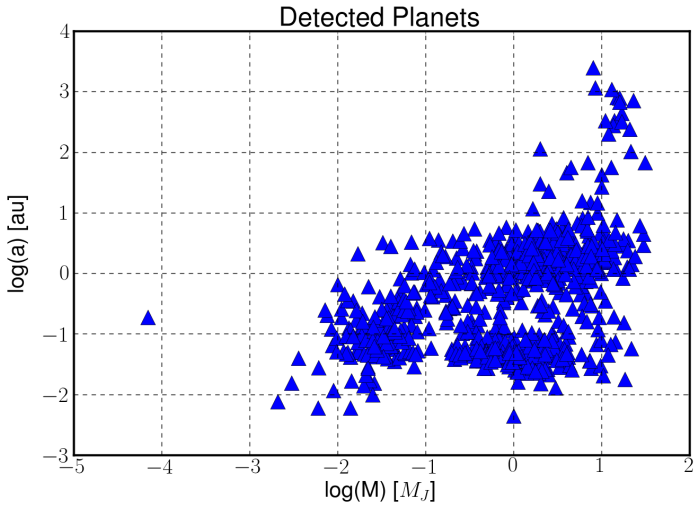

Figure 1.2.: Planet mass (in Jupiter mass units M_J, log scale) vs semi-major axis (in au, log scale) for the 816 confirmed extrasolar planets (up to date 11^{th} June 2013). Credits: `www.exoplanet.eu`

- A class of objects called Hot Jupiters have been detected. Those planets are giant planets orbiting very close to their hosting stars (a inside 0.5 au).
- Planet frequency is a function of metallicity: metal rich stars host more planets (Fischer and Valenti, 2005).
- Multiple planet systems are very common, although Hot Jupiters are usually lonely.
- Rocky planets in multiple system tend to be in very packed systems (Ragozzine and Kepler Team, 2012).
- Planets in multiple system show a very high rate of quasi-resonance orbits.
- The radii of giant planets are found to be larger then expected.

1.3. Extrasolar Planets: a theoretical prospective

Everything is self-evident.

[*R. Descartes*]

The first recognized theory of planet formation has been ascribed to Descartes and his theory of vortices, back almost four centuries ago (1644). According to this theory, planets form from vortices of particles that are in rotation around a star. This picture didn't involve a disc structure, nor was the rotation axis set to be the same for all the vortices. Moreover, the physics behind this theory was poorly described; Descartes was presenting more an idea than a scientific theory. Still, his idea would impact studies further down the road: indeed Weizsaecker in 1944 revisited the existence of these vortices in circumstellar discs, showing that they are likely to have

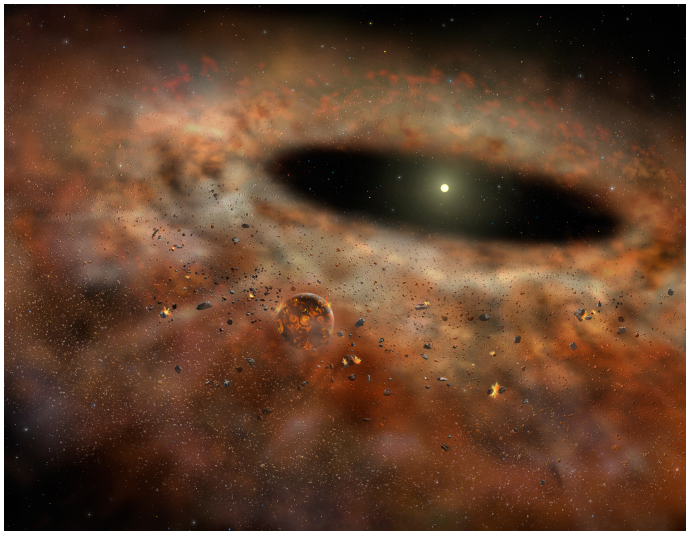

Figure 1.3.: Artist concept of circumstellar disc. Credits: `www.http://gemini.edu/`

the same rotation axis and investigated their role in angular momentum transfer in discs. In 1995 Barge and Sommeria (Barge and Sommeria, 1995) showed that vortices can actually be a preferential location in the disc that enhance particles coagulation, and therefore planet formation. A few years ago, Klahr and Bodenheimer (Klahr and Bodenheimer, 2003) showed in 3D simulations that vortices are expected to form in discs, giving back light to this four century old idea.

For the development of a more detailed theory of planet formation, we have to wait for the XVIII century, with Swedenborg's and Kant's nebular hypotesis, which would later be mathematically developed by Laplace. According to this theory, the birthplace for planets is inside contracting and cooling protostar clouds. As a cloud contracts, it flattens and forms a ring of particles, which will later collapse into the planets. The main problem with this theory is the distribution of angular momentum between the disc and the star: without any mechanism for angular momentum redistribution, almost all the angular momentum would end up in the star, in disagreement with the evidence from the Solar System. As a result, this theory was abandoned at the beginning of the 20th century, in favour of other ideas.

In 1972 Safronov (Safronov, 1972) presented the Solar Nebular Disc Model (SNDM), a revisited version of the Laplace theory. Moreover, in the same time window different observations (mainly young stars, such as Beta Pictoris) showed that stars are commonly surrounded by a circumstellar disc of cold material, as predicted by Laplace's theory. By the beginning of 1980th, the Solar Nebular Disc Model was the widely accepted model for planet formation.

1.3.1. The birthplace of planets: circumstellar discs

According to the state of the art theory, the birthplace of planets is the circumstellar disc. Those discs form from the collapse of molecular clouds, driven by self gravity and gas cooling (Inutsuka et al., 2010; Machida et al., 2010). The lifetime of such a disc can be divided mainly into three phases:

- **Early phase**, also called main accretion phase, is the initial stage of formation of the disc. Due to the initial non zero angular momentum and its conservation law, the gas collapsing from the molecular cloud sets down in a circumstellar disc. The material in the disc migrates inwards thanks to disc viscosity, and gets accreted into the protostar. This process though is not smooth, and phases of gas accretion from the cloud onto the disc are interspersed with quiet phases, during which the disc tends to reach hydrostatic equilibrium (Gammie, 2001). During this phase, the dynamic of the system is dominated by the disc mass. Indeed, when the disc forms its mass is 10-100 times larger then the protostar mass, and it tends to dominate the system during all this phase, which lasts 10^5 years. Such a massive disc is highly affected by gravitational instability and is likely to fragment, as discussed later.
- **Main phase**, also called T Tauri phase. It lasts 1-10 Myrs, based on the mass of the system. During this quiet phase, the gas sets in hydrostatic equilibrium in the disc, with a disc-star mass ratio on the order of ~ 10 %. During this phase, dust particles coming from the interstellar medium collide and interact both with each other and with the gas component. Thanks to these processes, the dust particles can grow from a few μ m up to planet-size objects.
- **Debris disc**. Circumstellar discs around mature stars are found to have lost the gas component. This is supposed to happen because of photoevaporation, a fast (on the order of a few 10^4 years) process that ends the disc main phase. During this phase, the radiation field from the star is shielded by the gas that gets accreted from the disc. While the disc is evolving, though, the available gas decreases, as there is no more accretion onto the disc from the environment. There is then a non-return point at which the gas is not sufficient anymore to shield the stellar irradiation, which takes over and cleans the disc from the gas. The system is therefore left with the central star surrounded by only the dust component[1].

In order to study the properties of a circumstellar disc, we will study first its gas component (which is the dominant component in mass in the first two phases) and then the dust component.

1.3.2. The dynamics of gas

The disc structure

The main component in a circumstellar disc is gas. The value of the dust-gas ratio is poorly constrained by observational data, as the detection of the dust component is not trivial. Nevertheless, in literature this ratio is usually assumed to be 0.01. Let's therefore begin the discussion from the prominent element: gas.

In a circumstellar disc the physical phenomena which are present are: hydrodynamic, gravity, viscosity (which determines the angular momentum redistribution), luminosity from the star and mass accretion. If we define $\Sigma(r,t)$ as gas density profile and $v_r(r,t)$ the radial velocity (with $v_r < 0$ for inflows), the continuity equation for an axisymmetric flow can be written as

$$r\frac{\partial \Sigma}{\partial t} + \frac{\partial}{\partial r}\left(r\Sigma v_r\right) = 0 \tag{1.3}$$

[1]Note that alternative mechanisms to explain the disappearance of the gas have been recently proposed (Owen et al., 2012)

and the angular momentum conservation becomes

$$r\frac{\partial\left(\Sigma r^2\Omega\right)}{\partial t}+\frac{\partial}{\partial r}\left(r^3\Omega\Sigma v_r\right)=\frac{1}{2\pi}\frac{\partial G}{\partial r} \tag{1.4}$$

with Ω the local keplerian angular velocity and G the net torque due to the viscosity stress. From Armitage (2010), we can assume G is

$$G=2\pi t\nu\Sigma r\frac{d\Omega}{dr}\cdot r \tag{1.5}$$

with ν the viscosity parameter. Therefore the evolution equation for the surface density of a thin disc is

$$\frac{\partial\Sigma}{\partial t}=\frac{3}{r}\frac{\partial}{\partial r}\left[r^{1/2}\frac{\partial}{\partial r}\left(\nu\Sigma r^{1/2}\right)\right] \tag{1.6}$$

In general, the viscosity is a function of the local conditions of the disc. This makes equation 1.6 non-linear, and therefore an analytical solution can not be found in general. However, by assuming that ν can be written as a power law in the radius, it is possible to solve it. Without going into the details of the solution, which can be found in Armitage (2010), under the assumption $\nu\propto r^\gamma$, the gas density profile is

$$\Sigma(\bar{r},t)=\frac{C}{3\pi\nu_1\bar{r}^\gamma}T^{(-5/2-\gamma)/(2-\gamma)}\exp\left[-\frac{\bar{r}^{2-\gamma}}{T}\right] \tag{1.7}$$

where C is a normalization constant, r_1 the initial radius of the disc, $\bar{r}=r/r_1$, $\nu_1=\nu(r_1)$ and $T=t/t_s+1$ with

$$t_s=\frac{1}{3(2-\gamma)^2}\frac{r_1^2}{\nu_1} \tag{1.8}$$

From this solution, it is possible to see that over time the disc mass decreases, while the disc expands in order to conserve angular momentum. Note that this derivation doesn't take into account mass accretion onto the disc, which would make an analytic solution for Σ derivable only in a steady-state case.

A circumstellar disc therefore has an exponential cut-off in the outer region. An inner cut-off radius is also expected to be present, due to the interaction with the star. Observational studies (Bouvier et al., 2007) indeed suggest that in accreting T Tauri stars the magnetosphere of the star destroys the inner circumstellar disc, leading to a magnetospheric mode of accretion, in which gas accumulates at the inner bounder and gets accreted onto the star periodically (Koenigl, 1991). The magnetic coupling between the star and its disc also allows angular momentum exchange and could be a mechanism to control the spin of young stars, although this argument is currently under debate (Armitage and Clarke, 1996; Collier Cameron and Campbell, 1993; Rebull et al., 2006).

The vertical structure of a circumstellar disc is assumed to be given by hydrostatic equilibrium. The pressure gradient is

$$\frac{dP}{dz}=-\rho g_z \tag{1.9}$$

with ρ the gas density. Assuming that there is no gravitational contribution from the disc, the vertical component of gravity is given by

$$g_z\sim\Omega^2 z \tag{1.10}$$

If the gas is isothermal in the vertical direction, then $P = \rho c_s^2$ with c_s sound speed. Therefore, the vertical density profile can be calculated as

$$\rho = \rho_0 \exp\left(-z^2/2h^2\right) \tag{1.11}$$

with h vertical scale hight, given by $h = c_s/\Omega$. The assumption of an isothermal gas can be considered valid if the disc luminosity is mostly derived from reprocessing starlight, and not from the release of gravitational potential energy as the gas flows inwards.

Gravitational Instability

The circumstellar disc that has been described in the previous section is in an equilibrium state. This is not always the case: a disc can undergo gravitational instabilities under certain conditions. The mathematical description of gravitational instability dates back to 1964, with Toomre's paper (Toomre, 1964).

Consider an arbitrary thin disc, rotating around a common center, not necessarily with uniform angular velocity but with exact equilibrium between gravitational and centrifugal forces. Imagine that this disc suffers a slight contraction over a relatively small region of length L. Due to this contraction, the local density μ increases by a factor ϵ. A material element previously located near the periphery of this contracting region will feel an additional gravitational force on the order $\epsilon G\mu$. On the other hand, due to the conservation of angular momentum, the contracting region has an increased angular momentum, which repels fluid elements in the neighbouring region. The increase of centrifugal force is roughly of the order of $\epsilon L\Omega_{loc}^2$ with Ω_{loc} local angular velocity. The perturbed region is therefore able to collapse as long as the increase of the gravitational force overcomes the increase of the centrifugal force:

$$G\mu\epsilon \geq \epsilon L\Omega_{loc}^2 \tag{1.12}$$

which leads to the condition

$$L \leq L_{crit} = \frac{G\mu}{\Omega_{loc}^2} \tag{1.13}$$

Random forces also play a role in preventing the collapse of regions in circumstellar discs. A region can not collapse as long as mass elements manage to travel relative to each other due to diffusion at least through a fraction of the perturbed length during the time the disturbance amplitude would otherwise have grown. This additional condition for stability can be written as

$$\sqrt{\frac{L}{G\mu}} \geq \frac{L^2}{\sqrt{< u^2 >}} \tag{1.14}$$

with $\sqrt{< u^2 >}$ velocity due to random motion. Collapse is therefore possible if

$$L \geq L_J = \frac{< u^2 >}{G\mu} \tag{1.15}$$

Combining conditions 1.13 and 1.15 we deduce that under the joint influence of rotation and moderate superposed velocity dispersion, the unstable disturbance is confined to an intermediate range of scales. Moreover, it appears evident that this range will shrink as the velocity dispersion

is increased. Beyond some value of the velocity dispersion, gravitational instability will be avoided altogether. This minimum velocity dispersion for stability is given by $L_{crit} = L_J$, which leads to

$$\sqrt{< u^2 >}_{min} = \frac{G\mu}{\Omega_{loc}} \tag{1.16}$$

All velocity dispersions smaller than this value will therefore make gravitational collapse possible. It is therefore possible to define the quantity Q, called the Toomre parameter, as

$$Q = \frac{c_s \Omega}{\pi G \Sigma} \tag{1.17}$$

for which it holds that $Q < Q_{crit} \simeq 1$ is the condition for gravitational instability in a circumstellar disc. Here, the velocity dispersion is assumed to be given by the gas sound speed.

Despite the fact that the derivation of the Toomre parameter herein presented is purely heuristic, the same result is found for a more mathematically correct derivation in linear perturbation theory, assuming that the perturbations are axisymmetric. Indeed Fujimoto (Fujimoto, 1987) shows that non axisymmetric perturbations are always stable in linear perturbation theory. Three-dimensional simulations of circumstellar discs, however, show that this result doesn't hold in reality. In non-axisymmetric discs with finite width, indeed, perturbations can grow and locally collapse as long as the azimuthal averaged Toomre parameter is lower then the threshold value $Q \lesssim 1.7$ (Durisen et al., 2007a). This collapse leads to the fragmentation of spiral modes, which can form for even higher values of the Toomre parameter, $Q \lesssim 2.0$, into clumps. This scenario is the so-called Gravitational Instability (hereafter GI) mechanism. This result underlines the importance of simulations in order to built a correct theory of GI.

By looking at the definition of the Toomre parameter, it appears that there are two factors that can play a role into setting the disc in a GI regime: local sound speed and local surface density. If the first factor decreases, the gas has less turbulence and therefore can collapse more easily. There is therefore a strong dependence on the cooling physics of the gas. The second factor is the local Σ: larger the local mass, indeed, stronger is the self gravity, and therefore GI becomes a more feasible process. The local value of Σ is determined by a lot of different factors, not all of which have been taken into account in the derivation presented in the previous section (e.g., effects of magnetic fields, interactions with the local dust component). Nevertheless, we know that in the early phase of life of a circumstellar disc, the disc component is quite massive due to accretion from the molecular cloud. Therefore, GI is likely to happen in the very first life phase (Machida et al., 2010).

Once GI sets in, the disc will react in order to stabilize itself, through mass rearranging and/or heating through dissipation. If locally the Toomre parameter gets lower than the critical value, local collapse will start, which will gravitationally attract more mass and therefore generate heating, which increases the Toomre parameter and therefore stabilize the disc. In a similar way, if the Toomre parameter gets too high values, the heating due to gravitoturbulence is weak, leading the disc to cool towards stability. There is therefore a feedback loop process that tends to keep the disc in the marginally stable regime $Q \simeq Q_{\rm crit}$. The effectiveness of this process is under debate (Lin and Pringle, 1987) (Lin and Pringle, 1990). Nevertheless, from both theoretical (Shlosman and Begelman, 1989) and simulation (Boley et al., 2010) studies it appears clear that the scenario in which cooling can be so rapid to lead to fragmentation before the disc heats is not unreasonable.

Simulation studies have shown that these clumps can form only in the outer part of the disc ($a > 50$ au).

1.3.3. The dynamics of dust

A circumstellar disc is composed not only of gas, but also of a second component: dust. According to the state of art, the ratio between dust and gas density is 1/100. The dust comes from interstellar particles, with an initial typical size on the order of $10\mu m$. The interaction between particles inside the disc, however, leads to collisions, aggregation and fragmenting these objects. The outcome of these interactions is that the size distribution of the grains changes with time, with grains becoming larger and larger, until they become rocky planets, icy planets or the cores of gas giant planets. The theory that describes this process is called Core Accretion (hereafter CA) (Youdin and Chiang, 2004).

While moving in a circumstellar disc, a dust particle will experience collisions with other particles. Considering two particles i and j, their collision can be driven by different mechanisms. In the following, we will describe the five more important ones for small size grains (up to meter-size). For larger particles, other mechanisms such as gravitational focusing, will play a role as well.

Brownian motion

According to brownian theory, the collisional velocity due to brownian motion is given by

$$v_{ij} = \sqrt{\frac{8K_B T(m_i + m_j)}{\pi m_i m_j}} \tag{1.18}$$

with K_B Boltzmann constant, T dust temperature, m_i and m_j mass for the particle i and j.

Turbulent motion

Collisions can happen because of the turbulent velocities of two particles. The source of turbulence in a circumstellar disc is not yet clear, therefore a complete theory of turbulence-induced collisional velocity is not available. The most common recipe used in this case is Ormel and Cuzzi (2007), based on the relative size of the dust particles and a comparison with that and the typical eddy size.

Radial motion

The main difference between the representation of gas and dust particles in circumstellar discs is that gas elements feels the pressure given by the surrounding gas elements. Because of this, the gas component experiences an extra force which pushes it away from the orbit; the gas component will therefore orbit at a sub-keplerian velocity. Dust particles, on the other hand, do not feel any kind of pressure, therefore they tend to settle in keplerian orbit. As the gas is moving subkeplerian, though, dust particles will feel a head-on wind, which will slow then down. For small size particles, this head-on wind is so strong that the dust is coupled with the gas and moves at the same speed. While the dust particle grows, the head-on wind gets less effective, until the particle is so big it doesn't feel the gas component anymore, and can move on a truly keplerian orbit. A complete description of this process is given in Whipple (1972); Weidenschilling (1977); Nakagawa et al. (1986).

Small particles which are coupled with the gas lose part of their angular momentum due to this friction. They therefore drift inward in the disc, with a radial velocity given by

$$v_r = \frac{1}{1+S^2}\left(u_g - 2S\eta v_K\right) \tag{1.19}$$

with u_g gas velocity, η quantity related to the gas pressure density, $v_K = \Omega_K r$ keplerian velocity and S Stokes number. The Stokes number expresses the degree of coupling between the gas and the dust:

$$S = \frac{s_i \rho_i \Omega_K}{\rho_m c} \tag{1.20}$$

with s_i dust particle size, ρ_i particle density, ρ_m mid-plane disc density and c local sound speed. Two dust particles with different size will therefore have different radial velocity, leading to possible collisions.

There is also a second physical mechanism that contributes to radial drift motion: as the central star emits light, the gas is pushed outwards. The grain particles therefore experience a second wind from the gas component, which has radial direction and outward verse. This wind makes them lose part of their angular momentum and migrate inward in the disc. This phenomena, though, is negligible in the early disc phase, when the stellar accretion rate is large enough to prevent the formation of a strong wind from the star (Armitage, 2010). Therefore, we do not take it into account in this context.

Azimuthal motion

Due to the same process described for the radial motion, in the azimuthal direction dust particles of different sizes have different velocities, given by

$$v_a = \frac{1}{2S}\left(v_r - u_g\right) \tag{1.21}$$

Vertical motion

Dust particles are distributed also in the z direction. They will naturally oscillate in this direction, due to the gravitational attraction from the gas mass present in the disc midplane. The vertical velocity has been evaluated in Birnstiel et al. (2010) as

$$v_z = -h\Omega_K \min\left(S, \frac{1}{2}\right) \tag{1.22}$$

with h vertical scale height for the particle.

Collisions

Two dust particles can collide due to both stochastic processes (brownian motion and turbulence) and to differences in velocity in the same direction (radial, azimuthal and vertical velocity). Once two particles collide, there are three possible outcomes: accretion, fragmentation (total or partial) and bouncing. A number of studies have been performed, both from a

theoretical (Dullemond and Dominik, 2005; Tanaka et al., 2005) and experimental (for a review see Blum and Wurm (2008)) point of view to be able to predict the size distribution of grains and compare it with the results from observations of discs.

The main problem that CA theory has been facing in the last years in this context is the so called meter size barrier: at 1 au from the star, dust particles which are mostly affected of loss of angular momentum due to the coupling with the gas are meter sized particles. According to the theory, these particles will drift inwards and be lost in the star in a few hundred years, which means that meter-size object can't be retained for a long enough time to be able to produce the planetesimals that are supposed to originate the rocky planets and the meteorites we observe. Some mechanisms to solve this problem have been proposed in the last couple of years, invoking the importance of the bouncing region (Windmark et al., 2012a), of a 3D treatment of the collisional velocity (Windmark et al., 2012b; Garaud et al., 2013), or the existence of pressure dominated regions inside the disc (Pinilla et al., 2012). None of these solutions seem to be definitive at the moment, although they all point towards a possible solution to this issue.

One other major issue regarding CA as a mechanism to form planets is the timescale issue. CA indeed needs tens of millions of years to be able to span the 12 orders of magnitudes in size between the μm interstellar dust particles and planetesimal sized objects. After this period, though, the disc has lost all its gas and therefore the planetesimals formed via CA can hardly become planets with an atmosphere or the cores of gas giant planets. In order to solve this problem, there are two possible roads that are currently followed: accelerating the CA process via gravitational focusing, pressure maxima and similar mechanisms, or treating CA and GI as coupled theories (Boley et al., 2010; Nayakshin, 2010).

1.3.4. Migration of protoplanets

GI and CA both form massive objects in the disc, which will interact with the environment. These interactions can be of different kinds:

- interactions between the protoplanet and the disc, which can be gaseous (early and main disc phase) or made up of remnant (debris disc phase);
- interactions within two or more massive protoplanets in an initially unstable system;
- tidal interactions between the protoplanet and the hosting star.

The result of these interactions will play a major role in the planet formation process outcome, determining the final physical properties of the survived planets. We present here a discussion on the interaction between protoplanets and a gaseous disc, as this interaction is the more critical one in the early stages of planet formation.

A protoplanet embedded in a gaseous disc experiences an exchange of angular momentum between itself and its surroundings. Assuming that the protoplanet is on a stable orbit, the interaction with the gas exterior to the orbit will move angular momentum from the protoplanet to the slower gas. As a result, the protoplanet is pushed inwards, while the gas is pushed outwards. In a similar way, the protoplanet gains angular momentum from the gas which is in the inner part of its orbit, being therefore pushed outwards while the gas is pushed inwards. The net result of the exchange of angular momentum between a protoplanet and the gas is therefore to repel the gas. The direction of the migration of the protoplanet is not easy to determine, and it is given by the result of integrating all the contributions to the net torque from the gas at different radii.

A powerful way to estimate the total torque exerted on the protoplanet is the decomposition at resonances locations (Goldreich and Tremaine, 1979; Tanaka et al., 2002). Let's assume that the protoplanet is on a circular orbit, with angular frequency Ω_p. The resonances it will feel are of two possible types: corotational resonance, exerted from the gas for which it holds

$$\Omega = \Omega_p \tag{1.23}$$

and Lindbald resonances, for which

$$m(\Omega - \Omega_p) = \pm k_0 \tag{1.24}$$

with m integer and k_0 epicyclic frequency, given by

$$k_0 = \frac{d^2\phi}{dr^2} + 3\Omega^2 \tag{1.25}$$

where ϕ is the stellar gravitational potential. In the case of a Keplerian disc, $k_0 = \Omega$, from which it is possible to estimate the positions where the Lindbald resonance condition holds:

$$r_L = \left(1 \pm \frac{1}{m}\right)^{2/3} r_P \tag{1.26}$$

For an orbiting test particle, resonances are the positions in the disc at which the protoplanet exerts strong perturbations. The flux of angular momentum exchange at each Lindbald resonance can be written as

$$T_{LR}(m) \propto \Sigma M_p^2 f_c(\epsilon) \tag{1.27}$$

with $f_c(\epsilon)$ the torque cutoff function (Artymowicz, 1993), which encodes the fact that torques close to the planet contribute very little to the net torque. The torque exerted by corotation requires more analysis, see Goldreich and Tremaine (1979); Tanaka et al. (2002); its expression is

$$T_{CR} \propto \frac{d}{dr}\left(\frac{\Sigma}{B}\right) \tag{1.28}$$

with B Oort parameter

$$B(r) = \Omega + \frac{r}{2}\frac{d\Omega}{dr} \tag{1.29}$$

Type I migration

For low mass protoplanets, the angular momentum flux due to the gravitational interaction between the protoplanet and the disc is negligible compared to the flux due to the disc viscosity. As a result, the surface density Σ can be considered unperturbed, and the net torque exerted on the protoplanet can be seen as

$$T_p = \sum_{ILR} T_{LR} + \sum_{OLR} T_{LR} + T_{CR} \tag{1.30}$$

where ILR stands for inner Lindbald resonances and OLR outer Lindbald resonances. From this formulation, the migration time can be derived as

$$\tau \propto \frac{M_p}{T_p} \propto M_p^{-1} \tag{1.31}$$

Type I migration is therefore more rapid for high mass protoplanets - as long as we are in the regime where the protoplanet does not alter the local density profile of the disc.

Evaluating the sum expressed in formula 1.3.4 is not easy; even being able to estimate the sign of it cannot be done analytically, as soon as not-isothermal discs are considered (the isothermal case is solved in Tanaka et al. (2002)). However, invariably it is found by simulations that the outer Lindbald resonances dominate the inner ones, and therefore the protoplanet migrates inward.

For the very low mass protoplanets, the Lindbald resonances dominate the evolution. As the mass of the protoplanet increases, the corotating component in the torque gets larger. What has been found is that the persistence of strong corotating torques depends upon whether or not they are saturated. Saturation indeed happens as corotation can only happen in a closed and relatively small region of the disc, next to the protoplanet. Moreover, the torque exerted via corotation depends upon the cooling timescale of this region.

Type II migration

For sufficiently large protoplanets, the angular momentum exchange is dominated by the gravitational torque between the protoplanet and the disc. As a result, the profile of the surface density is strongly affected, leading to the formation of a gas gap corresponding to the position of the protoplanet.

There are two conditions for the formation of this gap. The first is that the Hill radius of the protoplanet is larger or comparable than the local thickness of the disc. The second is that tidal torques are able to remove gas from the gap region faster than viscosity can fill it. There are many studies which analytically solve these two conditions simultaneously, (Goldreich and Tremaine, 1980; Lin and Papaloizou, 1980; Papaloizou and Lin, 1984). The state-of-the-art condition has been derived for laminar discs in Crida et al. (2006) and can be expressed as

$$\frac{3H}{4R_H} + \frac{50}{q\Re} \leq 1 \tag{1.32}$$

where H is the local disc scale hight, R_H the Hill radius, q the ratio between protoplanet and star mass and $\Re$ the disc Reynolds number.

Once a protoplanet is massive enough to be able to open a gap, its orbital evolution occurs on the same timescale as the local disc evolution. As small orbital radii the direction of migration will always be inwards, as the protoplanet will simply follow the disc gas which migrates towards the central star. As larger orbital radii, though, the motion of the gas can be outwards due to angular momentum redistribution inside the disc. The protoplanet migration can therefore also be outward.

Stochastic migration

All the analysis presented up to here on protoplanet migration is based on the idea that a circumstellar disc is a perfectly laminar object. This is of course not realistic. Angular momentum transport itself derives from turbulence, which can also change both in space and time inside a disc leading to local perturbations of the gas density profile. These fluctuations will exert random torques on the protoplanet. Assuming that these perturbations are uncorrelated with the presence of the protoplanet, then this random component usually dominates the type I

migration, which is supposed to be valid for small protoplanets (Baruteau et al., 2011). How important stochastic migration for planet formation is, is under debate, and depends, first and foremost, on the strength and nature of disc turbulence.

1.4. Methods

To err is human

and to blame it on a computer is even more so.

[*R. Orben*]

The evolution of the gas component of circumplanetary discs can be followed using codes that couple hydrodynamics and gravity. There are different ways to approach both these aspects. In this work we present the methods implemented in the code `Gasoline` (Wadsley et al., 2004), which has been used for the simulations analysed in Chapter 2. For a recent review of the implementation methods, I refer the reader to Springel (2010) and Price (2012)

1.4.1. SPH

The technique which `Gasoline` (as well as almost half of the astrophysical codes used in this contest) implements is called Smoothed Particle Hydrodynamics (SPH here after). SPH is based on the idea that a fluid can be approximated through the use of particles, which may be seen also as interpolation points. This idea was originally proposed in Lucy (1977) and Gingold and Monaghan (1977), more then 30 years ago.

As every numerical technique, SPH has advantages and disadvantages. On the bright side, SPH naturally leads to very accurate conservation of quantities such as energy, linear and angular momentum and entropy. Moreover, resolution is automatically higher in the regions with higher densities. Also, the formulation is manifestly Galilean invariant. All of these nice features come directly from how SPH is built. On the other side, SPH experiences the so-called mixing problem: regions with different properties (such as pressure, entropy, temperature and so on) tend to stay separate. As a direct consequence of this behaviour, shocks are hard to describe correctly (Agertz et al., 2007).

The key of SPH is the so called kernel interpolation (Gingold and Monaghan, 1982). Given a field $F(\mathbf{r})$, we can define its smoothed interpolated version $F_s(\mathbf{r})$ through a convolution with the kernel $W(\mathbf{r}, h)$:

$$F_s(\mathbf{r}) = \int F(\mathbf{r}) W(\mathbf{r} - \mathbf{r}', h) d\mathbf{r}' \tag{1.33}$$

with h the characteristic width of the kernel. The function $W(\mathbf{r}, h)$ must, by definition, be normalized to unity, to tend to the delta function for $h \to 0$, to be symmetric and to be continuous and derivable at least twice. The most currently used version of the kernel function (the spline kernel) has also a finite support (in order to save computational time), and in 3D it defined as

$$W(r,h) = \frac{8}{\pi} \begin{cases} 1 - 6q^2 + 6q^3 & \text{if } 0 \le q \le 1/2 \\ 2(1-q)^3 & \text{if } 1/2 < q \le 1 \\ 0 & \text{if } q > 1 \end{cases} \tag{1.34}$$

with $q = r/(2h)$.

Suppose now that we want to discretize the former expression, in order to be able to describe the field $F(\mathbf{r})$ for a set of points $\mathbf{r}_i$, i.e. $F_i = F(\mathbf{r}_i)$. Each point has an associate mass m_i and density ρ_i, with $\Delta\mathbf{r}_i \sim m_i/\rho_i$ the associated volume element. Substituting those expressions into the definition of the field $F_s(\mathbf{r})$, we find

$$F_s(\mathbf{r}) = \sum_j \frac{m_j}{\rho_j} F_j W(\mathbf{r} - \mathbf{r}_j, h) \tag{1.35}$$

In order to be able to evaluate $F_s(\mathbf{r})_i$, we need to know the local value of the density field. If we take $F_s = \rho_s$ the formulation becomes

$$\rho_s(\mathbf{r}) = \sum_j m_j W(\mathbf{r} - \mathbf{r}_j, h) = \rho_i \tag{1.36}$$

Therefore, once the position and mass of each particle is known, it is possible to derive every quantity. It is now clear why the kernel is preferentially with finite support. If that is not the case, indeed, the sum has to be done over all the particles in the sample, consuming computational time for evaluating neglectable contributions. With the finite support, on the other hand, only a certain amount of neighbouring particles are considered N_{ngb}. The kernel length h can be implemented so that the number of neighbours is constant, usually between 16 and 64. Larger values indeed create a collateral numerical problem, the so called *clumping* of the particles (Springel, 2010). With a fixed number of neighbours, the computational cost to calculate the field $Fs(\mathbf{r})$ is $O(N \log N_{ngb})$.

Hydrodynamics

Once we know how to describe the behaviour of a fluid, we need to know the equations of motion of the system. The Euler equations for inviscid gas dynamics in Lagrangian (comoving) form are given by

$$\frac{d\rho}{dt} + \rho\nabla\cdot\mathbf{v} = 0 \tag{1.37}$$

$$\frac{d\mathbf{v}}{dt} + \frac{\nabla P}{\rho} = 0 \tag{1.38}$$

$$\frac{du}{dt} + \frac{P}{\rho}\nabla\cdot\mathbf{v} = 0 \tag{1.39}$$

with $\mathbf{v}$ the velocity field, P the pressure, u the thermal energy per unit mass and $d/dt = \partial/\partial t + \mathbf{v}\cdot\nabla$ convective derivative. Eckart (1960) shows that these equations are equivalent to the minimization of the lagrangian

$$L = \int \rho\left(\frac{\mathbf{v}^2}{2} - u\right) dV \tag{1.40}$$

Using the SPH formulation, the lagrangian becomes

$$L_{\mathrm{SPH}} = \sum_i \left(\frac{1}{2} m_i \mathbf{v}_i^2 - m_i u_i\right) \tag{1.41}$$

Assuming that the fluid flow is isentropic, the thermal energy per unit mass can be written as

$$u_i(\rho_i) = A_i \frac{\rho_i^{\gamma-1}}{\gamma - 1} \tag{1.42}$$

with γ adiabatic index and A_i a function of the entropy. The value of A_i is taken to be constant. In a real fluid though, there are some physical processes that could modify the entropy, such as shocks. In order to describe them, an artificial viscosity is added to the fluid dynamic description. This term depends on the fluid velocity gradient, and changes the value of A_i. In the SpH implementation that has been used in this thesis, we modified the traditional prescription in order to have also a non constant adiabatic index: the implemented γ indeed is a function of both gas temperature and density, in order to improve the fluid description from a microscopic point of view.

We can solve the Lagrangian equation

$$\frac{d}{dt}\frac{\partial L}{\partial \dot{\mathbf{r}}_i} - \frac{\partial L}{\partial \mathbf{r}_i} = 0 \tag{1.43}$$

which with the Lagrangian given in eq 1.41 becomes

$$m_i \frac{d\mathbf{v}_i}{dt} = -\sum_{j=1}^{N} m_j \frac{P_j}{\rho_j^2} \frac{\partial \rho_j}{\partial \mathbf{r}_i} \tag{1.44}$$

where $\frac{\partial \rho_j}{\partial \mathbf{r}_i} = \nabla_i \rho_j + \frac{\partial \rho_j}{\partial h_j}\frac{\partial h_j}{\partial \mathbf{r}_i}$ is the total variation of density. We can combine this with the condition that the mass in the kernel volume should be constant $\rho_i h_i^3 = \text{const}$, which, after differentiation over $\mathbf{r}_i$, yields

$$\frac{\partial \rho_j}{\partial h_j}\frac{\partial h_j}{\partial \mathbf{r}_i}\left[1 + \frac{3\rho_j}{h_j}\left(\frac{\partial \rho_j}{\partial h_j}\right)^{-1}\right] = -\nabla_i \rho_j \tag{1.45}$$

The combination of those two expressions gives

$$\frac{\partial \rho_j}{\partial \mathbf{r}_i} = \left(1 + \frac{h_j}{3\rho_j}\frac{\partial \rho_j}{\partial h_j}\right)^{-1} \nabla_i \rho_j \tag{1.46}$$

From the definition of density in SPH formulation, the last term $\nabla_i \rho_j$ can be expressed as

$$\nabla_i \rho_j = m_i \nabla_i W_{ij}(h_j) + \delta_{ij} \sum_{k=1}^{N} m_k \nabla_i W_{ik}(h_i) \tag{1.47}$$

(with the abbreviation $W_{ik}(h_i) = W(\mathbf{r}_i - \mathbf{r}_j, h_i)$) and, combining these derivations we have the equation of motion for inviscid fluids in SPH:

$$\frac{d\mathbf{v}_i}{dt} = -\sum_{j=1}^{N} m_j \left[f_i \frac{P_i}{\rho_i^2}\nabla_i W_{ij}(h_i) + f_j \frac{P_j}{\rho_j^2}\nabla_i W_{ij}(h_j)\right] \tag{1.48}$$

with

$$f_i = \left[1 + \frac{h_i}{3\rho_i}\frac{\partial \rho_i}{\partial h_i}\right]^{-1} \tag{1.49}$$

From this procedure, it appears clear that energy and entropy conservation are assumed in the derivation, therefore SPH performs very well in their numerical conservation. In a similar way, mass conservation is given by construction: as long as no particles are lost, it will always be perfectly preserved.

A new equation of state

In the above section we derived the SpH formulation for the hydrodynamic component of an ideal gas, as postulated by using eq. 1.42. In Chapter 2, we developed a new Equation of State for a mixture of two ideal gases, and we implemented it into `Gasoline`. Appendix A shows the hole derivation of the Equation of State. We start by assuming that the gas is a mixture of atomic and diatomic hydrogen. We derive their partition functions and, assuming that the two components are in chemical equilibrium, we find a parametric Equation of State:

$$P = \frac{K_B T n}{2}(1+a) \tag{1.50}$$

with n the number density and a the dissociation parameter, given by the ratio of atomic hydrogen atoms and the total number of protons. The formulation for the thermal energy per unit mass is given by eq. A.22. Due to its complexity, we chose not to implement it directly into the code. Instead, we build three tables that give gas pressure, internal energy and density as a function of each other; the code calls those tables every time it needs to solve the equation of state.

1.4.2. Gravitational component

In the astrophysical context, the gravitational component is very important. Arguably, the best way to take gravity into account is to include it in the lagrangian of the system. We define the gravitational potential as

$$\Phi(\mathbf{r}) = G\sum_i m_i \phi(\mathbf{r}_i - \mathbf{r}_j, \epsilon_i) \tag{1.51}$$

with ϵ_i gravitational softening, used to prevent divergences. The lagrangian can be written as

$$L_{\mathrm{SPH}} = \sum_i \left(\frac{1}{2} m_i \mathbf{v}_i^2 - m_i u_i\right) - \frac{G}{2}\sum_{ij} m_i m_j \phi(r_{ij}, \epsilon_j) \tag{1.52}$$

with $r_{ij} = \mathbf{r}_i - \mathbf{r}_j$. Following the same procedure of the last section, we find that the equations of motion have an additional term, given by

$$m_i \mathbf{a}_i^{\mathrm{grav}} = -\sum_j G m_i m_j \frac{\mathbf{r}_{ij}}{r_{ij}} \cdot \frac{\phi'(r_{ij}, \epsilon_i) + \phi'(r_{ij}, \epsilon_j)}{2} - \frac{1}{2}\sum_{jk} G m_j m_k \frac{\partial \phi(r_{jk}, \epsilon_j)}{\partial \epsilon}\frac{\partial \epsilon_j}{\mathbf{r}_i} \tag{1.53}$$

In these additional terms, the sums are done over all the particles of the sample, as there is no kernel which is going to zero this time. This requires a lot of computational time, as the problem would scale as $O(N^2)$. There are different techniques to save computational time in this calculation. One of the most commonly used, which is implemented also in `Gasoline`, is called the *tree method* (Barnes and Hut, 1986). The treeSPH is based on a hierarchical grouping of the particles: for each particle, the code builds a tree in which the closest particles are considered one by one, while the ones further out are grouped and treated as a single larger particle. In this way, computational time is saved by not calculating all the interactions one by one, and the scaling of the system goes like $O(N \log N)$ instead of the prohibitive $O(N^2)$.

1.4.3. Gas Cooling

In realistic astrophysical contexts, pure hydrodynamic and gravity are not sufficient in order to give a complete description of the processes. There is the need for extra physical mechanisms to be added into the mathematical description: star formation, supernovæ explosions, magnetic fields, and more. In the following we take into account a cooling term, which is needed in the context of our interest: planet formation environments.

A realistic gas in a circumstellar disc will be heated by the star irradiation and by the background radiation. This is mainly given by ISM background radiation. Once it has been heated, it will re-emit part of this energy as a black body.

In a first simple implementation of the cooling term (Boley et al., 2010), at each simulation timestep each SPH particle loses a fraction of its internal energy. The energy loss per time per volume is given by

$$\Lambda = (36\pi)^{1/3}\frac{\sigma}{s}(T^4 - T^4_{\min})\frac{\tau}{\tau^2+1} \tag{1.54}$$

where τ is the optical depth, $s = (m/\rho)^{1/3}$ and σ is the Stefan-Boltzmann constant. A minimum background temperature must be assumed, which comes from environmental heating with typical values between 10 and 30 K. The optical depth is given by $\tau = \rho\kappa s$, where the opacity is approximated as

$$\kappa = \sqrt{\frac{T'}{64}}\ \mathrm{cm^2 g^{-1}} \tag{1.55}$$

for $T' = T$ if $T > T_{\min}$ and otherwise $T' = T_{\min}$ (see the next section for a description of the opacity treatment). While equation (1.54) is only approximate, it allows us to capture the general behaviour of radiative cooling. Indeed, it is capable of interpolating between the two different regimes of radiative cooling: the thin regime ($\tau << 1$), where $\Lambda \propto \tau$ and the thick regime ($\tau >> 1$), with the cooling term $\propto 1/\tau$.

One element is not taken into account at all in formula 1.54, is the energy emitted by one particle is not lost, but adsorbed by the neighbouring particles. This process can potentially be very important in the planet formation scenario, as it provides a heating term in a disc which can prevent GI. Indeed, Rogers and Wadsley (2011) show that a simulation which was showing fragmentation (Mayer et al., 2007) becomes stable against GI once a more accurate cooling scheme is considered.

A scheme that reintroduces the lost thermal energy into the neighbouring particles is called a flux-limited diffusion scheme. Rogers and Wadsley (2011) present a detailed description of the implementation of such a scheme inside `Gasoline`. In this scheme, a radiative flux term is added in the Euler equations for the conservation of angular momentum and internal energy. Also, a new equation for the conservation of radiation energy density is added to the conservation laws. The new Euler system of equations therefore becomes:

$$\frac{d\rho}{dt} = -\rho\nabla\cdot\mathbf{v} \tag{1.56}$$

$$\rho\frac{d\mathbf{v}}{dt} = -\nabla P + \frac{1}{c}\chi_F\rho\mathbf{F} \tag{1.57}$$

$$\rho\frac{dE/\rho}{dt} = -\nabla\cdot\mathbf{F} - \nabla\mathbf{v} : \mathbf{P} + 4\pi k_P\rho B - ck_E\rho E \tag{1.58}$$

$$\rho\frac{du/\rho}{dt} = -P\nabla\cdot\mathbf{v} - 4\pi k_P\rho B + ck_E\rho E \tag{1.59}$$

with E the radiation energy density, $\mathbf{F}$ the radiative flux and $\mathbf{P}$ the radiation pressure tensor. Furthermore, k_E is the energy mean absorption, k_P Planck's mean absorption and χ_F the flux mean total opacity.

In order to be able to solve this new system of equations, the code uses an implicit integration scheme

$$A_i^{n+1} = A_i^n + \Delta t \left[\frac{DA_i}{Dt}\right]^{n+1} \tag{1.60}$$

with A_i generic quantity evaluated for the particle i, Δt the length of the timestep, n and $n+1$ the timesteps considered. It is needed the use of an implicit scheme as the explicit form needs a very small timestep in order to be numerically stable, as it has already been noted for similar cases (Whitehouse and Bate, 2004).

Because of this implicit scheme, at each timestep the code needs to solve $2N$ coupled non-linear equations, with the unknown being the specific radiation and gas energies for each particle at the future time at $n+1$. The solution is obtained following the procedure illustrated in Whitehouse et al. (2005), which is based on iterations. For each particle we can rewrite the implicit specific gas energy equation in terms of the specific radiation energy and substitute the result into the implicit specific radiation energy equation. This results in a single non-linear equation for each particle, which can be solved by assuming that $T = u/c_v$. Convergence is achieved if the change in each particle specific energy over the iteration is small compared to the corresponding change over the entire time-step.

This method (called the Jacobi method) is guaranteed to converge only for linear systems: indeed it can happen then it doesn't converge in this situation. If that is the case, individual non-convergent particles are found to oscillate between two different values. This issue can be overcome by a relaxation method, with the new solution for the non converging quantity ψ given by

$$\psi_i^{(n+1)'} = \psi_i^n + \omega\left(\psi_i^{(n+1)} - \psi_i^n\right) \tag{1.61}$$

where ω is the relaxation parameter (Press et al. 2007).

The last numerical issue which needs to be solved in a complete flux limited diffusion scheme is the boundary condition. Indeed, in simulations of GI it is fundamentally important to correctly treat the emission of energy from the disc's photosphere, as this process drives the disc's cooling and therefore its fragmentation or stability. The way that the photosphere has been implemented in Rogers and Wadsley (2011) is based on a geometrical scheme. For each particle i, the code determines the geometry-independent outward direction by using $\nabla\rho_i$. Then it goes through its list of neighbours to find whether or not any reside within an angle of 50° in this direction. If no neighbour is found, then particle i is labelled as an edge particle.

The opacity

As already described in the previous section, opacity plays an important role in determining the cooling rate (see equation 1.54). As the cooling rate impacts the gas evolution in a non linear way, a realistic treatment of the opacity is crucial.

In a circumstellar disc, opacity is dominated by the dust component. Only in the very innermost region, where the temperature is higher then 1500 K, molecular opacity makes the largest

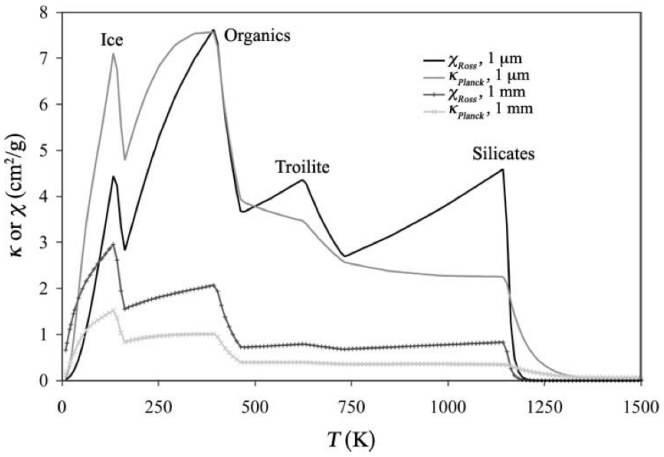

Figure 1.4.: Planck and Rosseland mean opacities as a function of temperature for grain size $s = 1\mu$m (solid curves) and $s = 1$ mm (thin curves). Credits: Boley et al. 2006.

contribution, as in this regime dust particles are destroyed. If we neglect this particular case, at a given position in the disc the opacity due to the dust is primarily dependent upon local temperature, chemical composition and grain size. The gas influences the opacity only in determining the local temperature, and therefore which species of dust particles are evaporated. The chemical composts that dominate are H_2O (ices), silicates, organic (containing C, H, O, and N), and troilite (FeS). Dust grains are assumed to be spherical, with size distribution a power law that mimics the ISM size distribution and which is for simplicity usually assumed to be constant in time (Mathis et al., 1977).

Assuming that the dust grains emit as a black body, it is possible to derive two mean opacities: Rosseland k_R and Plank k_P. The first is defined as

$$\frac{1}{k_R} = \frac{\int_0^\infty (1/k_\nu)(\partial B_\nu/\partial T)d\nu}{\int_0^\infty (\partial B_\nu/\partial T)d\nu} \tag{1.62}$$

where k_ν is the frequency dependent opacity and B_ν the Plank function. This mean opacity is used in optically thick regions, where the diffusion approximation is valid and the mean free path of a photon is much shorter than the thickness of the gas. In the opposite optically thin regime, photons can escape without being scattered by the gas, and the corresponding Plank opacity can be derived as

$$k_P = \frac{\int_0^\infty k_\nu B_\nu d\nu}{\int_0^\infty B_\nu d\nu} \tag{1.63}$$

Figure 1.4 shows the two opacities as a function of temperature for different grain sizes. The dips in the opacities are generated by the vaporization of different dust constituents at different temperatures. In the low temperature regime, up to $T \approx 160$ K, ices are the grain types which contribute the most to the total opacity. At this temperature, though, they evaporate, generating the dip in opacity. At higher temperatures, organic grains ($T \approx 470$ K), troilites ($T \approx 740$ K) and silicates ($T \approx 1140$ K) evaporate as well.

The chemical composition of grains is usually assumed to be a function of only the temperature of the gas. Although this is reasonable for a first order approximation, Podolak et al. (2011) show

that the grain composition is also a function of the temperature history of the gas. Indeed, if the gas undergoes a shock, given (in their study) by the presence of a spiral mode, some chemical components can evaporate and therefore the modified chemical composition of the dust modifies the opacity even if the gas cools afterwards. This generally leads to lower opacities than usually assumed, therefore enhancing gas cooling. This phenomena is supposed to play an important role in disc fragmentation due to GI, although a complete implementation of it has not been performed yet.

Figure 1.4 shows that gain sizes also play a major role in determining the total opacity. It is therefore important to include the description of grain size evolution in time and space in the model. This aspect is particularly crucial in the context of studying the collapse of clumps: grains tend to settle in the clump, creating an optically thick region in the center and an optically thin region in the outer part. This can affect the contraction timescale up to one order of magnitude (Helled et al., in preparation). Such a phenomenon can lead to major effects in the evolution and the fate of clumps.

The results presented in this thesis are obtained assuming a phenomenological law for the opacity, as a function of only the temperature (see Chapter 2 for a complete description). A more correct treatment of this quantity, which incorporates some of the features presented above, is currently being implemented.

1.5. Aims of this thesis

The aim of this thesis is to analyse the first stages of planet formation, from the point of view of both GI and CA. Analytical studies are coupled with the results of high resolution simulations, in order to shed light to this part of the planet formation scenario. Without a deep knowledge of the initial stage of the protoplanets, though, it is hard to make realistic prediction for the always increasing (both in number and in details) data that observation provide us.

Chapter 2 investigates the first phase of the collapse of a clump, since its formation as a fragment of a spiral arm generated through GI until it reaches second core collapse (SCC hereafter). The novelty of our study is both the focus on a realistic description of the initial condition for the clump, and the realistic description of the gas dynamic. Indeed, the initial condition for the clump is taken from a previous 3D simulation of a global fragmented disc (Boley et al., 2010). The clump therefore has a 3D complex structure, with an initial rotation and asymmetries. These are two aspects that have never been studied in detail before: analysis of collapsing clumps has been done previously for only perfectly spherical and non rotating clumps. Moreover, the version of the code that has been used in this study implements an equation of state for atomic and diatomic hydrogen in chemical equilibrium, which is expected to be more realistic in this context then an ideal equation of state (Boley et al., 2007).

This study presents a number of interesting findings. As a first result, we observe that a rotating asymmetric clump develops a bar mode which helps move the angular momentum outward, leading to a very fast initial collapse. For the same reason, only 40 % of the initial clump mass forms a spherical bound object which can be considered a protoplanet; the remaining mass settles into a proto-circumplanetary disc.

The most interesting finding though, is the estimate timescale for reaching SCC. Indeed, we don't follow the clump evolution until hydrogen dissociation happens, but we are able to extrapolate the increase of inner temperature and density, and therefore to calculate the timescale for SCC.

Our estimate is of the order of 10^4 years, one order of magnitude shorter than the value usually derived. We are able to explain this discrepancy due to the different technical implementations between our model and previous ones. This new timescale has a potentially large impact on the role of GI in planet formation: it is usually assumed that clumps which formed via GI cannot become real planets as they are disrupted by tidal interactions with the disc and the central star. A new shorter timescale estimate for the contracting time makes it plausible that these objects can become bound enough to survive these interactions, becoming the gas giant planets that we observe today.

In Chapter 3 we explore this possibility. We generate a set of 2000 synthetic clumps and evolve each of them separately inside a circumstellar disc. We couple their collapse, inward migration in the disc, tidal interaction with the central star, mass accretion from the disc and gap opening. Our results show that in the most realistic case, more than half of the initial clumps population survives and form two different populations. The first one has a typical mass of $1 M_J$ and orbits the star inside 0.5 au: these characteristics are therefore consistent with the observational results for a Hot Jupiter. The second, smaller population has a typical mass of $5 M_J$ and orbits the star at a few tens of aus. It could therefore be the progenitor of gas giant planets. These results therefore point toward a more central role of GI in the planet formation context.

Our study also stresses the crucial role of the disc viscosity on the clump survival; this quantity indeed determines whether or not a clump can open a gap in the disc, having therefore more chances to survive tidal forces. Despite this, its value is still very poorly constrained, both from theory and simulations and from observational data.

In Chapter 4 we analyse the first stages of CA in order to address two long standing problems of the theory of grain growth: the formation of large size particles (the so-called meter size problem at 1 au), which are observed in real discs but models have failed to produce, and the existence of a two-sized population of grains. We build and test a code to solve the grain size distribution evolution in time, starting from ISM grains at a fixed radius in a circumstellar disc. We recover a model presented in a previous work (Brauer et al., 2008) and find the same quantitative results. After this step, we improve the mathematical description of the model by assuming that the collisional velocity of a couple of grains is not given by a single value, but by a probability distribution function (pdf hereafter). As a first step, we assume that the pdf is maxwellian. We observe that this conceptually simple and physically motivated modification leads to the formation of grains which are larger by more then one order of magnitude. As a second step, the maxwellian pdf is modified with a pdf which takes into account the different nature of the collisional velocities: stochastic (brownian motion, turbulence) and deterministic with a preferred direction (radial drift, vertical settling and azimuthal velocity). This new improvement of the model leads to an even larger final grain size and to the formation of a two-sized grain population, consistent with the observational data.

2. The collapse of protoplanetary clumps formed through disc instability: 3D simulations of the pre-dissociation phase

This chapter is based on the publication:
M. Galvagni[1], T. Hayfield[2], A. Boley[3], L. Mayer[1], R. Roškar[1] and P. Saha[1]. **The collapse of protoplanetary clumps formed through disc instability: 3D simulations of the pre-dissociation phase**. MNRAS, 427:L1725-1740, December 2012.

Abstract

We present 3D smoothed particle hydrodynamics simulations of the collapse of clumps formed through gravitational instability in the outer part of a protoplanetary disc. The initial conditions are taken directly from a global disc simulation, and a realistic equation of state is used to follow the clumps as they contract over several orders of magnitude in density, approaching the molecular hydrogen dissociation stage. The effects of clump rotation, asymmetries, and radiative cooling are studied. Rotation provides support against fast collapse, but non-axisymmetric modes develop and efficiently transport angular momentum outward, forming a circumplanetary disc. This transport helps the clump reach the dynamical collapse phase, resulting from molecular hydrogen dissociation, on a thousand-year timescale, which is smaller than timescales predicted by some previous spherical 1D collapse models. Extrapolation to the threshold of the runaway hydrogen dissociation indicates that the collapse timescales can be shorter than inward migration timescales, suggesting that clumps could survive tidal disruption and deliver a proto-gas giant to distances of even a few AU from the central star.

2.1. Introduction

The combined efforts of RV and transit (see Wright et al., 2012; Borucki et al., 2011), mircrolensing (Sumi et al., 2011), and direct imaging surveys (Lafrenière et al., 2010) have revealed a wide range of planetary systems, with planets on both very short and very wide orbits. These increasingly large sample-size distributions of known planets, although still biased, can be used to constrain planet formation theories. Unfortunately, testable predictions by planet formation theories are not fully developed, and in some cases, there may be multiple ways to produce a particular planet (Boley et al., 2010) or to induce the observed disc structure (see Muto et al., 2012; Hashimoto et al., 2011). To complicate matters further, regardless of the

[1]Institute of Theoretical Physics, University of Zurich,Winterthurerstr 190, 8057 Zurich, Switzerland
[2]Max-Planck-Institute fur Astronomie, Koenigstuhl 17, D-69117 Heidelberg, Germany
[3]Department of Astronomy, University of Florida, 211 Bryant Space Science Center, USA

planet formation mechanism, planet-planet and planet-disc interactions can lead to large scale transport of planets throughout their natal discs (see Baruteau et al., 2011; Michael et al., 2011).

There are currently two main theories (for a review see Armitage, 2010) for the formation of massive planets: core accretion (hereafter CA) (Mizuno, 1980; Pollack et al., 1996) and gravitational instability (hereafter GI) (Boss, 1997; Mayer et al., 2002b). From these mechanisms, it is also possible to derive alternative scenarios, such as the tidal stripping theory (Boley et al., 2010; Nayakshin, 2010). In each paradigm, the formation of a gas giant planet proceeds in a very different way. In the first case the grains in the circumstellar disc aggregate until they reach a critical core mass at which there is a run away accretion of gas from the disc onto the solid core. The critical core mass for runaway gas accretion can vary due to conditions in the discs (Movshovitz et al., 2010; Rafikov, 2011); however, the large population of Neptune-mass planets on short periods discovered by *Kepler* suggests that the critical value may be $\gtrsim 10 M_{\oplus}$. Under the disc fragmentation paradigm, the giant planet is the result of a contraction of a massive self-bound clump of gas that forms due to fragmentation of GI-driven spiral arms.

The idea of forming giant planets by disc instability goes back to at least Kuiper (1951a). Renewed interest in disc instability as a planet-forming mechanism is largely due to the advancement of Boss (1997) and to recent discoveries of extrasolar planets on wide orbits (Bonavita et al., 2011; Nielsen et al., 2011; Quanz et al., 2012). The Toomre (1964) stability criterion measures the susceptibility of the disc to growing perturbations due to self-gravity; whenever

$$Q \equiv \frac{2c_s}{G\Sigma t_P} < 1, \tag{2.1}$$

axisymmetric ring distortions will grow in an infinitesimally thin disc. Here Σ is the disc surface density, c_s is the sound speed, and t_P is the epicyclic period, which will be close to the orbital period in nearly keplerian discs. For three-dimensional protoplanetary discs with finite width, numerical simulations have shown that spiral arms will grow whenever $Q \lesssim 1.7$ (Durisen et al., 2007a). The mass scale for self-gravitating distortions (Toomre mass), which is not necessarily the fragmentation mass, can be expressed as a sound horizon

$$GM_T/c_s^2 \approx c_s t_P, \tag{2.2}$$

which at plausible radii gives massive giant-planet to brown-dwarf masses within a square Toomre wavelength. Simulations have shown that when clumps do form, initial fragment masses can be a factor of a few or more smaller than the Toomre mass (Mayer et al., 2004; Boley et al., 2010; Rogers and Wadsley, 2012). After spiral structure develops in a disc due to self-gravity, spiral arms could regulate the instability and reach a marginally unstable state, with mass redistribution and energy dissipation balancing the effects of disc cooling. In the local limit, Gammie (2001) showed that for a cooling time $t_{\rm cool}$, GIs will lead to an effective α viscosity given by

$$\alpha = \frac{2}{9\pi\Gamma(\Gamma-1)}\frac{t_P}{t_{\rm cool}} \tag{2.3}$$

where Γ is the (2D) adiabatic index. If GIs cannot stabilize the disc, then spiral arms can fragment into bound clumps. The cooling time boundary for fragmentation, which sets a maximum α in the local limit (Rice et al., 2005), is still being debated in the literature (Meru and Bate, 2011a; Lodato and Clarke, 2011; Paardekooper, 2012), but appears to be within a factor of a few $t_{\rm cool}$.

Now consider the conditions in a disc that are favorable to disc instability. For $T = 100$ K and $t_P \sim 12$ yr, $\Sigma \gtrsim 3600$ g cm^{-2} for $Q \lesssim 1.7$. For comparison, a minimum-mass solar nebula has a

surface density $\Sigma \sim 150\,\mathrm{g\,cm^{-2}}$ at 5.2 AU, although we also remind the reader that that this value is a *minimum* and that the assumptions used to derive this mass are suspect (for an example, see Desch, 2007). For clump formation, higher surface densities than those considered above may be needed, as fragmentation seems to require an azimuthally averaged $Q < 1.4$ (Mayer et al., 2004). The exact threshold will depend on the equation of state. Because a low value of Q is needed for fragmentation, it is of interest to know where low values will most likely persist. In a Keplerian disc, $Q \propto r^{q/2-p-1.5}$ for disc radius r. We have assumed that the temperature and surface density profiles can be described by power laws with indices q and p, respectively. For a flared disc with $q \sim -0.5$, the surface density must drop more steeply than $p \sim -1.75$ to prevent the outermost regions of the disc from being the most susceptible to GIs. Furthermore, as the surface density drops and the disc becomes colder, the opacity of the disc will also drop and cooling can become more efficient, as long the gas has enough emissivity to radiate. Because the local dynamical times are long at large radii, cooling times can be much shorter than the local dynamical time, and disc fragmentation, not just instability, becomes likely (e.g., Rafikov, 2009; Boley, 2009).

When clumps do form, they are many orders of magnitude less dense than a giant planet, with radii of a few AU, and have significant angular momentum. Although there have been detailed numerical studies of clump evolution, they have been limited to spherical quasi-equilibrium models (Helled and Schubert, 2009). Simulations that follow the clump in 3D and within the context of a disc are too low resolution to capture the internal dynamics of the clump (Stamatellos et al., 2007). As long as clumps remain large and diffuse, it has been suggested that they might lose a significant fraction of their mass and become super-Earths as long as they can accrete enough mass in the core (Nayakshin, 2010; Boley and Durisen, 2010). However, even prior to considering tidal mass loss, the actual mass that goes into forming the planet (or brown dwarf) and the mass that contributes to an eventual subdisc (circumplanetary or circum-brown dwarf) is unknown and depends on the efficiency of angular momentum transport within the clump. As discussed in more detail below, when the central temperatures of the clump reach ~ 2000 K, H_2 dissociation will cause rapid collapse of the clump, forming a bound substellar companion (gas giants and brown dwarfs). At this point tidal mass loss will be negligible due to a very high central density.

In the present study we present high resolution 3D simulations of clumps that form through disc fragmentation at 80 AU. Their evolution is followed until the contaction approaches hydrogen dissociation and rapid collapse begins. The simulations are performed using a new version of `Gasoline` (Wadsley et al., 2004) that implements an equation of state (herein EOS) designed to model the relevant temperature-density regime. In some of the simulations we also include the effect of radiative cooling. Section 2.2 describes our methods. Section 2.2.3 shows simulation results, and discussions and conclusions are presented in section 2.4. A detailed derivation of the EOS is given in the appendix. The purpose of the present work is to follow the evolution of clumps in order to build a self-consistent picture of the types of objects that GI forms; this is a rich area of research, and this study represents an initial step toward this goal.

2.2. METHODS

2.2.1. EOS and Radiative Cooling

The internal structure of any single clump will go through a wide range of densities and pressures as the object cools and contracts, which can change the relative importance of the translational,

rotational, and vibrational modes of molecular hydrogen during the clump's evolution. In particular, the onset of H_2 dissociation in the clump's core will lead to dynamic collapse of the entire structure. For these reasons, we have modified the SPH code `Gasoline` (Wadsley et al., 2004) to include an EOS for a mixture of atomic and molecular hydrogen in chemical equilibrium (see appendix A). The EOS is taken to be

$$P = \frac{K_b T \rho (1+a)}{2 m_P}, \tag{2.4}$$

with P being pressure, k_B the Boltzmann constant, T temperature, ρ density, and $a = a(T, \rho)$ the dissociation parameter, given by the number of protons in the atomic case over the total number of protons, and m_P proton mass. In Figure (2.1), we show the dissociation parameter as a function of density and temperature. Dissociation becomes more likely as the temperature increases and as the density decreases. In order to highlight the regime of interest in this context, the evolution of one of our simulations is also shown.

For a clump to evolve from the initial low-density, low-temperature state to the H_2 dissociation threshold, it must radiate away energy. In the following, we present simulations with and without cooling. The latter is referred to as the adiabatic case, and serves as a base for comparisons. We implement cooling in `Gasoline` for these simulations with a simplified prescription that uses local gas conditions only (as done in Boley et al., 2010). Let the energy loss per time per volume be given by

$$\Lambda = (36\pi)^{1/3} \frac{\sigma}{s} (T^4 - T_{\rm min}^4) \frac{\tau}{\tau^2 + 1} \tag{2.5}$$

where τ is the optical depth, $s = (m/\rho)^{1/3}$ and σ is the Stefan-Boltzmann constant. Here, a minimum background temperature $T_{\rm min} = 10$ K is assumed, which is the reference background radiation field for the ISM. The clump explored here forms in the outermost regions of the disc, where the tempertature can become dominated by the radiation background, which is what we assume. The optical depth is given by $\tau = \rho \kappa s$, where the opacity is approximated as

$$\kappa = \sqrt{\frac{T'}{64}} \ {\rm cm}^2 {\rm g}^{-1} \tag{2.6}$$

for $T' = T$ if $T > T_{\rm min}$ and $T' = T_{\rm min}$ otherwise. While equation (2.5) is only approximate, it allows us to capture the general behavior of radiative cooling. Namely, cooling is most efficient at an optical depth $\tau \sim 1$. The opacity law used here is also very approximate, but is chosen to be monotonically increasing with temperature for two reasons: (1) Only a local optical depth is used, where the proper optical depth is integrated along a path. (2) The geometry of the problem places the densest material at the highest temperatures. Although sublimation of ices, organics, and dust can all cause the opacity to drop suddenly, the integrated optical depth for radiation to leave the clump from any of these regions will likely be large. The simple form for the opacity permits fast evaluation of radiative cooling, allowing us to focus on investigating the effects of the EOS on the clump's evolution. The effects of radiative transfer in addition to the new EOS will be investigated in future work.

2.2.2. Initial conditions

We present four high-resolution simulations of gaseous clumps that have formed through disc fragmentation. Clump initial conditions (ICs) are taken directly from global simulations of a fragmented protoplanetary disc (Boley et al., 2010), but with the resolution increased by a factor

Table 2.1.: Simulations parameters for the global simulation presented in Boley et al. 2010 and for the high resolution simulations presented in this work.

	Mass [M_J]	Radius [AU]	N. particles	Grav.Softening	N. neighbours
Global Sim.	3.7	7.0	1.5×10^4	0.5 AU	32
Clump Sim.	3.7	7.0	1.5×10^5	0.045 AU	32

of 10 (see below for a description of the procedure). The clump was extracted from the global simulation when the fragment's central density was one order of magnitude larger than the background value. Its radius was taken to be twice the bound radius. In this way we can follow correctly the clump contraction, as all the particles which will follow into it are included, and part of the environment is as well. We did not try different radii, but we observe during the evolution that most of the initial gas do not collapse into the clump. Therefore, we can safely assume that considering twice the bound radius is safe. We selected a clump that has a stellar separation of about 80 AU and is not distorted due to tidal effects from other close clumps. This choice ensures that the clump has a simple morphology and that it is not strongly affected by the presence of other objects or the central potential (see Figure 2.3). By using ICs based on the results of global simulations, we are confident that the initial conditions of the presented simulations are self-consistent with the formation of clumps by disc instability. We refer to the ICs that are produced by this direct extraction method as IC1. As the aim is to follow the collapse of the object through several orders of magnitude in density, the simulations are quite computationally expensive.

We increased the effective resolution in the extracted clump by resampling the "parent" particles (i.e. those taken from the global simulation) by ten "child" particles, randomly distributed within a volume defined by the SPH kernel smoothing length h determined using 16 neighbors. The child particles inherited equal fractions of the mass from their parents as well as their velocity. However, in order to preserve the multiphase structure of the clumps, the hydrodynamic quantities were distributed to the child particles using a standard SPH scatter scheme. The temperature has been rescaled to take into account the change in the mean moleclar weight μ and in the adiabatic index γ between the global simulation and the high resolution ones used in this study. To simplify the software development, we reused the neighbour-finding methods of the well-known group-finding code `SKID` (Stadel, 2001) and tailored them to our needs.

The ICs produced by direct extraction can be used to produce a second, quieter set of ICs. This second set (IC2) is produced by symmetrizing the mass and the temperature profiles of IC1 and by setting the initial velocity field, which is mostly rotational, to zero. This gives us a spherically symmetric IC that can be used to isolate the effects of rotation on clump contraction. For each IC, one simulation is run adiabatically (no cooling) and a second is run with the radiative cooling described in section 2. The adiabatic case will help to isolate the EOS effects from clump cooling during the early stages of the system evolution.

We check whether the tidal potential of the central star can affect the clump evolution by running an adiabatic simulation with IC1 for ~ 10 of its internal dynamical times with the central star explicitely included. We found negligible differences between clump evolution with and without the central star. At the time that the clump was extracted from the global simulation, the clump is at large stellar separation and well within its Hill sphere. Tidal effects only play a role in the outer, low-density layers of the clump, which appear to be unimportant for the evolution of the clump as studied here (see section 2.3 for a detailed analysis).

The extraction method used to create the initial conditions prevents us from studying the effects

of gas accretion from the disc onto the clump during its evolution. This is a limitation for these simulations. Gas accretion potentially plays an important role in the evolution, although it is not clear in which direction it would lead. As a first approximation, it would speed up the collapsing timescale as it increments the clump mass. At the same time, though, this process would influence the density and the temperature of the object, leading to a different cooling rate which is not easy to predict due to the non-linear nature of cooling. In order to correctly quantify the effects of gas accretion, then, long term simulations on large scale are needed, which are beyond the aim of this work.

Table 2.1 summarizes the numerical parameters used in this study, including the initial clump mass and radius. Figure 2.4 shows the temperature, density and cumulative angular momentum profiles of the initial clump resampled at higher resolution (see next section). The angular momentum barrier R_b is the radius that the object would have if it were rotationally supported, where $R_b(< r) = J(< r)^2/GM(< r)$ with specific angular momentum inside r $J(< r)$. As the initial radius is 2.5 AU and the corresponding angular momentum barrier is 0.17 AU, the clump is only partially rotationally supported. This is confirmed by the initial ratio between rotational and gravitational energy, which is 0.18.

Figure 2.5 shows the different components of the energy as a function of the radius for the initial condition (kinetic, thermal and gravitational). It is evident that the the gravitational component is dominant and that the clump is out of equilibrium. The virial equilibrium condition $2(E_{\rm kin} + E_{\rm the}) = -E_{\rm gra}$ [1] is not completely fulfilled, as the initial condition is missing 4% of the internal energy needed for it to be in virial equilibrium. This out-of-equilibrium condition is due to the low resolution of the global disc simulation from which we are extrapolating the clump, as in that condition the clump was not allowed to properly collapse because of a gravitational softening of 0.5 AU. This artificial out-of-equilibrium state leads to a fast initial collapse phase, which lasts for $4t_{\rm dyn}$. The clump evolution is then self-consistent after this initial transient.

2.2.3. Determining a Resonable Clump Resolution

The resolution of the clump as taken from the global simulation has been increased by a factor of 10 through particle splitting. This value of 10 has been selected based on the results of a resolution study, where IC2 has been evolved adiabatically for different resolutions, increasing slowly its initial number of particles. Convergence for clump evolution is found when the increasing factor is 10. The initial temperature is kept constant for all particles that are split from their parent. The new particle mass is rescaled so that the total mass is constant between different resolution runs and the softening ($h_{\rm hsm}$) is rescaled so that $h_{\rm hsm} \times (N_{\rm par})^{1/3}$ is constant. Figure 2.6 shows the evolution of the half-mass radius and of the inner density in different runs; there is convergence for both quantities at increasing number of particles. The temperature profiles for three runs at different resolutions at different times are shown in Figure 2.7. In this case, the convergence at high resolution is clear. Moreover, in the low-resolution case, the inner part of the clump does not reach as high of temperatures as found in the high-resolution runs, as the simulation is not resolved well enough to follow the collapse.

[1] Note that only the translational component of the thermal energy goes into pressure support. If the total thermal energy is used, then the virial condition is dependent on the volume-averaged adiabatic index, such that $2E_{\rm kinetic} + 3(\bar{\gamma} + 1)E_{\rm thermal} = -E_{\rm grav}$.

2.3. RESULTS

Using the simulations presented here, we follow the evolution and fate of clumps as they evolve toward second core formation. This evolution is strongly correlated to the rotational state of the object, so our analyses first focus on the effects of rotation and angular momentum transfer due to the growth of structures in the clump. These processes affect the evolution of the clump, which we quantify by studying its half-mass radius, inner density and temperature for the simulated timescale. Lastly, we give an estimate of the clump entropy and compare it with the values usually assumed in long-term contraction and cooling simulations.

Radius and angular momentum evolution

We follow the evolution of the clumps in four different cases: IC1 and IC2 are evolved using the adiabatic and cooling cases. The evolution of the half-mass radius (Figure 2.8) shows that the initial rotation of the clump (IC2) helps to prevent the collapse. This is a trivial result, but note how this effect is quite drastic and fast. In only a few dynamical times the difference between the two initial conditions is evident. Naturally, including a cooling term exacerbates the initial collapse.

The presence of initial asymmetries in the IC1 simulations leads to the development of Fourier modes, which are due to low-amplitude spiral structure. They are presumably initially seeded by the self-gravity of the disc and then amplified during the collapse phase by the clump dynamics. The stellar potential does not play a role during this phase of the evolution.

The strengths of the asymmetries are given by the global Fourier amplitudes,

$$A_m = \frac{(a_m^2 + b_m^2)^{1/2}}{\pi \int \rho_0 \bar{\omega} d\bar{\omega} dz}, \tag{2.7}$$

with

$$a_m = \int \rho \cos(m\phi) \bar{\omega} d\bar{\omega} dz d\phi, \text{ and} \tag{2.8}$$

$$b_m = \int \rho \sin(m\phi) \bar{\omega} d\bar{\omega} dz d\phi. \tag{2.9}$$

Integration is extended out to 7 AU. From this analysis it is clear that the clump develops an m-2 mode, which becomes weaker with time (see Figures 2.9, 2.10 and 2.11). These structures move the angular momentum outward, as can be seen in Figure 2.12, where, after the fast initial collapse, the cumulative angular momentum profile appears to be flattened in the inner part. When the modes start to become unimportant, this angular momentum transport becomes weaker, with the clump developing a spherical core (with only 46% of the initial mass collapsed into the core in the cooling case) surrounded by a rotating circumplanetary disc. In the adiabatic simulation, although the m-2 mode lasts for a longer time, the effects due to the angular momentum transfer are weaker compared to the cooling case. The total angular momentum is conserved in both simulations up to 5%[2].

Figure 2.13 shows the evolution of the ratio between rotational and gravitational energy $T/\|W\|$ for IC1 in the adiabatic and cooling cases. In both cases this ratio initially increases, as the

[2]The conservation of the total angular momentum can not be seen from Figure 2.12 as the x-axes are only up to 1.5 AU, so the component from the outer part is not shown.

collapse is very fast and wins over the angular momentum transport. After the first few dynamical times, the collapse becomes slower and the m-2 modes move angular momentum outward. Eventually the T/‖W‖ stops increasing and instead decreases. This phase is faster in the adiabatic case as the clump's collapse is less efficient. It is worth pointing out that the initial condition IC1 is not spherical, so the values of T/‖W‖ are not a straighforward indicator of the modes evolution of the clump. Indeed, we detect the presence of several fourier modes throughout the collapse, although the ratio hardly reaches 0.274, which is the threashold value for a bar mode in a spheroidal (Durisen et al., 1986).

While the clump is largely a spheroid, it can also be decomposed into core-like and disc-like structures. For the disc portion, the Toomre Q (1964) parameter can be used to explore the susceptibility of the system to the growth of non-axisymmetric structure. However, this must be taken with caution, as portions of the disc have significant pressure gradients, making a strict application of the Toomre Q difficult. Figure 2.14 shows the evolution of Q in the cooling case IC1 outside the half-mass radius for five different times. Although early in the clump's evolution the clump's Q value approaches the instability threshold for a thick, 3D disc (e.g. Mayer et al., 2004), the disc evolves toward a stable state.

At the final stage of the simulation, the protoplanetary disc can be defined as the region between the clump radius and one third of the Hill radius, which is the maximal disc extent found in previous works (Ayliffe and Bate, 2009; Martin and Lubow, 2011). Although these previous works address clumps formed via CA, with gas accreting onto solid cores, the disc which forms in the simulation herein presented has very similar properties. Figure 2.15 shows the disc's morphology; the disc gas mass is 46% of the total mass, giving the clump and disc having comprable mass. Moreover, the clump velocity is sub keplerian in the core-like structure due to pressure support, while it approaches keplerian values in the disc-like structure. The ratio H/r where H is the disc hight is comparable to the values found in previous works.

Density and temperature evolution

To understand if a clump is going to survive inside a disc, it is essential to study the evolution of the clump's inner temperature and density, where we use inner to refer to the values that are averaged over the particles inside one gravitational softening from the center of the clump. This average is used because the gravitational softening is larger than the particles' smoothing length. This also implies that the presented simulations underestimate the contraction, regardless of their high-resolution. The evolution of inner density and temperature are shown in Figures 2.16, 2.17, 2.18 and 2.19. The density profile evolution in both the adiabatic and cooling cases shows that a fraction of the mass lies outside the Hill radius (13.1 AU in the initial condition), which will be stripped away due to the interaction with the host star, reducing the mass of the clump. This process will happen on a timescale comparable to the rotational time of the material at the Hill radius, which is (for our IC1) about 760 yr. This timescale is longer than the duration of the simulations, so neglecting the star is not expected to alter the evolution of the high-resolution simulations. However, the timescale is shorter than the contraction timescale, which means tidal effects could still play some role in the evolution of the clump over the contraction timescale. This effect is expected to be small for the conditions considered here, as the clump becomes highly concentrated over the duration of the simulation.

The simulations with cooling show that the clump will eventually reach the second core collapse. It is not possible to state with certainty the same for the adiabatic simulations, as it is not clear which physical phenomena will lead to the collapse after the removal of the m-2 mode. Without

Table 2.2.: The last density of the clump as taken directly from the simulations, as well as extrapolations for two evolutionary timescales and two thermodynamic values just priori to dissociation and collapse. See the text for further details.

Quantity	IC1: adiabatic	IC1: cooling	IC2: adiabatic	IC2: cooling
Last density [g/cm^3]	4.20×10^{-9}	1.57×10^{-7}	4.28×10^{-7}	4.30×10^{-6}
1300 K Timescale [yrs]	2.3×10^4	2.2×10^3	–	1.38×10^2
Dissociation Timescale [yrs]	–	6.3×10^3	–	6.3×10^2
Extr. density [g/cm^3]	–	7.3×10^{-6}	–	1.3×10^{-4}
Extr. Specific Entropy [k_B]	–	14.8	–	15.2

cooling, the clump should eventu ally reach an equilibrium. In the cooling case, it is possible to estimate the timescale for reaching the dissociation of molecular hydrogen[3] by extrapolating temperature and density (the first quantity is extrapolated linearly, while the latter using a parabolic function). For IC1 the extrapolation is done using the last 15 $t_{\rm dyn}$, while for IC2 it is done using the last 1.5 $t_{\rm dyn}$. Although it is initially unclear whether such extrapolation is reasonable, as after the 3D simulations end, the clumps must still go through a wide range of temperatures and densities before collapsing to the second core, the simple extrapolation does place the inner values on a sensible trajectory (see Fig. 1). The speed of collapse will be dependent, in part, on the adopted cooling approximation for radiative cooling, but also on the opacity and metallicity of the clump, where for a given metallicity the opacity is only known to factors of a few. These extrapolations are crude, but we expect the resulting timescales to be within the range of plausible evolution scenarios for realistic clumps. See table 2.2 for the estimated timescales and physical quantities.

Entropy evolution

It is usually assumed that CA and GI lead to the formation of protoplanets with different properties. In the first case, called the cold model ($s/k_B < 10$), these objects are supposed to have a lower specific entropy than in the second case, the so called hot model ($s/k_B > 10$) (Spiegel and Burrows, 2012). With our simulations we are able to give an estimate of the actual value of the specific entropy when the clump reaches $R = 10R_J$ by extrapolating the entropy evolution (see table 2.2). The specific entropy of the clump changes very slowly with time, and the extrapolated value agrees with the hot model range found in previous works.

The evolution of specific entropy changes depending whether the inner or the outer part of the clump is considered. It is interesting to notice that, in all the performed simulations, the specific entropy of the inner part of the clump decreases with time, while it increases for the outer part. This points towards the existence of a redistribution mechanism of the entropy between the clump and its envelope. Figure 2.20 shows the evolution of the specific entropy profile for IC1 in both the adiabatic and cooling case. Overall redistibution is evident, although the simulation with cooling develops a more complex specific entropy profile with a peak and a trough at $r_p = 0.48$ AU and $r_t = 2.38$ AU, respectively. This effect is due to the more effective collapse seen

[3]From a 1D study of clump collapse we don't present here, we know that when hydrogen dissociation starts the dissociating gas becomes locally almost isothermal, therefore triggering even more collapse, temperature raising and hydrogen dissociation in the nearby molecular gas. Because of this back feeding behaviour, we observe that once the dissociation parameter `a` is 1 % the collapse becomes so fast that we can safely assume that the clump has reached SCC. In this work we use as a safe threshold `a` = 10 %, which will give us an overestimate in the contraction timescale.

in the simulations with cooling, so that at $r = r_p$ the density has significantly decreased compared with the adiabatic case (factor of 5), which leads to a local entropy increase.

2.4. Discussion and Conclusions

Gravitational instabilities in the outer regions of circumstellar discs can lead to disc fragmentation and the formation of clumps, but at the moment it is unclear whether these clumps can survive to become gas giant planets or other bound objects. In this work, we have analyzed the initial collapse of realistic clumps using a set of high-resolution, 3D simulations that include an EOS that is appropriate for clump densities and temperatures. Our results allow us to estimate the long-term evolution of these clumps, which can be used to address their survival and whether they can continue to contract to form a companion (in this case, a gas giant planet).

Our timescale estimates for the collapse are usually smaller than the values found in previous work. In Helled and Schubert (2008) the timescale estimated to reach an inner temperature of 1300 K (value at which the dust component evaporates) is 1.6×10^4 years for a clump with $3M_J$. It is possible to make a comparison between this case and our IC1 simulation in the cooling case as it implements a similar physics and as the initial conditions have comparable values for both mass and luminosity[4] (see Helled and Bodenheimer, 2011). Our result for estimated timescale to reach the same inner temperature shows that a 3D treatment of the clump evolution describes a faster collapse (see Table 2.2). This difference is due to a combination of factors, above all the different treatment for contraction. Indeed (Helled and Schubert, 2008) implements a 1D quasi-static model, which means that the collapse goes through a series of equilibrium states. In this way if reactions take place on a dynamical timescale that is smaller than the sound crossing time, the shells are not able to communicate and each of them has to wait for the evolution of the others to react to it, while non-axisymmetric and dynamical instabilities can occur in our 3D simulations.

The estimated timescales presented in this work have important implications for the evolution and survival of clumps formed by disc instability. The clump contraction timescales and central mass concentrations determine whether fragments can survive tidal stripping forces as they move throughout the disc. It is possible to estimate the minimum distance from the central star that the clump can reach before tidal forces will overwhelm the clump's stability and prevent collapse to a second core. To calculate this, use the Hill radius definition:

$$a_{\min} = R \left(\frac{3M_{\text{star}}}{m_{\text{clump}}} \right)^{1/3} \tag{2.10}$$

with $M_{\text{star}} = 0.3M_{\odot}$. Using the results from the more realistic simulation (IC1 with cooling), i.e., the values from the last output, we find $a_{\min} = 5.97$ AU. It is also possible to extrapolate the half-mass radius of the clump to its value as the clump reaches collapse to a second core by $R = R_{\text{last}} \left(\rho_{\text{last}}/\rho_{\text{extr}}\right)^{1/3} = 0.32$ AU, so that $a_{\min} = 2.52$ AU. This means that if the clump collapses before getting closer to the star than $a_{\min}$, it can become bound enough to survive further tidal effects. This is expected to be the case, as the migration timescale for such an object has been found to be of the order of 10^4 yr (compare Baruteau et al., 2011; Michael et al., 2011), which is longer than the extrapolated time to molecular hydrogen dissociation in the

[4]The luminosities are evaluated at half-mass radius in order to exclude the circumplanetary envelope. The initial value is 4.5×10^{29}erg/s, while the end value for the IC1 simulation with cooling is 4.0×10^{28}erg/s.

clump. There is the possibility that the clump gets disrupted at pericenter passages in the early stage of migration through clump-clump scattering, clump-spiral arm excitation, or birth on an eccentric orbit. If migration remains smooth, then the clump can remain well inside its Hill sphere for plausible migration rates.

Although rapid collapse could be a common evolutionary scenario for clumps, there is still the potential for rich dynamics to occur prior to molecular hydrogen dissociation. This is best illustrated by noting the total angular momentum of the IC1 clump with cooling at the end of the simulation, which is $L = 5.4 \times 10^{47}$ g cm^2 s^{-1}. This result is in agreement with the calculations shown in Machida et al. (2008) which give a slightly larger value for L (less than factor of 2) for a clump with the same mass. In both cases, the total L is two orders of magnitude larger than the angular momentum estimated for Jupiter ($L_j = 4.14 \times 10^{45}$ g cm^2 s^{-1}). Moreover, as the clump evolves, the amplitude of the fourier modes get weaker in these simulations, leading to a less efficient removal of the angular momentum from the clump. This implies that there has to be a second mechanism, later in the evolution of the clump, in order to match the simulation results for L with Jupiter. This mismatch could, for example, be due to the neglect of magnetic effects. The temperature and density regimes that the clump will experience do allow for possible development of some magnetic drag, due to thermal ionization, that would lead to angular momentum loss (compare with Perna et al., 2010). The presence of magnetic fields in the protoplanet could also lead to a transfer of its angular momentum to a circumplanetary disc due to coupling of the planetary dipole field lines to the disc fluid, as discussed in Takata and Stevenson (1996). Although the Takata and Stevenson derivation applies only for the very last stage of the planet formation, when its radius is only a factor of ten larger than its final value, the mechanism they describe can lead to the decreasing of L by a factor of $3 - 4$ in this very last phase. Self-gravitating instabilities could also become important again as the clump contracts and the core spins up. If $T/||W||$ once again reaches ~ 0.27, then dynamic bar instabilities can be rejuvenated.

The simulations that have been performed allow us to confirm that the clumps formed via GI are described by the so called hot state model. As stressed in Spiegel and Burrows (2012), this is particularly interesting as it can allow the next generation of observational surveys to discriminate between the GI and the core accretion model.

The present work points toward a more central role for the GI theory in the direct formation of gas giant planets, as the contraction of disc instability clumps may be very rapid, at least for some if not many conditions. The possibility that protoplanetary clumps retain most of their mass even when they reach distances close to the star as a result of inward migration opens new scenarios for the origin of close-in extrasolar plantes. Indeed, while previous work has suggested that partial stripping and concurrent core formation could turn clumps into super-Earths and/or Neptunes (Boley et al., 2010; Nayakshin, 2010), our findings suggest that in principle a fraction of clumps formed at large radii by GI can become giant planets on close-in orbits. Nevertheless, it is worth pointing out that this result comes from extrapolated values, and not from a self-consistent study of a clump's contraction over the full range of its first core phase. This work is a first step towards a full description of clump contraction, which appears to be a very complex and computational demanding problem. Note also that the EOS herein implemented does not really affect the clump evolution in the presented simulations, but it is expected to play a major role in the later evolution. A more realistic cooling prescription using radiative transfer, which is only mimicked here, as well as simulations taking into account gas accretion from the disc onto the clump, will need to be included in future models. These points will be addressed in future work.

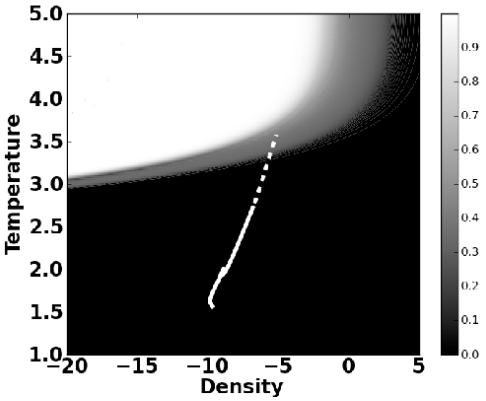

Figure 2.1.: Dissociation parameter `a` as a function of temperature and density. The x and y axes are in log scale (cgs units). The white solid curve represents the evolution of the clump from the IC1 simulation in the cooling case, the white dotted curve is the extrapolated evolution.

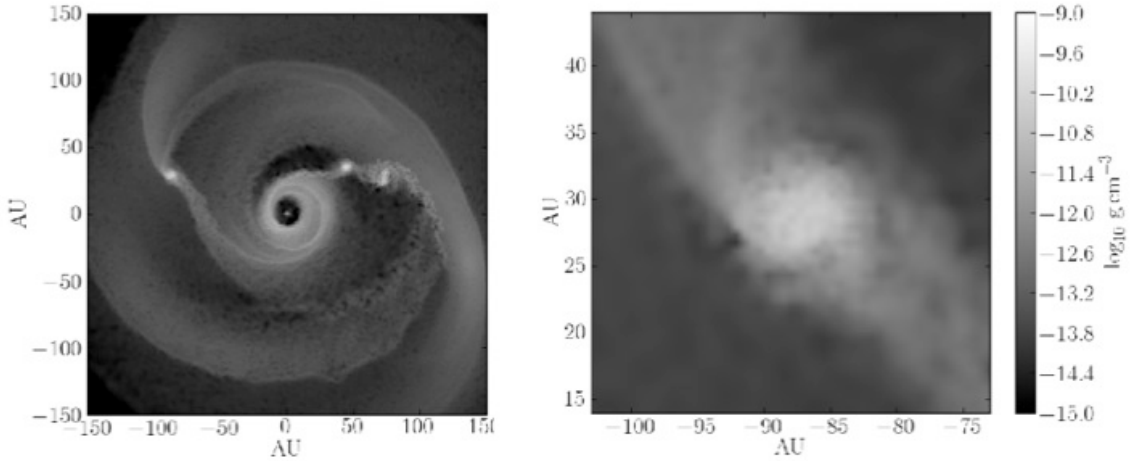

Figure 2.2.: Density map for the initial condition. On the left, the propoplanetary disc simulation presented in Boley et al. 2010. On the right, a zoom on the selected clump. Axes are in AU, density in cgs (log scale).

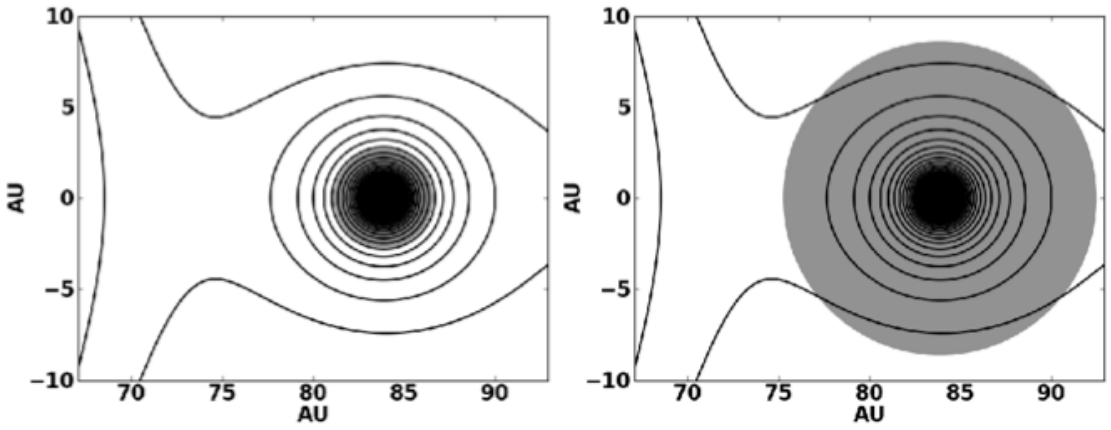

Figure 2.3.: Roche map of the protoplanetary disc. The black curves represent the gravitational potential, the gray circle the extracted clump at half mass (left) and 80% mass (right). Axes are in AU.

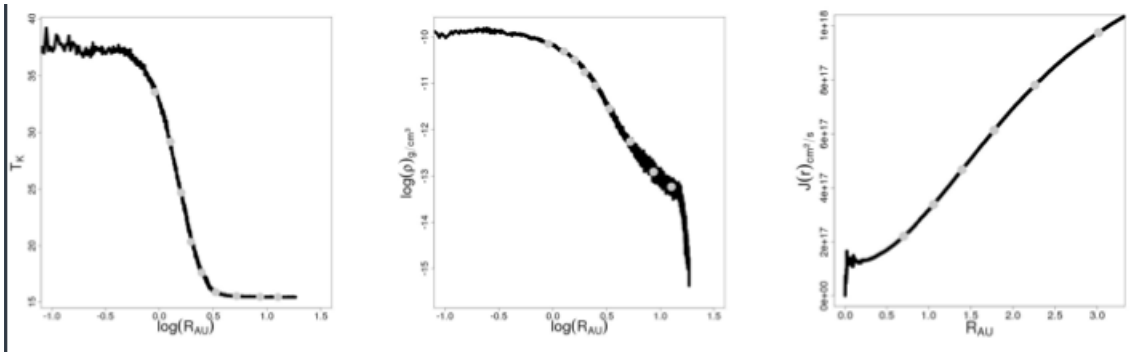

Figure 2.4.: Temperature (on the left), density (on the middle) and cumulative angular momentum (on the right) profile of the initial clump. The gray dots represents shells containing 10% of the mass.

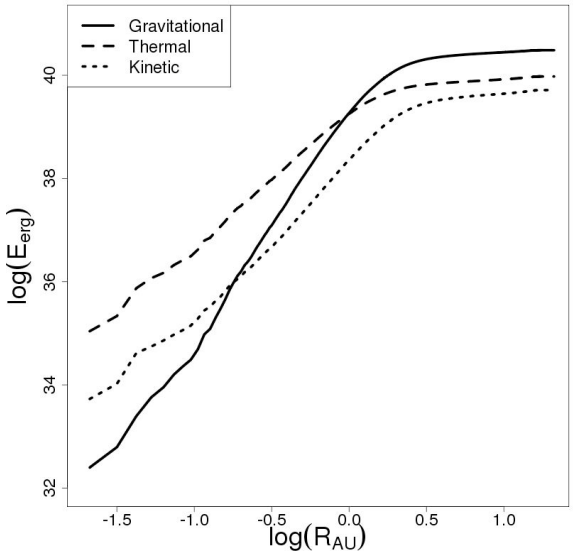

Figure 2.5.: Cumulative energies (gravitational, kinetic and thermal) in log scale (cgs units) as a function of the radius (in AU) for the initial condition.

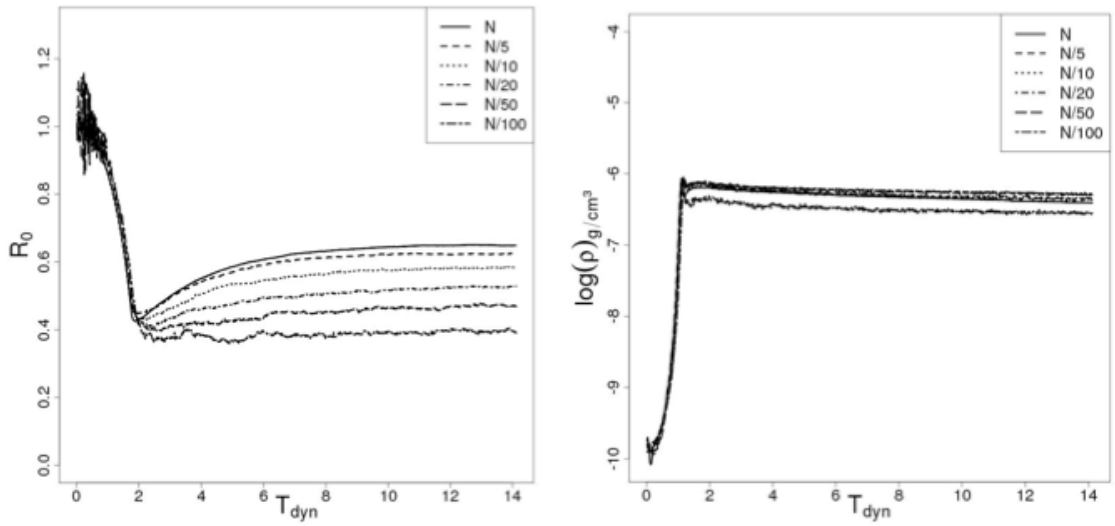

Figure 2.6.: Evolution (in dynamical times) of the half-mass radius (in unit of its initial value) and inner density (in log of cgs) for IC2 in adiabatic case for different number of particles. N is the number of particles in the high-resolution case.

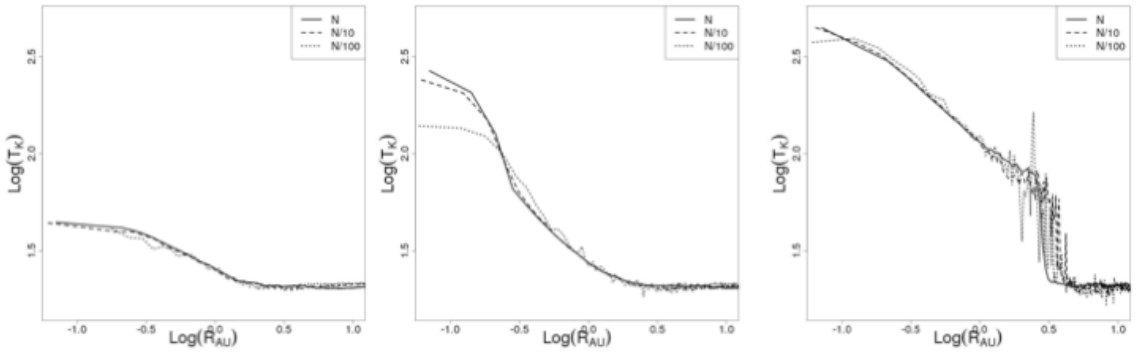

Figure 2.7.: Temperature profiles for runs at different resoltions and at different times: from left to right $t = 1T_{dyn}$, $t = 1.5T_{dyn}$, $t = 3.0T_{dyn}$. As in the previous figure, N is the number of particles in the high-resolution case.

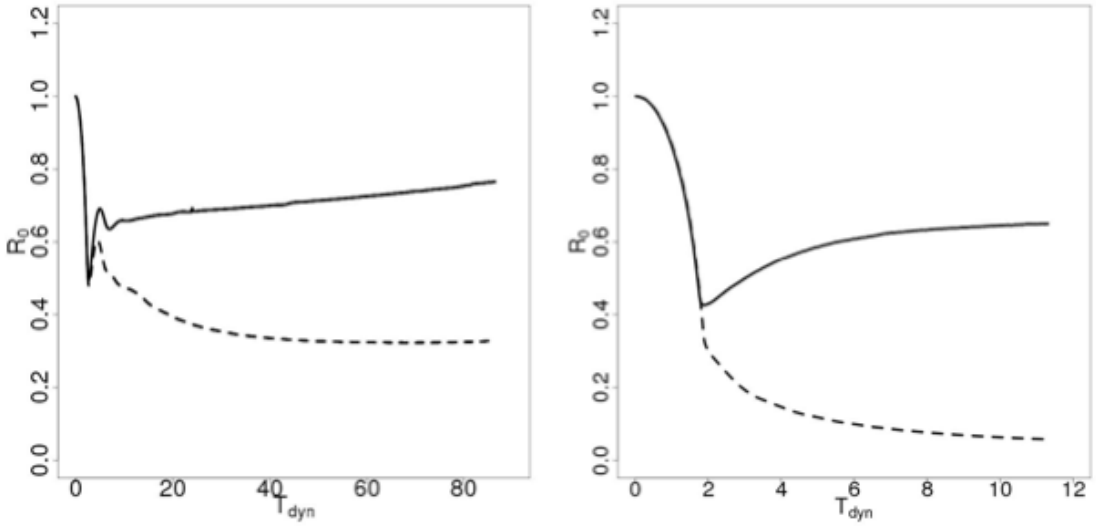

Figure 2.8.: Evolution (in dynamical times) of the half-mass radius (in unit of its initial value) for IC1 (left) and IC2 (right) in adiabatic (solid line) and cooling (dashed line) cases.

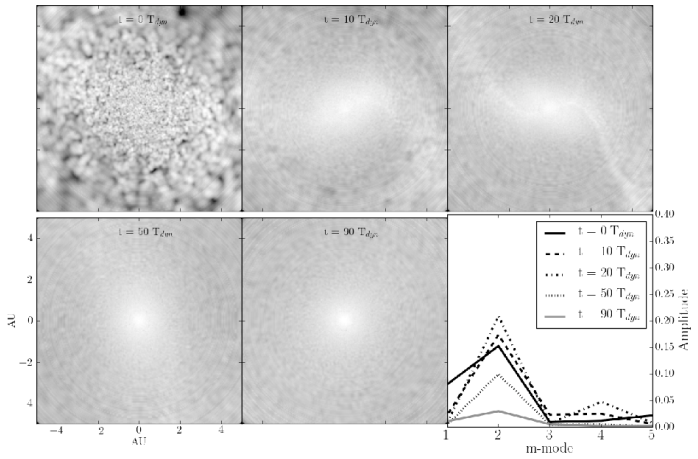

Figure 2.9.: Fourier analysis of the evolution of IC1 at different times: adiabatic case. The maps show the difference between the density and the mean density calculated from the surface density profile of the clump. Axes are in AU, see the bottom left corner. On the bottom right, corresponding amplitude vs Fourier modes

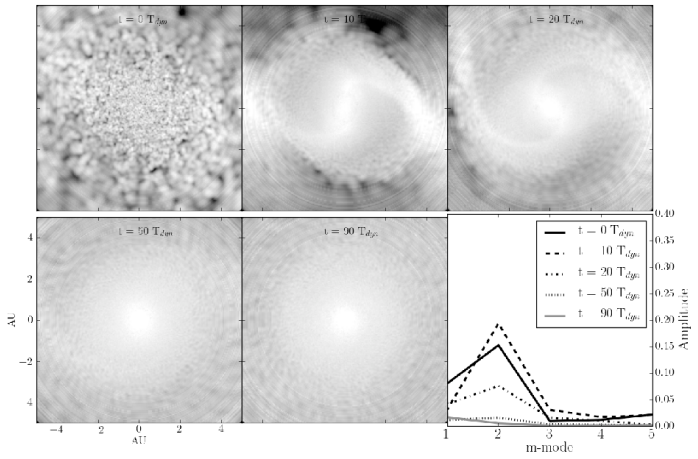

Figure 2.10.: Fourier analysis of the evolution of IC1 at different times: cooling case. The maps show the difference between the density and the mean density calculated from the surface density profile of the clump. Axes are in AU, see the bottom left corner. On the bottom right, corresponding amplitude vs Fourier modes

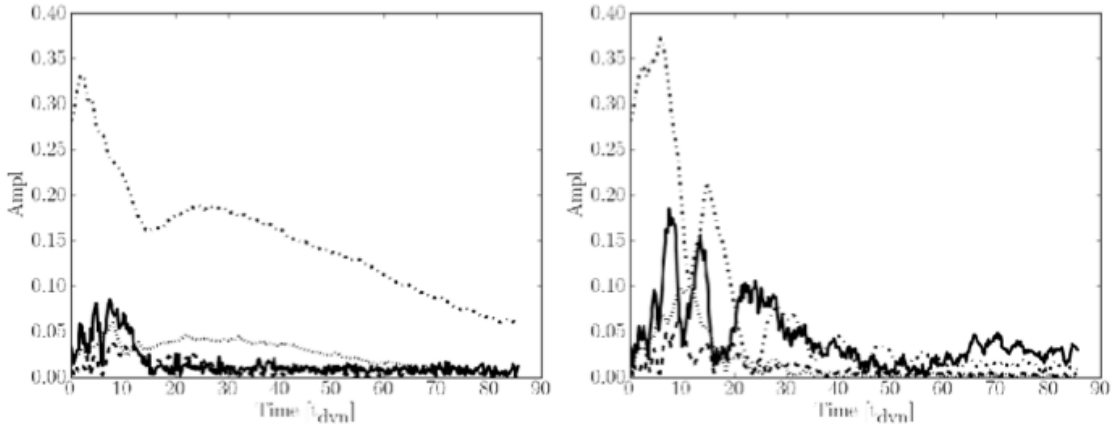

Figure 2.11.: Evolution (in dynamical times) of the amplitude of the first four fourier modes in the adiabatic (left) and cooling (right) cases using IC1. The solid line corresponds to m=1, the dotted-dashed line to m=2, the dashed line to m=3 and the dotted line to m=4.

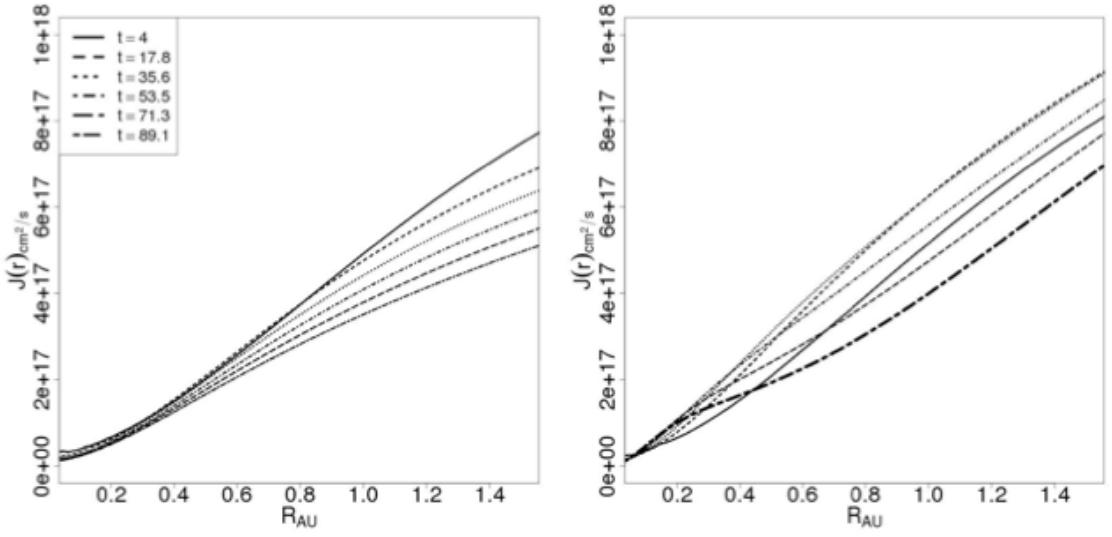

Figure 2.12.: Evolution of the cumulative angular momentum profile in the adiabatic (left) and cooling (right) case for IC1. The transient phase (earlier than $4t_{\rm dyn}$) is not shown.

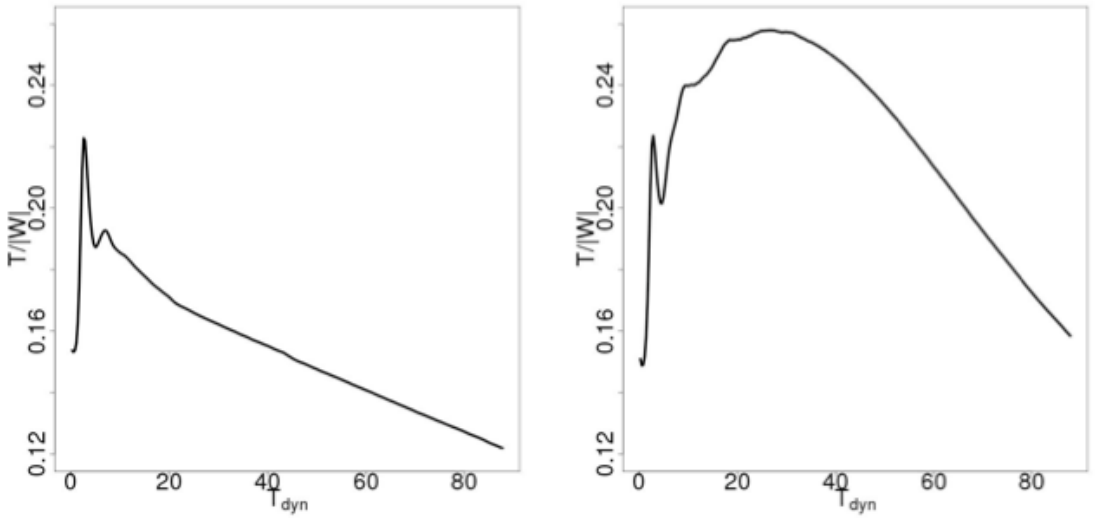

Figure 2.13.: Evolution of the ratio between rotational and gravitational energy $T/||W||$ for IC1 in the adiabatic (on the left) and cooling (on the right) cases.

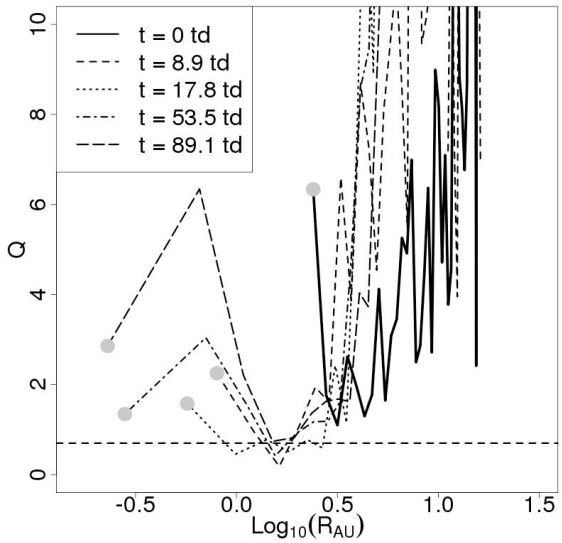

Figure 2.14.: Toomre parameter Q as a function of radius (in log scale) at five different times for the cooling evolution of IC1. The horizontal line is the threashold 0.7 for a thick, 3D disc (see, e.g., Mayer et a. 2004).

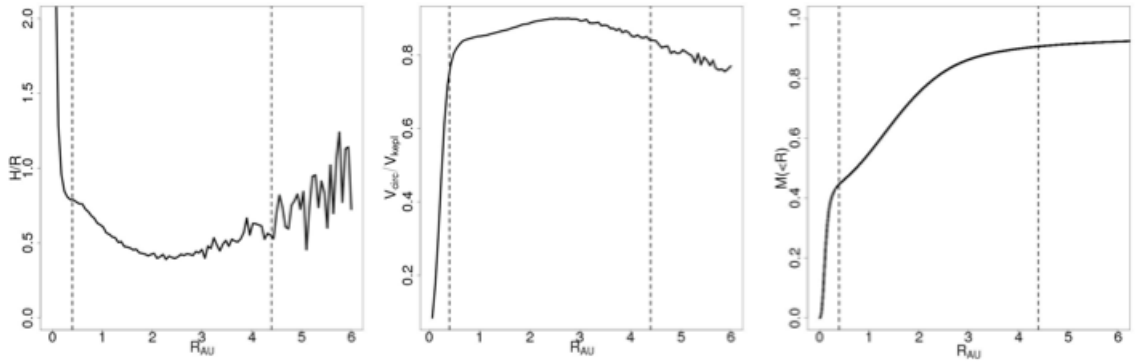

Figure 2.15.: Circumplanetary disc properties at the last stage of IC1 simulation in cooling case. The left panel shows the ratio between the disc hight and the disc radius, the central panel the gas circular speed to the Keplerian speed, and the right panel the mass enclosed within a given radius. All profiles are shown versus clump radius. In each panel, the vertical lines represent the clump core and the disc boundaries.

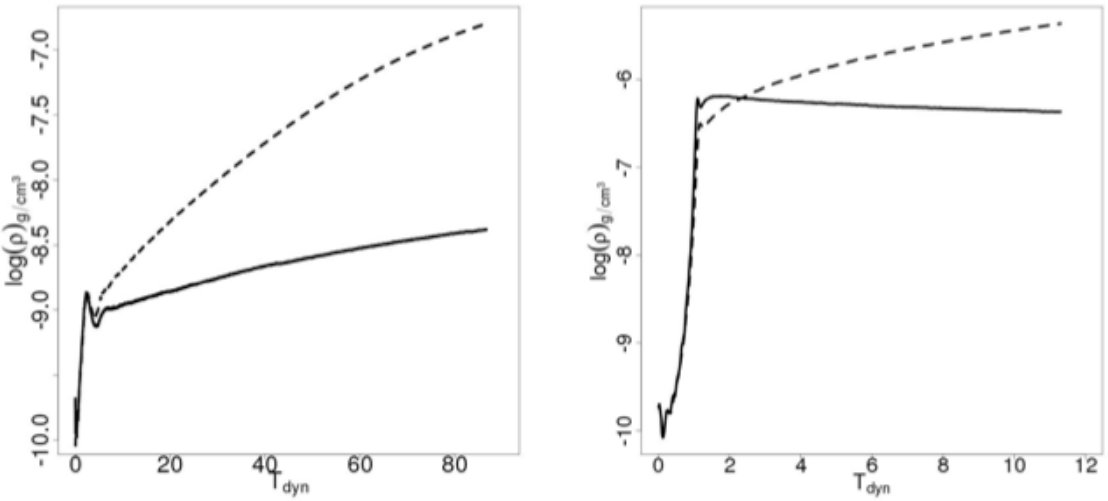

Figure 2.16.: Evolution (in dynamical times) of the inner density (log scale of cgs units) for IC1 (left) and IC2 (right) in adiabatic (solid line) and cooling (dashed line) cases.

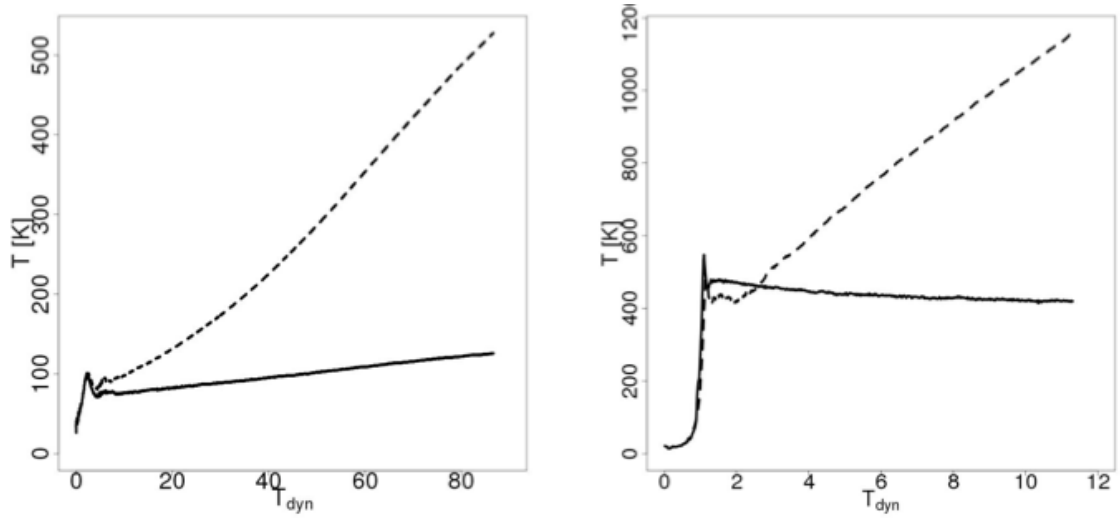

Figure 2.17.: Evolution (in dynamical times) of the inner temperature for IC1 (left) and IC2 (right) in adiabatic (solid line) and cooling (dashed line) cases.

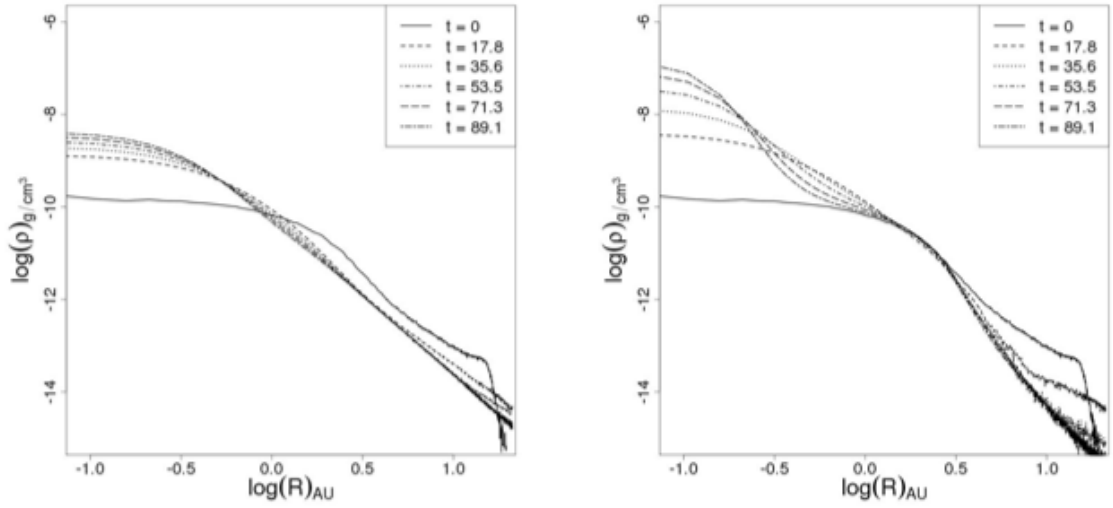

Figure 2.18.: Density profile evolution for IC1 in the adiabatic (on the left) and cooling (on the right) cases.

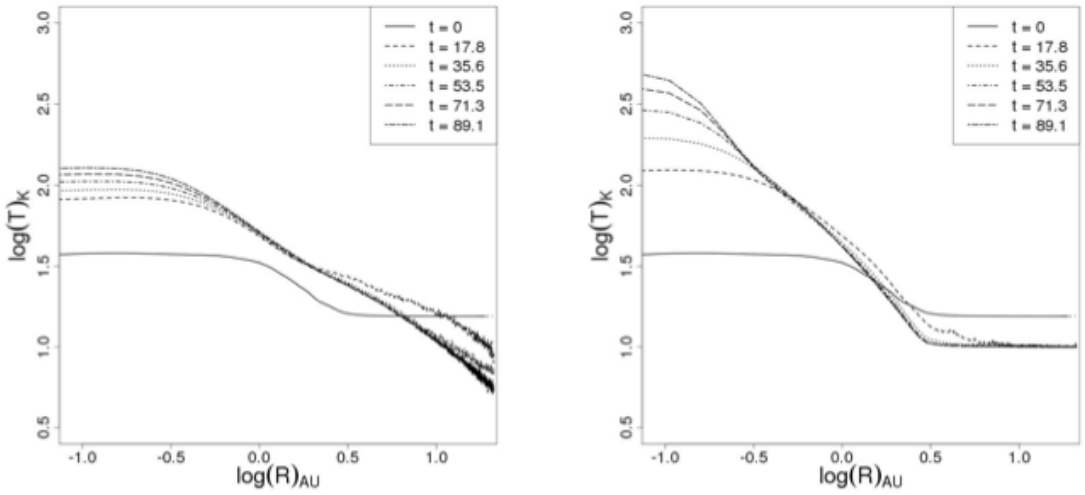

Figure 2.19.: Temperature profile evolution for IC1 in the adiabatic (left) and cooling (right) cases.

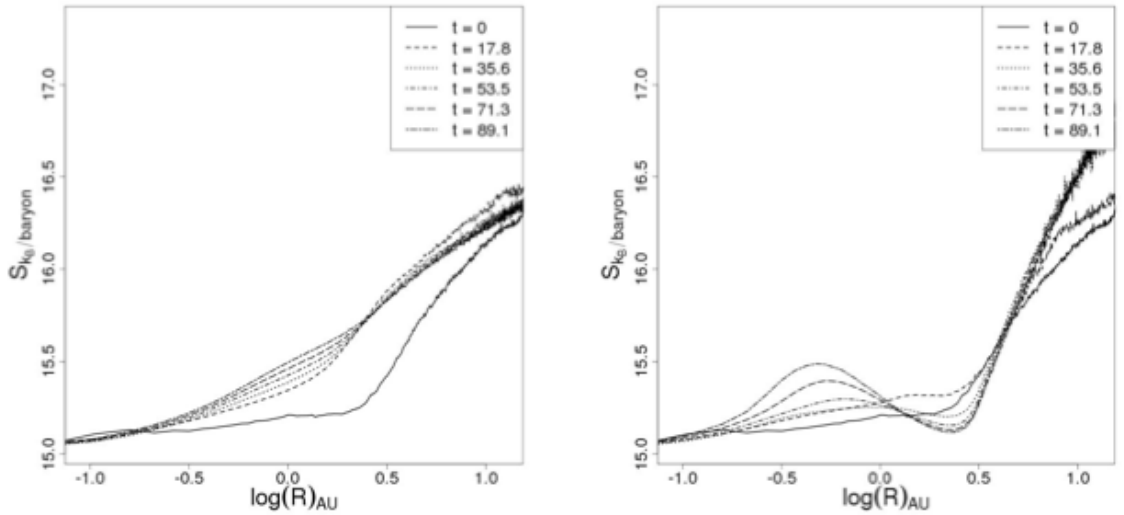

Figure 2.20.: Specific entropy profile evolution for IC1 in the adiabatic (on the left) and cooling (on the right) cases.

3. Early evolution of clumps formed via gravitational instability in protoplanetary discs; precursors of Hot Jupiters?

This chapter is based on the publication:
M. Galvagni[1] and L. Mayer[1]. **Early evolution of clumps formed via gravitational instability in protoplanetary discs; precursors of Hot Jupiters?** Submitted to MNRAS.

Abstract

Although it is fairly well established that Gravitational Instability (GI) should occur in the early phases of the evolution of a protoplanetary disc, the fate of the clumps resulting from disc fragmentation and their role in planet formation is still unclear. In the present study we investigate semi-analytically their evolution following the contraction of a synthetic population of clumps with varied initial structure and orbits coupled with the surrounding disc and the central star. Our model is based on recently published state-of-the-art 3D collapse simulations of clumps with varied thermodynamics. Various evolutionary mechanisms are taken into account, and their effects are explored both individually and in combination with others: migration and tidal disruption, mass accretion, gap opening and disc viscosity. It is found that in general, at least 50% of the initial clumps survive tides, leaving behind gas giants over a wide range of orbits after $\sim 10^5$ *yr of evolution in the disc. The rest might be either disrupted or produce super-Earths and other low mass planets, provided that a solid core can be assembled on a sufficiently short timescale, a possibility that we do not address in this paper. Extrapolating to million year timescales, all our surviving protoplanets lead to close-in gas giants. This outcome might in part reflect the limitations of the migration model adopted, and is reminiscent of the analogous result found in core-accretion models in the absence of fine-tuning of the migration rate. Yet it suggests that a significant fraction of the clumps formed by gravitational instability could be the precursors of Hot Jupiters.*

3.1. Introduction

The study of planet formation has been boosted in the last decade due to unprecedented observational campaigns of extrasolar planets enabled by new telescopes and techniques (see Wright et al., 2012; Borucki et al., 2011; Sumi et al., 2011; Lafrenière et al., 2010). The large diversity of physical characteristics that these objects show (Ma and Ge, 2013) leads to the idea that there must be more then one mechanism to generate them. Indeed, there is a great variety

[1]Institute of Theoretical Physics, University of Zurich, Winterthurerstr 190, 8057 Zurich, Switzerland

in mass, composition (from rocky planets to gas giants), radii and position in the disc (from a few fractions up to hundreds of au from the central star).

The state-of-art primary formation scenarios are Core Accretion and Gravitational Instability (for a review see Armitage, 2010). While CA is generally recognized as the mechanism by which most planets should form, and is by construction meant to form gas giants as well as rocky planets, GI has received revived interest with the discovery of gas giants at large distances from their parent stars (semimajor axis > 30 au) since this is the region where discs are likely undergoing fragmentation in the early stages unless they are stabilized by strong irradiation (Rafikov, 2009; Boley, 2009; Zhu et al., 2012). On the theoretical side, GI, which has been traditionally restricted to explain gas giants (Boss, 1997; Mayer et al., 2002a), has been developed in a new direction in the last few years as it has been recognized that Tidal Downsizing coupled with accretion of solids and core formation within gas clumps can in principle lead to Super-Earths and other rocky planets (Boley et al., 2010; Nayakshin, 2010). Furthermore, recent work has shown that radial migration plays an important role in GI as it is already known to play in CA (Baruteau et al., 2011), possibly leading to planets at distances much lower than those of their formation site. It is therefore clear that the fate of clumps produced by GI depends on several mechanisms, many of which the same that are also crucial in CA. While this adds complexity, it is also a sign that GI has now become a far more mature theory, within which predictions can now be made beyond the short timescales probed by simulations (Zhu et al., 2012) by combining analytical calculations of several processes, as it has been done in CA for a few years (Alibert et al., 2005). This potentially allows us to start making predictions that can be verified or falsified by observations, as has been done now for a few years with CA, and finally allows us to compare both formation theories on the same ground.

Indeed, although the concept of GI as a giant planet formation model has been around for a long time (Kuiper, 1951b), studies of the long term dynamical evolution of clumps formed in GI are just now beginning to appear (Zhu et al., 2012). This isn't the case for CA, where studies of population synthesis models (Mordasini et al., 2009) have been proposed over the last few years, making it possible to produce statistics for the characteristics of extrasolar planets formed via this mechanism.

While fully radiative 3D simulations are too expensive to allow us to carry out studies of clump evolution on long timescales (Boley et al., 2010), simpler 2D simulations with phenomenological cooling prescriptions (Vorobyov, 2013) have recently been used to study the likelihood of whether fragments are the progenitors of the giant planets and brown dwarfs that are detected at tens of au from the hosting star (Marois et al., 2008; Kalas et al., 2008). These works find that most of the clumps migrate inwards rapidly and are destroyed by tides in the inner region of the disc before they can become fully fledged planets, leading to the conclusion that successful planet formation by GI is a rare occurrence in general. However, these simulations have low resolution (a few AU with their grid size), which likely leads to artificial clump disruption by tides at small radii, an effect that is known to have plagued simulations of self-gravitating collapse with non-adaptive grid techniques in other fields of astrophysics, such as star formation and cosmological structure formation (Durisen et al., 2007b; Mayer and Gawryszczak, 2008, for effects of resolution on disc fragmentation in various numerical techniques). Futhermore, no existing numerical simulation of self-gravitating protoplanetary discs by either grid-based or SPH codes, has enough resolution to resolve the internal structure of the clumps and allow us to study their collapse properly. Clump collapse is crucial since it will determine the response of the clumps to migration and tides by affecting its density, mass and temperature, as shown by analytical studies that focus on this process (Helled and Bodenheimer, 2011; Vazan and Helled, 2012).

In order to be able to make prediction for the characteristics that a population of extrasolar planets formed via GI would present, more accurate studies of the very early stage of clump formation and evolution are needed. Indeed, the main question regarding GI is: are the clumps that form going to survive the interaction with the disc and hosting star, or will they be disrupted?

Fortunately, the first high-resolution 3D fully hydrodynamical simulations of clump collapse have been performed (Galvagni et al., 2012, and Galvagni et al. in prep.), adding a new important step that goes in the direction of answering these questions properly. The results of the published collapse simulations constitute the backbone of this paper.

As a first approximation, we can divide the lifetime of a clump into two parts: pre-dissociation and post-dissociation phase. It is indeed known that, while a clump contracts, it will eventually reach an inner temperature and a density high enough to dissociate molecular hydrogen (Masunaga et al., 1998). This dissociation phase makes the clump momentaneously isothermal, as the gravitational energy from the collapse goes into breaking the molecules. This leads to a fast collapse that shrinks the clump into a more compact object. Once the clump has undergone this process, it can be safely assumed to be so compact that it could resist interaction with the disc and hosting star, being then a real protoplanet.

Due to its much longer timescale phase the key phase is thus the first phase of the clump life: if it is able to reach the dissociation of hydrogen (called second core collapse, hereafter SCC) without being priorly disrupted, then we can assume it is a real protoplanet.

Nayakshin and Lodato (2012); Zhu et al. (2012); Forgan and Rice (2013) recently presented first attempts towards a population synthesis model for GI, by coupling the evolution of clumps during the first collapse phase with their interaction in the disc.

However, none of these works relies on accurate clump collapse simulations, rather they assume a timescale for the collapse in the first phase, or they compute that while assuming quasi-static collapse based on the notion that the dynamical time is always much shorter than the cooling time. However, detailed studies of clump collapse assuming near hydrostatic equilibrium at all times obtain clump collapse timescales that are up to 2 orders of magnitude longer relative to those found in the 3D hydro simulations. Since the relationship between the timescale of the various processes involved is ultimately what will decide the fate of the clumps (Zhu et al., 2012), starting from a self-consistent model of internal clump evolution becomes a pivotal factor.

The aim of the study presented herein, is to address the following questions : how many of the clumps formed via GI in a standard circumstellar disc will survive to SCC? What will their characteristics be? The answer will give an estimate of how lucky GI is to be a valid mechanism for forming planets. Nevertheless, this work does not represent a synthesis population model for GI, as the final characteristics of the population of planets formed via this mechanism still depend on the evolution that the clump undergoes afterd SCC. Our results give an estimate of the final position and mass of the planets, but should not be taken as a prediction, as a description of SCC and the following stage is beyond the scope of this work.

The paper is organized as follows: the next section presents the methods, with detailed explanation of the implementation of the different physical mechanisms taken into account. Section 3.3 presents the results of our simulations, which are discussed in section 3.4. The conclusions are given in section 3.5.

Table 3.1.: Physical mechanisms implemented in the different scenarios.

	Migr+Tidal Disr	Mass Accr	Gap opening	Mass Accr during gap
Set A	Yes	No	No	No
Set B	Yes	Yes	No	No
Set C	Yes	Yes	Yes	Yes
Set C_m0	Yes	Yes	Yes	No

3.2. METHODS

We consider the evolution of a set of clumps formed via GI inside a disc, from the fragmentation of spiral arms to SCC. Since our focus here is to study the fate of clumps *provided that they form by GI*, rather than the conditions to form clumps by GI in discs, we will not include a model of a Toomre-unstable disc as done in eg. Zhu et al. (2012). Instead, we will assume that clumps are already present and study their evolution under the combined action of all the key mechanisms: collapse, migration, mass accretion, and tidal effects. As in all the semi-analytical works on the subject so far, we will not include the effect of the dynamical interaction between different clumps, which is known to take place in 3D disc simulations, leading occasionally to clump-clump merging and rendering their orbital dynamics more stochastic than expected if only inward radial migration takes place (Boley et al., 2010; Zhu et al., 2012). Therefore, in our model we are essentially considering the simple situation in which there is one clump per disc and, therefore, by generating a population of clumps as we will do, we are following a population of protoplanetary discs in which fragmentation has taken place. What fraction of the overall disc population the latter population represents is beyond the scope of this paper. While this might appear somewhat idealized, the highest resolution radiative disc simulations published so far show that only very few clumps form in discs which undergo fragmentation (Mayer et al., 2007; Boley et al., 2010; Meru and Bate, 2011b), while 2D simulations, which are less realistic but can probe a larger parameter space, show that in most cases clump-clump interactions are not the dominant process (Zhu et al., 2012).

We generate a population of clumps in a random way (see section 3.2.1) and evolve each of them independently. Three different scenarios are explored (see table 3.1). In all scenarios, clump contraction, migration and tidal disruption are taken into account. In scenario B, mass accretion from the disc onto the clump is added. Scenario C implements also a gap opening criteria. For each scenario, different sets of simulations are run, changing the initial conditions and exploring different gap opening implementations.

This study concentrates on the formation of gas giant planets; we therefore neglect as a first approximation grain coagulation and core formation. Due to this approximation, we are unable to capture the formation of rocky planets through tidal downsizing.

The disc model and initial conditions are presented in 3.2.1; all the phenomena implemented in the different scenarios are presented from 3.2.2 to 3.2.5.

3.2.1. Disc model and Initial Conditions

In a protoplanetary discs self-gravitating clumps can form from the fragmentation of spiral arms in Toomre unstable discs (Boss, 1997; Mayer et al., 2002a). Recently, a new mechanism has been proposed for the formation of these objects (Hopkins and Christiansen, 2013), based on

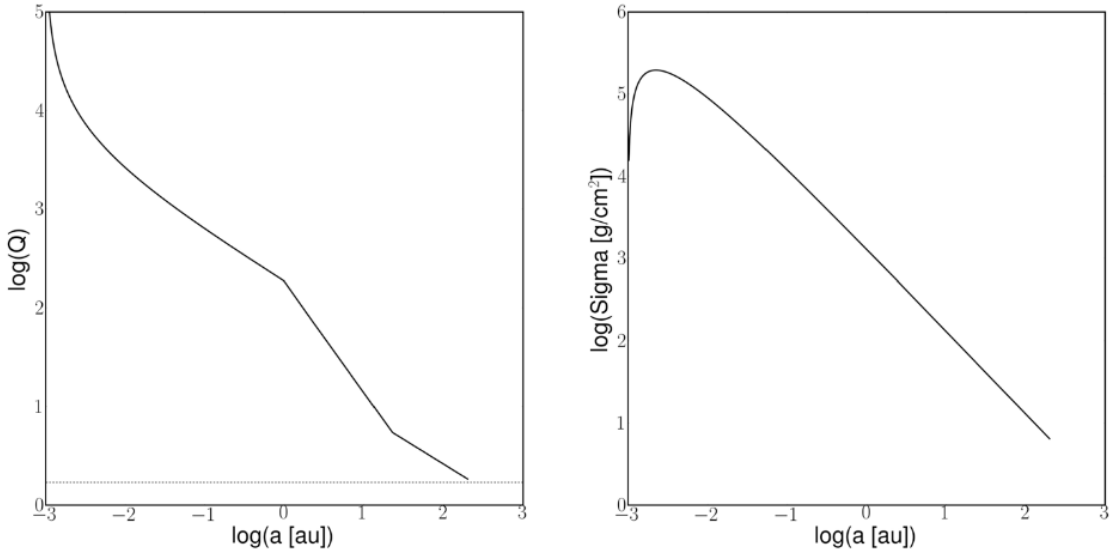

Figure 3.1.: On the left, surface density profile of the circumstellar disc. On the right, Toomre parameter profile. The horizontal dashed line corresponds to the critical fragmentation value $Q_{\rm cr} = 1.7$. Scales are logaritmic.

turbulence-induced fragmentation in self-gravitating discs occurring even when the disc is Toomre stable. We will not consider this case, as it is a less likely occurrence and requires closer scrutinity. The focus is then on clumps which form from the fragmentation of spiral arms when $Q_{min} < 1.4$ (Durisen et al., 2007b), as found by a wide range of calculations. We also assume that a disc self-regulates to a marginally stable steady state immediately after fragmentation ($Q_{min} = 1.7$, see disc Q profiles in Figure 3.1), neglecting the possibility of recurrent fragmentation epochs sustained by either disc mass loading or sudden opacity changes which shorten the cooling time, since this would require following the disc evolution (Vorobyov and Basu, 2009a). We emphasize once again that our model is intentionally simple and errs on the side more effects that would favour clump formation and survival rather than the opposite (see Summary/Discussion section on caveats).

Our starting point is thus the disc configuration soon after fragmentation. We generate two different sets of initial conditions. In each case, the only quantities we need to specify for the clumps are: initial semimajor axis a, mass clump $M_{\rm clp}$ and radius r.

Fragmentation is more likely in the early stage of the disc lifetime, when the disc is still quite massive due to gas accretion from the environment and the star is still growing significantly in mass via accretion, as in Class 1-2 phases (Machida et al., 2010; Eisner, 2012). We therefore assume that the star mass is $M_{\rm star} = 0.6 M_{\odot}$ while the disc mass is $0.3 \times M_{\rm star}$. Note that high mass tail of T Tauri discs, which occur much later, would also match this choice. The observational dissipation timescale for a circumstellar disc is of the order of Myr (Haisch et al., 2001), while the typical timescales for the evolution of clumps formed via GI is of the order of 10^5 yr (collapsing and migrating timescales, see the next sections). We can therefore safely neglect the time evolution of the disc. Due to this simplification, we can adopt a steady state disc as our background disc model, whose surface density profile Σ is given by the numerical solution of the

equation

$$\frac{\partial}{\partial a}\left[a^{1/2}\frac{\partial}{\partial a}\left(\nu\Sigma a^{1/2}\right)\right]=0 \tag{3.1}$$

as implied by the diffusion equation for a thin viscous disc in Lynden-Bell and Pringle (1974) when assuming $\partial\Sigma/\partial t = 0$. Figure 3.1 show the surface density and the Toomre parameter profiles obtained.

In the above equation $\nu = \nu_0 a$ is the viscosity of the gas. We assume that the radius of the disc is 150 au, the range often found in GI simulations (Mayer et al., 2002a; Rice et al., 2005; Boley et al., 2010). By fixing the total mass of the disc, the ratio K/ν_0 is determined, where K is a constant of integration. Hence the viscosity remains a free parameter only if the mass of the disc is specified.

In both sets, the initial semimajor axis a is assumed to be in the region where the Toomre parameter is near the minimum, where it is most likely that clumps have been formed (while the disc profile adjusts as the disc self-regulates no large radial excursions are seen in the location of the minimum Q as long as the physical conditions in the disc do not change, see eg Mayer et al. 2004). As it can be seen in figure 3.1, the latter region is between 80 au and 120 au. In the first set of clump initial conditions (hereafter IC) the initial mass $M_{\rm clp}$ and radius r of the clumps are taken to match typical values found in GI simulations (Boss, 2011; Galvagni et al., 2012): r is taken in $1.0 - 6.0$ au while $M_{\rm clp}$ lies in the range $0.5 - 5.0 M_J$. The mass range is consistent with (Boley et al., 2010), where it has been found that the typical mass of a fragment is nearly an order of magnitude lower than the local Toomre mass due to effects in the nonlinear regime of gravitational instability. A second set of more massive initial conditions (hereafter ICM) is generated. In ICM the clump mass is assumed to be in the range $5 - 12 M_J$, and the clump radius has been rescaled to $2 - 12$ au in order to have a similar initial density in the two sets of initial condition. This second more massive set is meant to include, in a very first approximation form, the possibility of multiple fragmentation followed by merges between the clumps. It is indeed still unclear if the outcome of GI is usually single or multiple clump formation. In the latter case, merges between the clumps are expected, as they are massive (gravitational focusing) and they form in a relatively small region. Moreover, this second set of more massive clumps is consistent with the initial conditions assumed in Vorobyov (2013) and Forgan and Rice (2013), or also with the masses of clumps formed in the earliest phases of protostellar disc evolution soon in the first few 10^4 years following the collapse of the molecular cloud core (Hayfield et al., 2011) , making comparisons with other works more feasible.

3.2.2. Clump contraction and migration

The fate of the clumps is determined from the competition between contraction and tidal disruption due to the presence of the central star, modulated by mass accretion and radial migration which affect contraction and disruption. The contraction/collapse timescale is assumed to be the time to reach SCC, as it is known that when a clump undergoes second core collapse its size shrinks and its density increases by order of magnitude (Masunaga et al., 1998), making it safe from tidal disruptions and therefore a real protoplanet. The tidal disruption timescale on the other hand will depend on the migration timescale of the clump, as it can be disrupted only if it gets close enough to the star that its radius becomes large enough that the outer part is no longer gravitationally bound to the clump.

In this work the contraction timescale to reach SCC is assumed to be the time needed for the dissociation parameter[1] in the inner part of the clump to reach 1 % [2]. We use the results presented in Galvagni et al. (2012) to determine the contracting timescale for each clump. Galvagni et al. (2012) present 3D high-resolution study of the collapse of a realistic clump formed via GI, also taking into account its initial rotation and non axisymmetric state. The timescales therein presented are therefore the more realistic ones currently available. This work shows that when a clump forms from the fragmentation of a spiral mode due to GI, it undergoes a rather fast phase (on the order of a few dynamical times) where the initial asymmetries lead to a redistribution of the angular momentum. After this phase, the clump becomes spherical and its contraction becomes constant, so that it becomes possible to extrapolate the evolution of the inner density and temperature, and therefore the contraction timescale.

Due to the presence of this first unstable phase, the clumps we generate as initial conditions are not the clumps that form just after fragmentation of the spiral mode, but a few dynamical times after that. In this way, it is possible to use the extrapolation results comfortably, which are obtained in the previous paper. Postponing the initial evolution time of the clumps leads to an uncertainty in the position of the clump in the disc, as it still undergoes migration in the very first phase we are neglecting. Nevertheless, as this neglected phase is fast, and as there already is an uncertainty on the initial semimajor position of the clump, we can safety assume that this procedure does not affect our results.

The main consequence of neglecting this initial phase is that the initial temperature and density of the clump have larger values than the ones usually observed in simulations for clumps formed into spirals. The initial values for density and temperature are calculated by rescaling the clump simulated in Galvagni et al. (2012) to fit the mass and radius of the new clump:

$$\rho' = \rho_0 \frac{M'}{M_0} \left(\frac{r_0}{r'}\right)^3 \tag{3.2}$$

$$T' = T_0 \frac{M'}{M_0} \frac{r_0}{r'} \tag{3.3}$$

with r_0, M_0, ρ_0 and T_0 the radius, mass, inner density and temperature of the clump in Galvagni et al. (2012) and r', M', ρ' and T' the values for the randomly generated clump. The first rescaling comes from the definition of density. The second rescaling comes from assuming that the ratio between gravitational and thermal energy stays constant between different clumps. Figure 3.2 presents the distribution of contracting timescales, initial inner temperature and density for the two set of clumps generated in this work (IC and ICM).

The derived collapsing timescale depends on the initial rotational status of the clump, and how it redistributes the internal angular momentum. However we can assume that the derived collapsing timescales are a safe overestimate. Indeed, the initial ratio between rotational and gravitational energy is $T/|W| = 0.15$ for the reference clump in Galvagni et al. (2012), but quickly increases during the first collapsing phase. Therefore, if the initial value were lower, it would mean that the clump were a very slow rotator, and the collapsing timescale would decrease. On the other hand, if the initial value of $T/|W|$ were higher, the strong rotational component would lead to the formation of a bar instability, which is a very effective structure for angular momentum

[1] The dissociation parameter is defined as the ratio between protons in the atomic form of hydrogen and the total number of protons in the gas.

[2] SCC is a non linear effect, with a strong back feeding component. When dissociation of hydrogen starts, the fast collapse locally increases the gas temperature, triggering dissociation in parts of the gas where it was still unactive. Dissociation parameter of 1 % is therefore a safe assumption with which treat all the clumps in SCC phase, as already discussed in Chapter 2

redistribution. Therefore, the angular momentum of the inner part of the clump would be transferred outwards, leading also in this case to a decrease of the collapsing timescale.

Once the clump forms in the outer part of a disc, it starts migrating due to the interaction with the disc. The migration characteristics are strictly related to the local disc properties; it is usually inwards, although it could be outward in some particular cases (Bate et al., 2003; Nayakshin and Lodato, 2012). In this work, we assume that the migration is inwards, following the result presented in Baruteau et al. (2011). Equation 3.4 describes the migration timescale for a clump in a similar mass and radius range as the one we study:

$$\tau = T_{\rm orb} 5.6(3.8-\sigma)^{-1}\gamma Q \left(\frac{q}{h^3}\right)^{-1} \left(\frac{h}{0.1}\right)^{-2} \tag{3.4}$$

with $\sigma = 1.3$ power of the density surface of the disc, $\gamma = 5/3$ adiabatic index, Q local Toomre parameter calculated from the disc profile, q ratio between clump and star mass, h disc aspect ratio. The inward migration is stopped when the clump reaches 0.01 au, as at that distance the magnetic field coming from the star prevents it from migrating even further in.

The contraction and migration timescales are both of the order of 10^4 years. This means they have comparable values and therefore we need to follow the evolution of each clump in the disc in order to predict its fate.

3.2.3. Tidal disruption

While the clump moves inwards, the outer part feels the gravitational interaction from the host star. If the clump gets close to it faster then it contracts, the outer part is stripped away. The distance at which this happens is usually assumed to be the distance at which Hill radius $R_h = a \times (M_{\rm cl}/(3M_{\rm star}))^{1/3}$ and clump radius are equal. We assume that the outer part of the clump is disrupted when its radius equals one third of the Hill radius. This factor of 1/3 arises when the rotation of the clump is taken into account, which makes it more prone to being disrupted. Boley A. C. and T. Hayfield (private communication) show that a typical clump formed in GI simulations is a fast rotator, and that the rotation affects how tightly bound it is by this factor. A similar factor has been found in the work of Zhu et al. (2012), where the clumps' radii are close to half the Hill radii. We choose to follow the factor 1/3 as it arises from 3D simulations, while the second study has been performed with 2D simulations.

When tidal disruption strips away the outer part of the clump, its mass is reduced accordingly. The contraction timescale will be affected by tidal stripping, although in which way this phenomena plays a role (increasing or decreasing it) is still unclear, as non linear effects happen. In this work, we assume that clump contraction proceeds according to the instant value for clump radius and mass; further analysis are currently under development. The tidal stripping makes the clump smaller, which leads to a larger migration timescale (see equation 3.4). The clump then slows down, so that it can have enough time to contract and to get out from the tidal-interaction disruption region. The clump therefore could survive a tidally downsizing phase.

3.2.4. Mass accretion

While the clump moves in the disc, it can accrete mass from the disc itself. In this work the mass accretion rate is calculated starting from equation (17) in Boley et al. (2010). In the latter,

nevertheless, the clump is in the outer part of the disc, so that when this formula is used in the inner region, where the disc gas density is larger by orders of magnitude, it leads to unphysically large mass accretion rates. In order to fix this, we assume that for every order of magnitude increase in Σ, the mass accretion rate increments by only of a factor of three, as has been described in Shabram and Boley (2013). The formula for the mass accretion rate then becomes:

$$\dot{M} = 1 \times 10^{-7} \times 3^{\log[\Sigma/\Sigma_{100}]} \left(\frac{M_{\rm cl}}{M_J}\right)^{2/3} \left(\frac{M_{\rm star}}{M_\odot}\right)^{-1/6} M_\odot/{\rm year} \tag{3.5}$$

with Σ_{100} surface density at $a = 100$ au. While the clump accretes mass, it radiates away the extra gravitational energy that comes from this accretion. If the timescale for the accretion is lower than the timescale to radiate this energy away, then the accretion gets stopped from the radiation pressure coming from the clump itself. The timescale over which the radiation happens is called the Kelvin Helmotz timescale, and can be evaluated as the ratio between the gravitational potential and the luminosity of the clump. If it is assumed that the clump radiates as a black body, the Kelvin Helmotz timescale is then

$$T_{KH} = \frac{U}{L} = \frac{GM_{\rm cl}^2}{4\pi\sigma_{SB}T^4 r^3} \tag{3.6}$$

with σ_{SB} the Stephan Boltzmann constant and T the mean temperature of the clump. If this timescale is longer then the accretion timescale $T_M = M_{\rm cl}/\dot{M}$, the mass accretion is stopped from the radiation pressure, and the mass accretion has an upper limit equal to $\dot{M}_{\rm max} = M_{\rm cl}/T_{KH}$. When the clump is at 0.01 au from the star, the mass accretion is zero, as at this location the disc has been cleared from the magnetic field of the star (Koenigl, 1991).

We compare the mass accretion rates found using this criteria with those presented by Nayakshin and Cha (2013), where the back-reaction of clumps onto the disc due to hydrodynamics feedback is analyzed. We find that the accretion rates are similar, as would be expected as the formulae we are using have been derived from simulations where gas cooling and radiative feedback are implemented.

When the clump accretes mass, its gravitational energy increases as well. In order to keep the ratio between gravitational and thermal energies constant, the clump radius increases accordingly. We can assume that this process happens isothermally by comparing the accretion and cooling luminosities. The accretion luminosity is given by $L_{\rm acc} = GM\dot{M}/R$, and has typical values on the order of 10^{30} erg/s. The cooling luminosity can be evaluated as the black body luminosity emitted by the clump $L_{cool} = 4\pi r^2 \sigma_{SB} T_{ps}^4$ where $T_{ps} = 2.7 \times 10^5 (v_{ff}/100)$ K is the post-shock temperature and v_{ff} gas free fall velocity in km/s. Typical values of the cooling luminosity are approximately 10^{41} erg/s. Such a large value of the L_{cool} compared to L_{acc} leads to a very loss of the heat generated by the accretion shock. As the clump temperature stays constant during this process, the radius rescales with the following rule:

$$r' = r + \delta r = r\left(1 + \frac{\delta M}{M_{\rm cl}}\right) \tag{3.7}$$

3.2.5. Gap opening

While the clump is migrating in the disc, it can open a gap if it is massive enough that the gravitational torques that it excerts on the disc overcome the local torque given from the disc

viscosity ν. In this work we adopt the gap opening criteria presented in Crida et al. (2006) and Kley and Nelson (2012):

$$\frac{3}{4}\frac{H(a)}{R_h} + \frac{50}{q\Re} \leq 1 \tag{3.8}$$

with $H(a)$ the local disc scale hight from vertical hydrostatic equilibrium condition $H(a) = c_s \times a/v_K$ (v_K local Keplerian velocity) and $\Re = a^2\Omega^2/\nu = (a^2\Omega)/(\alpha H(a)^2)$ Reynolds number (ω Keplerian angular velocity at a, α viscosity parameter). Although this result has been obtained for viscous discs, we adopt it also in a self-gravitating disc case.

When a gap is opened, the migration timescale becomes similar to the local viscous diffusion timescale (Lin and Papaloizou, 1986):

$$\tau_{\rm vis} = \frac{a^2}{\nu} \tag{3.9}$$

For a typical case of gap opening at 50 au, the local viscous diffusion timescale is between 10^5 yrs and 10^6 yrs, depending on the assumed viscosity value.

The mass accretion onto the clump is affected as well from the gap opening process. The local Σ decreases by a factor of 10 (cfr figure 1 in Crida et al. (2006)). We therefore assume that the mass accretion is the same one would have if the clump were embedded in a disc with this lower density surface. This is not completely correct, though, as it assumes that mass accretion would proceed in the same way even though the clump is not actually embedded in the disc gas now. Therefore, we run a second set of simulations, where mass accretion is completely stopped when the gap is opened. These two extreme cases give a lower and a higher limit on the final mass of the clump.

3.3. RESULTS

We create a set of 1000 clumps built with IC and 1000 clumps built with ICM and evolve each of them in four different scenarios: A,B,C and C_m0. Clump collapse, migration and tidal disruption are implemented in all these four configurations. The other physical mechanisms are implemented in different ways between the sets, in order to separate the effects of each of them on the clump evolution. Table 3.1 highlights the differences between the scenarios.

As there is no general consensus in the community about the value for the viscosity parameter α, scenario C is run for two different spatially and temporally uniform values: $\alpha = 0.05$ and $\alpha = 0.005$. This is considered to be a realistic range from simulations and model studies. Indeed, the results of circumstellar evolution models presented in Vorobyov and Basu (2009a,b) show that values of $\alpha \geq 0.1$ lead to the destruction of the disc in less then 1 Myr, incompatible with the observational data. Moreover, they show that values of $\alpha \geq 0.01$ manage to reproduce the mass accretion rate of gas onto young discs but decreases the change to have GI. Smaller values of α have been derived in studies which try to enligth the physical processes that generate turbulence; the study Nelson and Papaloizou (2004), for example, where turbulence is generated via ideal MHD, gives a value $\alpha = 7 \times 10^{-3}$. Our choice $\alpha = 0.05$ and $\alpha = 0.005$ is therefore chosen so as to explore all the range of possibilities. In the first case, the clumps are never able to open a gap; therefore the results from simulations C with $\alpha = 0.05$ are the same as simulation B (not shown). In the second implementation ($\alpha = 0.005$), mass accretion onto the clump when the gap opening criteria is fullfilled is implemented in the two limiting cases described in section 3.2.5. See table 3.1 for the details of the sets of simulations performed.

Table 3.2 shows the probabilities for the different outcomes of the clump evolution in the simulations sets: clump survival without undergoing tidal disruption, clump survival after being affected by tidal downsizing and clump disruption. It is also shown the probability of gap opening in scenario C. Figures from 3.3 to 3.5 show the distribution of final mass, radius and semimajor axis for the survived clumps. Figure 3.6 shows mass, radius and semi-major axis position of the clumps that are able to open a gap in scenario C. Figure 3.7 shows the evolution of two clumps (one from the set IC, one from ICM) in the four different scenarios.

We run the models until the protoplanet has reached the second collapse phase, so this is the time that we indicate as *final* from now on. From this point onwards the clump will collapse dynamically to a very small size, becoming virtually insensitive to tidal effects, but can in principle continue to accrete mass and will continue to migrate. However, to date there are no 3D numerical simulations exploring this late phase of the protoplanetary collapse based on which to construct a simple model and, furthermore, disc evolution, driven by accretion onto the star and irradiation/photoevaporation, should be accounted if we had to probe longer timescales. Therefore we decide to postpone the study of the late phase to a future work. However, in the discussion section we comment on the results of trial runs in which we have continued to evolve the protoplanets while neglecting disc evolution.

The survival rate is larger then 50 % in all cases. Survival of clumps without undergoing tidal downsizing is rare, and happens mainly when the gap opening is implemented. In this case moreover, the survival probability becomes higher, reaching 90 % in the case with massive initial conditions.

The final mass distribution depends both on the initial conditions chosen and the number of mechanisms that we take into account. When the gap opening is not implemented, indeed (scenario A and B) only small clumps manage to survive, as the larger ones have migration timescales very short and get disrupted. Clumps have masses up to $3M_J$ (with typical value of $1.5M_J$) for the initial condition IC and $5M_J$ (with typical value of $3M_J$) for initial condition ICM (with few exceptions). Once the gap opening is added, though, even more massive clumps can survive. Indeed gap opening is more likely to happen for massive clumps, and once the gap has been open the clump will be able to survive. This leads to a mass distribution spread up to $15M_J$ in the case with initial condition ICM, when the probability of a clump opening a gap is quite high (see table 3.2). Once the gap has been open, mass accretion is still possible in scenario C, while it has been stopped in scenario C_m0. These two different implementations do not significantly affect the final mass of the clumps, as the gap is opened in the external part of the disc, where mass accretion onto the clump is anyway insignificant.

The final distribution of the clump radius shows that only clumps that are able to collapse to very small objects can survive. Moreover, more massive clumps (ICM) need to collapse more than the low-mass ones (IC) to survive, as their Hill radii are shorter. The inclusion of gap opening prevents the disruption of some of the large clumps by preventing them from getting too close to the star. The final radius distribution shows that the typical final radius is of the order of tens of Jupiter radii, with the largest values found for those clumps which are able to open a gap, therefore never experiencing tidal disruption, and can be has high as $10^4 R_J$. This result is confident with what has been observed in Helled and Bodenheimer (2011): in this work only clumps in isolation were studied, which are comparable to our case of clumps that open a gap. The final radius that has been found is of the order $10^3 - 10^4 R_J$ also in their work. This result is not surprising, as SCC and the successive slow contraction still have to happen, and those processes are expected to reduce the radius by order of magnitudes.

Table 3.2.: Survival probability without tidal interaction (TD), survival probability after tidal interaction, disruption and gap-opening probability for the clumps in the eight different sets of simulation.

Set	IC				ICM			
	Surv	TD	Disr	Gap Open.	Surv	TD	Disr	Gap Open.
A	4 %	53 %	43 %	-	0 %	10 %	90 %	-
B	0 %	57 %	43 %	-	0 %	30 %	70 %	-
C	6 %	51 %	44 %	5 %	16 %	72 %	12 %	79 %
C_m0	6 %	51 %	44 %	5 %	16 %	72 %	12 %	79 %

The final semimajor axis distribution shows that survived clumps tend to sit very close to the star: almost all of them have a final semimajor axis inside 1 au from the star. When the initial clump is less massive (IC) it can sit also at larger distances (up to 75 au), while massive clumps always get very close to the star. This is due to the very short migration timescale for massive clumps. The inclusion of a gap opening helps the massive clumps to be retained at larger distances, between 25 and 75 au. Still, a significant fraction of the survived clumps (15 %) sit in a very inner orbit.

Figure 3.6 shows the mass, radius and semimajor axis of the clumps when they open a gap in scenario C for both the sets of initial conditions. The clumps that are able to open a gap are the more massive ones. The semimajor axis is between 25 and 70 au, making the formation of proto giant planets at these distances from the star possible.

3.4. Discussion

The results presented in this work represent a first step towards a more detailed model of the formation and evolution of clumps via GI. Despite the simple physics implemented, we can already conclude that GI appears to be a likely mechanism to explain the formation of gas giant planets. From the results presented it is possible to extrapolate some general behaviour:

- the survival rate for the light clumps is never lower than 50 %. In the case of massive initial conditions, the survival rate is very low (the miminum being 10 %) as long as gap opening is not taken into account. Once this is implemented survival rates are even higher than in the low mass case, as a more massive clump is more prone to open a gap and therefore survive (up to 88 % of surviving rate). This means that the probability of a clump formed via GI to become a proto-gas giant planet is quite high. Not only: the semi-major axis and mass distribution of the surviving clumps shows that these proto-planets are in the position and have the right mass to be considered in most cases the progenitors of Hot Jupiters.
- The inclusion of a gap opening affects the final fate of clumps only if the disc viscosity is low, $\alpha = 0.005$. Larger values, $\alpha = 0.05$, indeed, do not affect the clump evolution. If this is the case, we observe that the gap is always opened between 25 and 70 au. Once the gap is opened, the clump migrates on a viscous timescale. Moreover, a gap opening is easier for massive clumps, which are those more subject to being tidally destroyed. Combining these two factors together, the net result of including gap opening in a low viscosity disc is to create a population of survived clumps with high masses and further out in the disc.
- The simpler scenario A for light clumps and the gap opening scenarios (for both initial

conditions) shows that there is a (small) population of clumps which survives without ever undergoing a phase of tidal disruption. In the first case this happens as light clumps have large migration timescales, so they are able to reach SCC before they get close to the star, while in the second case the gap prevents some clumps from getting in the inner part of the disc.

- None of the clumps undergo tidal downsizing twice. If they survive the first downsizing, they will become small enough to have the contraction timescale win over the migration one.

This paper aims to give well physically motivated estimates for the evolution of clumps formed via GI by using the latest results from simulations and other works. Despite this, in most cases we had to include only a first order approximation of the physical mechanisms involved, partially for simplicity and partially because a complete description of some of these mechanisms is still missing. As an example, the contracting timescales derived herein are supposed to be a better estimates compared to the ones currently available, which derive from 1D collapse (Helled et al., 2006; Forgan and Rice, 2013). Once 3D asymmetries and angular momentum transport inside the clump itself are taken into account, indeed, the contraction is quicker than usually calculated. Nevertheless, improvements on these estimates are expected through a more detailed description of the physics involved in the collapsing phase. In particular, the inclusion of flux limited diffusion in the cooling routine is a natural improvement which is supposed to slow down the contraction. A detailed study of the inclusion of this effect (Galvagni et al. in preparation) nevertheless shows that this time increase is within one order of magnitude; we can therefore use the currently available timescale as a first approximation study. Moreover, there are some physical mechanisms which have not been taken into account and which could lead to a shortening of the contracting timescale. One case is the opacity evolution due to the chemical changes in the dust composition during the collapse, which have been shown to shorten the contracting timescale (Helled and Bodenheimer, 2011). The contracting timescale used herein can therefore be considered conservative.

The description of tidal downsizing is done as a first order approximation, neglecting effects due to the reaction of the clump to the tidal field. Nevertheless, the use of $R_h/3$ instead of the more common R_h as the maximum radius the clump can have before being tidally disrupted should take care of these second order effects, leading our work to more confident results. A more precise study of the dependence of the reducing factor of the Hill radius on the characteristics of the clump and of the local disc is currently under investigation. A more precise treatment of the tidal downsizing phase would impact mainly the clump radius evolution. Indeed, taking into account the heating which comes from the tides between the star and the clump would increase the clump radius. The final radius distribution for the survived clumps is therefore not completely trustable.

The clumps have been studied in isolation, as if each of them formed alone in the disc from the fragmentation of spiral modes induced from GI. From simulation studies (Boss, 2011; Vorobyov, 2013) and from the existence of multi-companion systems that could have formed via GI (Marois et al., 2010), it appears that the formation of two or more clumps at the same time is not rare. The study of the more massive set of initial condition ICM is meant to partially cover this scenario. Despite this, our study neglects the clump-clump interaction (in a similar way to what has been done for CA synthesis population studies), which could play a major role in determining the final population of survived clumps. It has to be noted, though, that in most simulations which show the formation of only two clumps, the spiral fragments at the opposite extremes, so that the reciprocal interaction of the clumps can be considered a second order effect.

One other effect that has being neglected in our study is photoevaporation from the star onto the clumps (Nayakshin and Lodato, 2012) once they reach the inner part of the disc. From our study, it appears that at that stage clumps are already dense enougth to be able to survive this phenomena, at least partially; nevertheless a consistent investigation of this effect needs to be included.

The inclusion of magnetic fields could also play a major role, as it is known that MRI influences the disc viscosity and surface density profile (Mohanty et al., 2013), which dominate the interaction between the clump and the disc. A detailed study of the dependence of the clump evolution on the disc structure is still needed.

The migration considered in this work is always inward migration. It is known (Bate et al., 2003; Baruteau et al., 2011) that migration of clumps is usually not smooth in one direction, and could even be outward. Nayakshin and Lodato (2012) relates the migration time to the mass evolution of the clump, with particular focus on the tidal downsizing phase. According to their findings, it is possible to have outward migration driven by mass loss. In the description given in this work of the tidal downsizing process though, the mass loss rate is quite slow (on the order of a few Jupiter masses per thousand years), so that the change in angular momentum due to this process is not able to significantly affect the migration rate.

In this study, core formation has been completely neglected, therefore we cannot make any quantitative predictions on the formation of rocky/icy planets through tidal downsizing. A comparison between the time that it takes for the clumps evolved in this study to be subjected to tidal downsizing and the temperature evolution of the core given in Forgan and Rice (2013) would show that, if the cores that form at the center of a clump were able to survive the tidal downsizing phase, they would for the most part be in the rocky state. The inner temperature would have overcome the critical value of 130 K far before tidal downsizing starts, due to the fast collapsing timescales assumed. A secondary effect of these fast timescales would be that the cores would be smaller that usually calculated (Forgan and Rice, 2013), as they have less time available to grow inside the pressure maxima of the clump.

Finally, as we have explained above, we stop running our models at the beginning of the phase of second core collapse, which starts no later than 10^5 yr after the initial time. Therefore, strictly we only make predictions for the properties of a population of protoplanetary clumps in the pre-dissociation phase. While tidal effects will cease to be important once the clump collapses dynamically to planetary sizes and densities, migration and accretion can still be important. We have run a subset of the clumps forward in time, finding that, irrespective of whether or not they are allowed to open a gap, in about a million years all the protoplanets end up at the inner boundary. This is nothing other than the *fast migration* problem encountered in population-synthesis models for planets forming via core-accetion (Alibert et al., 2005; Mordasini et al., 2012; Mordasini, 2013).

Therefore, in disc instability, as well as in core-accretion, one needs to invoke a suppression of migration or some stochastic effects that lead to a variable direction of migration, with some clumps moving outwards rather than inwards. That the latter can happen is suggested by numerical simulations of fragmenting discs in which multiple clumps form (Durisen et al., 2007b; Boley et al., 2010; Boss, 2011). Additionally, if the gas disc is rapidly dissipated, dynamical scattering of protoplanets can lead to fast rearrangement of their orbits, accompanied by mass segregation (Papaloizou and Terquem, 2001).

3.5. Conclusions

The study presented herein aims to understand the fate of clumps formed via GI in circumstellar discs. In order to do that, we studied the evolution of a set of clumps, one at a time, coupling their contraction with the interaction with the disc and the central star. We performed four sets of simulations, in order to add mass accretion and gap opening (for both a low and a high viscosity disc) step by step.

Our results show that a large fraction of the clumps survives, contrary to previous claims in the literature.

The higher surviving fraction is due to the fast collapse timescales in the dissociation phase. Most importatly, such a fast collapse timescale is estimated for the first time based on the results of 3D hydro collapse simulations (Galvagni et al., 2012, and Galvagni et al. in prep.). Furthermore, most of the clumps formed via GI could in principle be precursors of Hot Jupiters.

Taken at face-value, the chance that they are the progenitors of massive gas giant planets at distances between 20 and 75 au from the star is not negligible as well. However, a naive extension of our models beyond the pre-dissociation phase leads to the prediction that all clumps must become Hot Jupiters or be engulfed by their host star since migration timescales are always shorter than 1 Myr, no matter whether or not gap opening takes place. This reflects the same problem found in core-accretion: migration has to be much slower or be somehow stochastic, with inward-directed migration being only one of the possibilities, in order to be consistent with the wide range of semi-major axis found among the exoplanet population. Alternatively, disc dissipation has to be faster than the migration time so that protoplanets can stop migrating sooner and undergo gravitational scattering that redistributes their orbits.

The physical mechanism that seems to play a major role in shaping the properties of the population of clumps until the pre-dissociation phase is gap opening. The efficiency of gap opening is strongly tied with disc viscosity in turn. For a low viscosity disc the survival probability for the clumps approaches 50 % for low mass clumps and 90 % for massive ones. In reality, disc viscosity will be spatially and time dependent, likely transitioning from a high viscosity state soon after fragmentation has taken place (when the disc is still unstable and therefore gravitoturbulent) to a lower viscosity state in which gap opening will be effective. Models incorporating disc evolution and a more realistic prescription for viscosity will have to be investigated in the future.

In summary, our results show that GI can in principle produce a large fraction of the population of present-day gas giants, including Hot Jupiters, as much as CA. Yet problems associated with excessive migration occur here as they do in CA. While clumps form at much larger radii than cores in the core-accretion model, and hence have a larger distance to cover before they reach the inner disc, they also have more time to do so since GI is expected to happen early in disc evolution. Future studies will have to elucidate the role of the migration of clumps in long-term simulations in order to construct a more realistic model for the orbital evolution of clumps relative to what we have done here.

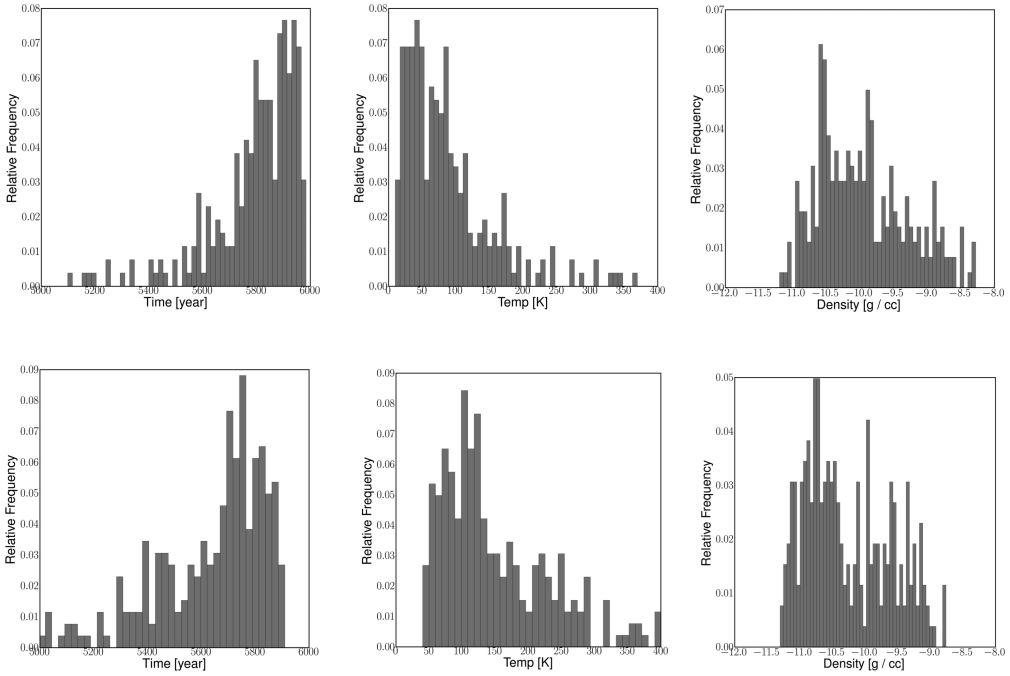

Figure 3.2.: Histograms of the initial conditions for the clumps in the set IC (on the top) and ICM (on the bottom). For each line: on the left, histogram of the contracting timescale for the clumps evolved; in the middle and on the right, respectively, histogram of the inner temperature and density (in log scale).

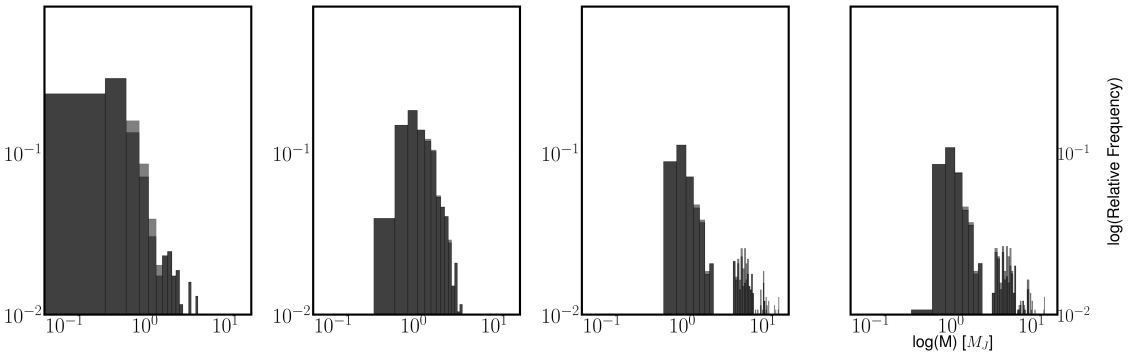

Figure 3.3.: Histograms of the final mass distribution for surviving clumps (in M_J units). From left to right: scenario A,B,C and C_m0. In black, clumps that survive after tidal downsizing. In grey, clumps than never undergo tidal downsizing.

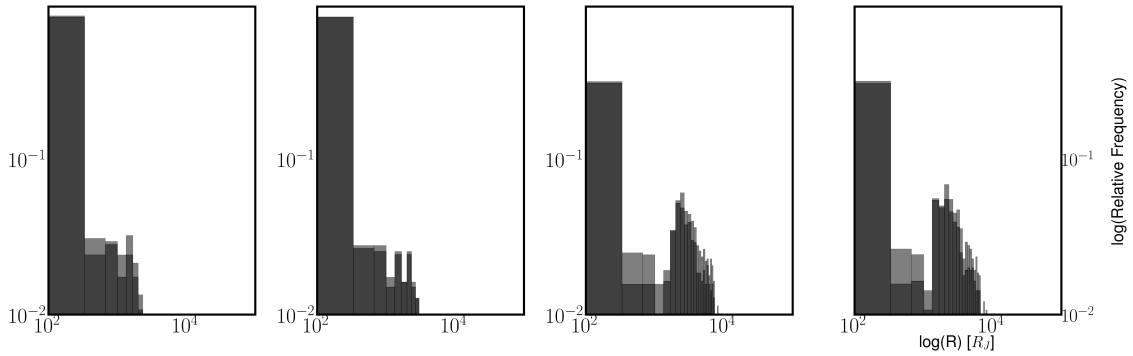

Figure 3.4.: Histograms of the final radius distribution for surviving clumps (in R_J units). From left to right: scenario A,B,C and C_m0. In black, clumps that survive after tidal downsizing. In grey, clumps than never undergo tidal downsizing.

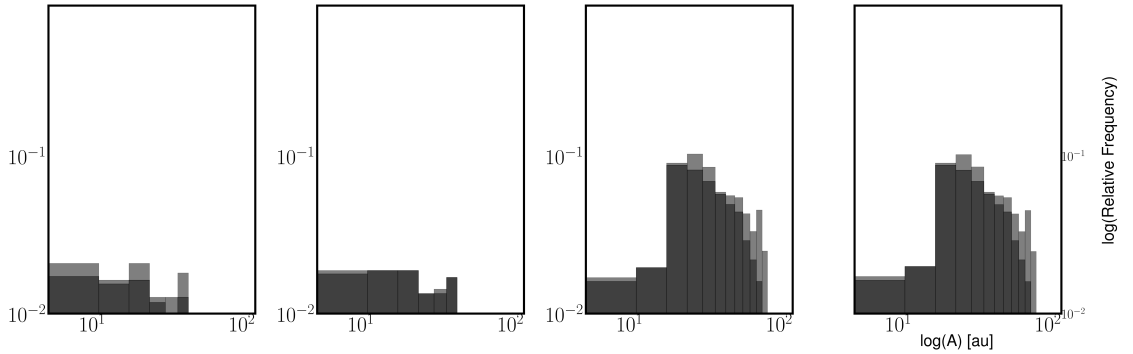

Figure 3.5.: Histograms of the final semimajor axis distribution for surviving clumps (in au units). From left to right: scenario A,B,C and C_m0. In black, clumps that survive after tidal downsizing. In grey, clumps than never undergo tidal downsizing.

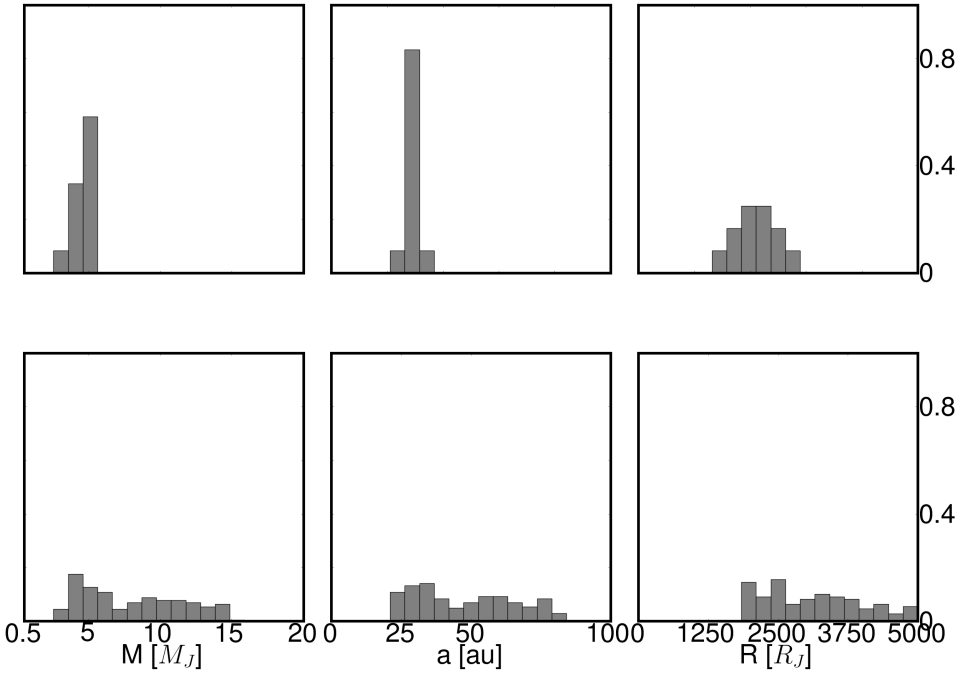

Figure 3.6.: Histograms of (from left to right) the mass (in M_J units), semimajor axis (in au units) and clump radius (in R_J units) for the clumps when they open a gap in the disc in scenario C with $\alpha = 0.005$. On the top: initial condition IC. On the bottom: initial condition ICM

.

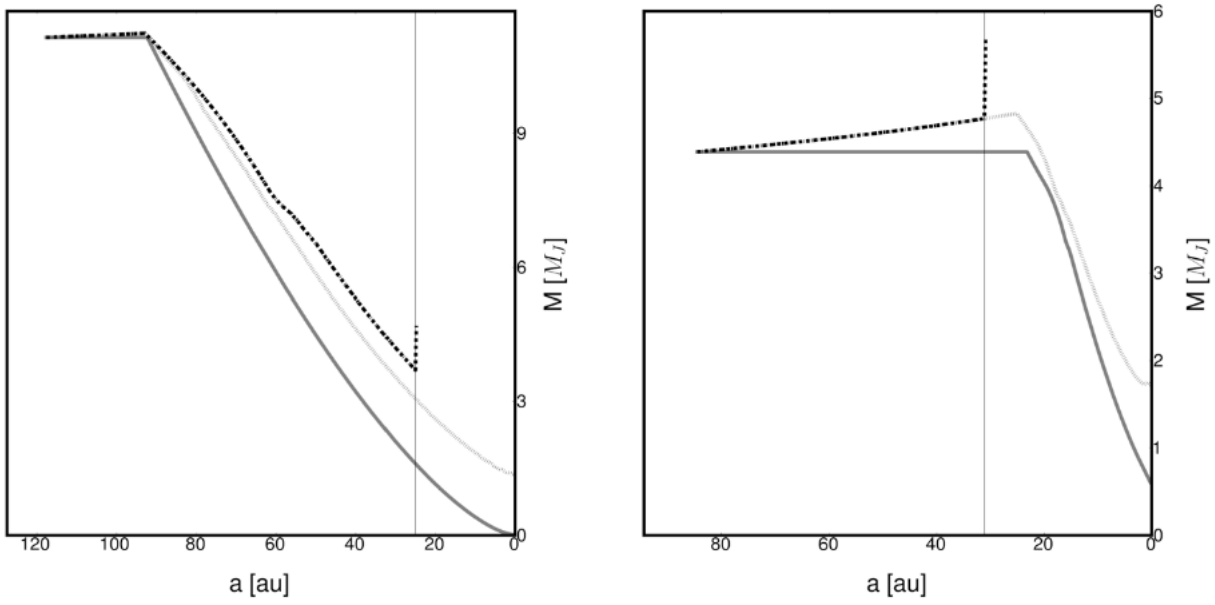

Figure 3.7.: Evolution of the clump mass as a function of semimajor axis. On the left, one clump from the initial condition set IC, on the right one clump from the initial condition set ICM. The lines represent scenario A (solid gray line), scenario B (dashed gray line) and scenario C with $\alpha = 0.005$ with (dashed black line) and without (dashed black line) mass accretion during gap opening. Units are Jupiter masses and au.

4. A Grain Growth model with a 3D probability distribution function for collisional velocity

This chapter is based on the following proceeding and publications:
1) M. Galvagni[1], P. Garaud [2], C. Olczak[345] and F. Meru[67]. **Improving the grain growth model in the outer part of a circumstellar disc**. Proceeding of ISIMA 2011 summer school.
2) P. Garaud [2], F. Meru[67], M. Galvagni[1] and C. Olczak[345] **From dust to planetesimals: an improved model for collisional growth in protoplanetary disks**. The Astrophysical Journal (2013), Vol:764, art. id:146.
3) F. Meru[67], M. Galvagni[1] and C. Olczak[345] **Growth of grains in brown dwarf discs**. Accepted for publication in Astrophysical Journal Letters.

Abstract

Observations of circumstellar discs and theoretical models for fragmentation and coagulation of grains show some inconsistencies. Among the most important ones, there is the meter size problem (and the physically equivalent millimeter size problem), which consists of the failure to grow 1 mm size objects at 1 au around a solar-type star, and the observational evidence of the presence of a long standing population of small size particles. In this work we present a new theoretical model for coagulation and fragmentation of grains. The main novelty of our study is the inclusion of a three-dimensional probabilistic treatment for the collisional velocity: the collisional velocity is no longer considered as a single value, but a probability distribution function peaked around the most probable one. This simple and natural improvement in the physical description of the collisions leads to surprisingly strong results. Not only are grain particles able to growth large enough to overcome the meter size problem, but also our simulations show the development of a two particle population, predicting therefore the existence of a small grain population that lasts with time, in accordance with the observational results.

4.1. Introduction

Planets are born in circumstellar discs typically found around young stars, which form from the collapse of a molecular cloud core. Circumstellar discs are made up of two components: gas and

[1]Institute of Theoretical Physics, University of Zürich,Winterthurerstrasse 190, 8057 Zurich, Switzerland
[2]Department of Applied Mathematics and Statistics, UC Santa Cruz, 1156 High Street Santa Cruz
[3]Astronomisches Rechen-Institute (ARI), Zentrum für Astronomie Universit ä t Heidelberg, M önchhofstrasse 12-14, 69120 Heidelberg, Germany
[4]Max-Plank-Institute fü r Astronomie (MPIA), Königstuhl 17, 69117 Heidelberg, Germany
[5]National Astronomical Observatiories in China, Chinese Academy of Sciences (NAOC/CAS), 20A Datun Lu, Chaoyang District, Beijing 100012, China
[8]Institute für Astronomie und Astrophysik, Universität Tübingen, Auf der Morgenstelle 10, 72076 Tübingen, Germany
[7]Institute für Astronomie, ETH Zürich, Wolfgana-Pauli-Strasse 27, 8093 Zürich, Switzerland

dust. Observations have shown that in the outer parts of discs, grain sizes can reach values as large as millimeter or even centimeter (Wilner et al., 2005). This is in contrast to theoretical predictions for the collisional growth of grains, which struggle to produce grains of these dimensions at large distances (Dullemond and Dominik, 2005). Furthermore, even if they were able to grow to this size, they would be rapidly lost due to radial drift. Indeed as a particle is growing, it must pass through a phase where its radial velocity component is a large fraction of its orbital speed (Weidenschilling, 1977), making it rush towards the central star in 10-100 orbital times. Therefore, it is possible to retain particles and form even larger ones only if coagulation is very efficient. This issue is usually referred to as the mm size problem at 100 au, physically equivalent to the more familiar meter size problem at 1 au.

Observations of circumstellar discs also bring a second issue for grain growth models: the long standing existence of a population of small grains (Kessler-Silacci, 2006; Furlan et al., 2009; Oliveira et al., 2010). This feature cannot be explained with a model of coagulation of grains only. The first way to overcome this issue has therefore been the inclusion of a fragmentation description in the model Dullemond and Dominik (2005). This new degree of freedom though, introduces a second growth barrier: it gets very difficult for the grain particles to grow to sizes comparable to the observed ones once fragmentation is included, as has been pointed out by Birnstiel (2011).

A number of ideas have been proposed to overcome one or both those barriers. In the recent publication Windmark et al. (2012a) the importance of a bouncing region for keeping a reservoir of small size particles has been explored; these small grains not only would explain the observations of their long standing population, but would also enhance the formation of large particles by providing a reservoir of small grains that can be swept up by a few large bodies. Pinilla et al, in Pinilla et al. (2012) study how the existence of local pressure maxima can provide a mechanism to locally stop radial drift and therefore solve the first growth barrier. In this work we present a probabilistic treatment of the collisional velocity, which has been developed during the ISIMA 2011 summer school and presented in its proceeding Galvagni et al. (2011), and further developed in the publications Garaud et al. (2013) and Meru et al.. To our knowledge, the first work to introduce a probabilistic treatment for the collisional velocity was presented by Okuzumi et al. (Okuzumi et al., 2011), although they only concentrated on very small particles, with brownian motion and a mean drift being the only source of collision. In the present work we take into account a wider range of physical phenomena that are characteristic for collisions of larger particles. In the work of Windmark et al. (Windmark et al., 2012b) a very similar probabilistic treatment has been proposed and presented in an independent way, although a comparison between our approaches pointed out a mathematical error on their side.

4.2. METHODS

The model

The evolution of the circumstellar disc is dominated by the gas, as this component dominates the total mass. The theory which describes the structure and evolution of gas discs was developed in 1974 by Lynden-Bell and Pringle (Lynden-Bell and Pringle, 1974); they derived the radial velocity of the gas u due to mass and angular momentum conservation inside a viscous disc with viscosity ν:

$$u(r) = -\frac{3}{\Sigma\sqrt{r}}\frac{\partial}{\partial r}\left(\Sigma\nu\sqrt{r}\right) \tag{4.1}$$

where r is the radius and Σ gas surface density. This quantity can be evaluated starting from the mass conservation equation and vertically integrating it:

$$\frac{\partial \Sigma}{\partial t} + \frac{1}{r}\frac{\partial}{\partial r}\left(r\Sigma u\right) = 0 \tag{4.2}$$

This equation admits self similar solutions:

$$\Sigma(r,t) = \frac{M_{disc}}{2\pi r R_0 T^{3/2}} \exp\left(-r/R_0 T\right) \tag{4.3}$$

with M_{disc} is the initial disc mass, R_0 the initial disc radius, $T = t/\tau_\nu + 1$, where $\tau_\nu = R_0^2/3\nu_t(R_0)$ is the viscous spreading time (the viscosity is $\nu_t(r)$).

There are five fundamental physical mechanisms that determine the velocity of dust particles: radial drift, azimuthal velocity, turbulence, vertical settling and brownian motion. The dominant mechanism depends on the particle size (eg, brownian motion dominates the collisions of very small particles, while turbulence is most important if the grains have very different sizes).

The gas component feels the pressure, while dust grains don't. This implies that gas settles in a sub-keplerian orbit, while the grains tend to settle into keplerian orbits. This difference between the two components generates a head-on wind on the grains, which will make them lose part of their angular momentum and drift inward in the disc. This process is called radial drift, and depends on the coupling between the gas and dust components: a small grain will travel with the gas speed, while a large grain will settle into a keplerian orbit, as the head on wind can be neglected. The velocity of collisions generated by radial drift is the difference between the velocities given by

$$v_R(s) = \left(u - 2\eta\tau\Omega\frac{\rho_0}{\rho}\right) / \left[1 + \left(\rho_0\tau\Omega/\rho\right)^2\right] \tag{4.4}$$

with ρ being the gas density, $\tau = \left(\rho(s)s\right)/\left(c\rho_0\right)$ the stopping time of the particle, with $\rho(s)$, s the density and size of the particle, c the local sound speed, $\rho_0 = 1g/cm^3$, $\Omega = \sqrt{(GM_{star})/r^3}$ the keplerian frequency and $\eta = -\frac{c^2}{\Omega\rho}\frac{\partial\rho}{\partial r}$. The stopping time gives an idea of the influence of the gas pressure on the grains, and depends mainly on the grain size and the gas density.

The azimuthal collisional velocity, in a similar way, is given by the difference between the azimuthal velocities of the two particles, given by

$$v_A(s) = \frac{1}{S}\left(v_R(s) - u\right) \tag{4.5}$$

The relative velocities of particles induced by their interactions with turbulent eddies were calculated by Ormel and Cuzzi (2007) and depends on the ratio of the particle stopping time with the eddy turnover time:

$$\Delta v_T(s_i, s_j) = \begin{cases} \left[\frac{[\tau(s)-\tau(s')]^2}{\tau_d[\tau(s)-\tau(s')]}\right]^{1/2} v_e & \text{if } \tau(s),\tau(s') \leq \tau_\nu \\ v_e & \text{if } \tau(s') \leq \tau_d \leq \tau(s) \\ \left[\frac{\tau_d}{\tau_d+\tau(s)} + \frac{\tau_d}{\tau_d+\tau(s')}\right] v_e & \text{if } \tau_d \leq \tau(s), \tau(s') \\ \frac{3}{\tau(s)+\tau(s')}\left(\frac{max(\tau(s),\tau(s'))}{\tau_d}\right)^{1/2} v_e & \text{otherwise} \end{cases} \tag{4.6}$$

where $v_e \simeq \sqrt{\alpha}c$ is the velocity for the smaller eddy, $\tau_d = \sqrt{GM(<r)/r^3}$ is the dynamical timescale of the disc and $\tau_\nu = \tau_d Re^{-1}$ is the dissipation timescale of the disc, with $Re \simeq 10^{14}$ Reynold number for a viscous disc. Heuristically, this can be interpreted in the following way: the first case corresponds to two small particles both being trapped within the smallest eddy, so highly affected by the turbulence. In the second case, one of the particles is larger and its motion is still affected by the eddies, but no longer dominated by them, while the second particle is. In the third case, both particles have large enough stopping times to be just slightly influenced by the turbulence. The fourth case covers all the other possibilities (eg, one particle is no longer inside the smaller eddy, but has not yet decoupled from the turbulence).

The vertical settling velocity describes the velocity acquired by the particles that are above the midplane while they fall on it. In this case we adopt the same scheme as in Birnstiel (2011):

$$v_S(s) = \min(0.5, \tau(s)/\tau_d) h(r) \min\left(1.0, \sqrt{\frac{\alpha}{(1+(\tau(s)/\tau_d)^2)\min(0.5, \tau(s)/\tau_d)}}\right)\Omega \tag{4.7}$$

where Ω is the Keplerian angular velocity. The relative settling velocity generating the colliding velocity is simply $\Delta v_S(s, s') = v_S(s) - v_S(s')$.

The brownian motion gives relative velocities:

$$\Delta v_B(s, s') = \sqrt{8 k_B \frac{m(s) + m(s')}{\pi m(s) m(s')}} \tag{4.8}$$

where k_B is the Boltzmann constant. Using these equations, we visualize the relative collision velocity of two particles over a range of sizes.

4.2.1. Coagulation - Fragmentation solver

There are three main scenarios from the interactions between dust particles: coagulation, fragmentation or bouncing. The combination of all these encounters determines the evolution of the grain size distribution. Mathematically, these can be modelled by the standard Smoluchowski coagulation/fragmentation equations (Smoluchowski, 1916), which, for $i = 1..N$, has the form:

$$\frac{dN_i}{dt} = \frac{1}{2}\sum_{j,k=1}^{N} C_{jki} N_j N_k - \sum_{j=1}^{N} K_{ij} N_i N_j + \frac{1}{2}\sum_{j,k=1}^{N} F_{jk} N_j N_k N_{ijk}^f - \sum_{j=1}^{N} F_{ij} N_i N_j \tag{4.9}$$

where N_i is the number density of particles of mass m_i. The first two terms represent the coagulation part, the latter two the fragmentation. As we are following the evolution of particles for several orders of magnitude in mass density, it is necessary from a numerical point of view to use a log-spaced mass range distribution. This implies that, given two particles m_i and m_j, the particle resulting from their coagulation will have mass $m_k = m_i + m_j$ which usually falls between two points of the particle mass: $m_{k-} < m_i + m_j < m_{k+}$. It is therefore necessary that a solver assigns part of this mass to the two nearest mass mesh points in a consistent way. This is the origin of the C_{ijk} term, which is defined as in Brauer et al. (2008)

$$C_{ijk} = \begin{cases} p_{ij} & \text{if } k = k- \\ (1-p_{ij}) & \text{if } k = k+ \\ 0 & \text{otherwise} \end{cases} \tag{4.10}$$

with

$$p_{ij} = \frac{m_{k+} - (m_i + m_j)}{m_{k+} - m_{k-}} \tag{4.11}$$

K_{ij} and F_{ij} are the coagulation and fragmentation kernel, so the probability that particle i and j coagulate/fragment into particle k as a result of a collision. The second and fourth terms of equation 4.9 represent how particles i and j disappear after collision: either because of coagulation (second term) or because of fragmentation (fourth term). The coagulation/fragmentation kernels are given by the product between the mean collisional cross section $A_{ij} = \pi(s_i + s_j)^2$, the collisional velocity Δv_{ij} and the coagulation/fragmentation efficiency ϵ^c_{ij} and ϵ^f_{ij}:

$$K_{ij} = A_{ij}\Delta v_{ij}\epsilon^c_{ij} \tag{4.12}$$

$$F_{ij} = A_{ij}\Delta v_{ij}\epsilon^f_{ij} \tag{4.13}$$

The third term represents the number density of particles m_i which are generated by fragmentation due to the collision of particles m_j and m_k, when $m_i < m_j + m_k$. Once two particles collide and fragment, we assume that the number density of the generated fragments follow a power law with index $\epsilon = 1.83$, as given by laboratory experiments (Mathis et al., 1977; Draine and Lee, 1984). Therefore, the term in equation 4.9 becomes

$$N^f_{ijk} = a_{jk} m_i^{1-\epsilon} \theta(M - i) \tag{4.14}$$

with a_{jk} the normalization factor, $\theta(M - i)$ the discrete Heaviside function and M index of the largest generated fragment.

Tests

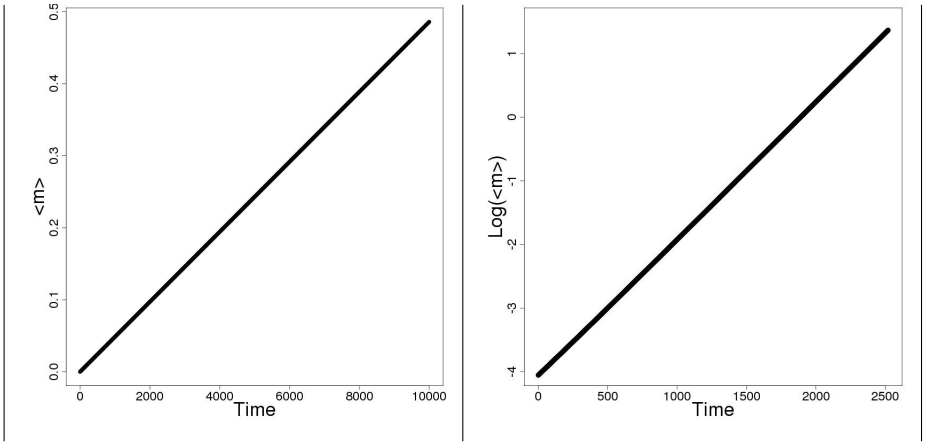

Figure 4.1.: Time evolution of the grain mean mass ¡m¿ in the two test cases presented: constant kernel (on the left) and linear kernel (on the right). The y-axis of the right plot is in log scale.

The integrator solver designed for this problem has been tested. Here we report two of the tests that have been done, following the ones presented in Ormel's PhD thesis (Ormel, 2008).

Constant Kernel

Assume that the initial condition is a monodisperse grain mass distribution, with mass m_0. Assume that the kernel is constant, so that

$$\frac{dN_i}{dt} = K \tag{4.15}$$

From this equation, the evolution of the mean grain mass is simply given by

$$< m >= m_0(1 + 2t) \tag{4.16}$$

Linear Kernel

In a similar way as before, assume that the initial condition is a monodisperse grain mass distribution, with mass m_0. This time, the kernel is taken to be linear:

$$\frac{dN_i}{dt} = m_i + m_j \tag{4.17}$$

The solution is given by an exponential increase of the mean mass:

$$< m >= m_0 \exp(t/2) \tag{4.18}$$

Figure 4.1 shows the results for the two tests. The grain mean mass evolves as predicted by the analytic results.

The reference Model

Once the numerical model has been set, we need the information about the outcome of the collisions to feed the kernels. For this reason, a number of laboratory experiments (Blum and Wurm, 2008; Blum, 2010) and simulations have been performed. The results of these experiments have been recently implemented in numerical models simulating the evolution of the grain size distribution in a circumstellar disc. In this work we will call *Brauer model* the model implemented in a work by Brauer (Brauer et al., 2008) and we will use it as a reference. This scheme includes only fragmentation and coagulation, but ignores cratering[1]. Given a critical fragmentation velocity $v_f = 30$ m/s, the fragmentation efficiency ϵ_f is assumed to be

$$\epsilon_{ij}^f(\Delta v_{ij}) = \left(\frac{\Delta v_{ij}}{v_f}\right)^{\psi} \Theta(vf - \Delta v_{ij}) + \Theta(\Delta v_{ij} - vf) \tag{4.19}$$

with $\psi = 1$ and Δv_{ij} the colliding velocity for particles i and j, assumed to be the largest between the five possible colliding velocities. The coagulation probability in this scheme is $\epsilon_{ij}^c = 1 - \epsilon_f$. Fig. 4.3 shows the coagulation and fragmentation probabilities given a critical fragmentation velocity $v_f = 30$ m/s. Note that for relative velocities larger than the critical value, the coagulation probability is always zero. This means that once the particles have grown large enough that collisional velocities are always larger than this threshold, it is impossible for

[1] When a small particle collides with a larger one, a possible outcome which has been observed in laboratory experiments is that the small particle craves the surface of the larger one. This sort of partial fragmentation has been defined as cratering.

them to grow further and only fragmentation can happen. This means that this prescription causes the so-called fragmentation barrier.

Laboratory experiments show the existence of a bouncing region between the collisional and fragmenting ones. The inclusion of this phenomena in our model is straightforward, by assuming that the critical velocity at which fragmentation starts is larger, and not equal, to the critical velocity at which coagulation stops, which can be defined as the bouncing velocity v_c. The equation for the fragmentation efficiency will not change, while the equation for the coagulation efficiency becomes

$$\epsilon_{ij}^{c}(\Delta v_{ij}) = \Theta(v_c - \Delta vij) - \left(\frac{\Delta v_{ij}}{v_c}\right)^{\psi} \Theta(vb - \Delta v_{ij}) \tag{4.20}$$

The Tail Model

In this work we present an alternative model for the representation of the collisional velocity. We will hereafter refer to this alternative scheme with the name Tail model. Let us assume that the fragmentation probability function is a step function, with value 1 for relative velocities larger than v_f and 0 in the other case. The relative collisional velocity is usually assumed to be a fixed value; the largest between the values that are generated in the different mechanisms that lead to collisions. A more physically correct approach must take into account all the collisional velocities at the same time. As it is not possible to know the exact angle between the different velocity components, neither can we assume that the relative velocities have no error given by local peculiarities, it looks more physically motivated to use a probability distribution function (pdf) instead of a single value for the collisional velocity. We choose a Maxwellian as the velocity pdf, peaked at the most probable collisional velocity:

$$\Delta v = \sqrt{(\Delta v_R)^2 + (\Delta v_A)^2 + (\Delta v_T)^2 + (\Delta v_B)^2 + (\Delta v_S)^2} \tag{4.21}$$

We take into account that the relative velocity of colliding particles is not fixed by Eq.s 4.4 - 4.8, but follows a Maxwellian distribution peaked at the value determined by these equations.

The coagulation/fragmentation kernel formulae need to be changed accordingly. If we rewrite equation 4.12 in the integral form, and take into account the velocity pdf $p(\Delta v_{ij})$, the new kernels will be given by

$$K_{ij} = A_{ij} \int_0^{\infty} \Delta v_{ij} p(\Delta v_{ij}) \epsilon_{ij}^{c} d(\Delta v_{ij}) \tag{4.22}$$

$$F_{ij} = A_{ij} \int_0^{\infty} \Delta v_{ij} p(\Delta v_{ij}) \epsilon_{ij}^{f} d(\Delta v_{ij}) \tag{4.23}$$

So, it is possible to return to the standard formulation expressed in 4.12 by substituting the efficiency with a mean value:

$$\bar{\epsilon}_{ij}^{c} = \frac{\int_0^{\infty} \Delta v_{ij} p(\Delta v_{ij}) \epsilon_{ij}^{c} d(\Delta v_{ij})}{\int_0^{\infty} \Delta v_{ij} p(\Delta v_{ij}) d(\Delta v_{ij})} \tag{4.24}$$

and an equivalent formulation for the fragmenting efficiency. The efficiency ϵ_{ij}^{c} and ϵ_{ij}^{f} are assumed to be Heaviside functions, with $\epsilon_{ij}^{c} = \Theta(v_c - v)$ and $\epsilon_{ij}^{f} = \Theta(v - v_f)$.

Table 4.1.: Table of the simulations' properties: model used, bouncing velocity v_c, fragmenting velocity v_f and mass transfer size ratio s_c (when applied).

Sim	Model	v_c [m/s]	v_f [m/s]	Mass Transfer
Br	Brauer	30.0	30.0	–
$\mathrm{Br_{b1}}$	Brauer	30.0	50.0	–
$\mathrm{Br_{b2}}$	Brauer	30.0	50.0	–
$\mathrm{Br_{mt}}$	Brauer	30.0	30.0	100
T	Tail	30.0	30.0	–
$\mathrm{T_{b1}}$	Tail	30.0	50.0	–
$\mathrm{T_{b2}}$	Tail	30.0	100.0	–
$\mathrm{T_{mt}}$	Tail	30.0	30.0	100

It is possible to solve the equation for the new coagulation efficiency via a simple integration; we therefore obtain

$$\bar{\epsilon}^c_{ij} = 1 - \left[\left(\frac{v_c}{\sigma_{ij}}\right)^2 + 1\right] e^{-v_c^2/2\sigma_{ij}^2} \tag{4.25}$$

with $\sigma_{ij} = \sqrt{\pi}\Delta v_{ij}/4$. With a similar procedure, the new fragmenting efficiency is

$$\bar{\epsilon}^f_{ij} = \left[\left(\frac{v_f}{\sigma_{ij}}\right)^2 + 1\right] e^{-v_f^2/2\sigma_{ij}^2} \tag{4.26}$$

Note that in this scheme the coagulation efficiency is never zero, and for large velocities behaves like $\propto \Delta v^{-4}$; this implies that there is no theoretical maximum size for successful coagulation, only the probability gets very low. Note also that, if one assumes $v_f = v_c$, then $\epsilon_f + \epsilon_c = 1$; if instead $v_c < v_f$ there is a region where $\epsilon_f + \epsilon_c < 1$ which naturally defines a bouncing region. In figure 4.4 we show the coagulation and fragmentation efficiency for the Tail model with and without bouncing.

Finally, recent laboratory experiments (Blum, 2010) show that collisions of porous dust aggregates on compact objects reveal a second coagulation regime beyond the bouncing region (in velocity space), so that in high-velocity encounters, fragmentation does not occur. This phenomena is called mass transfer. We have implemented it into the Tail model by imposing that the coagulation efficiency is one for size ratios larger than a critical value s_c, which is assumed to be 100 in this work. We can safely assume this value as in the work by Garaud et al. (Garaud et al., 2013). It is shown that the actual value of this parameter doesn't play a major role in the evolution outcome.

In Fig. 4.5 we compare the coagulation efficiencies that are determined implementing the different models presented in this section.

4.3. RESULTS

This section presents the results of our simulations. We studied the evolution of the grain size distribution at $r = 100$ AU for a T Tauri disc using different coagulation-fragmentation schemes. Table 4.1 summarizes the parameters for the simulations presented.

4.3.1. Initial conditions

The initial grain size distribution is assumed to be a Gaussian, peaked at $s = 10\mu$m, a typical value found for the grains in the interstellar medium. More simulations (not shown here) show that the grain size distribution converges to the same shape within a few hundreds years regardless of the initial distribution. The circumstellar disc is assumed to have a time-invariant surface density profile, which has a radial dependence:

$$\Sigma(r) = \frac{M_{disc}}{2\pi R_0 r} \tag{4.27}$$

Here we focus on the outer disc at $r = 100$ au. Our disc parameters are those observationally determined for the TW Hydrae disc (Wilner et al., 2005): $M_{\rm star} = 0.8 M_\odot$, $M_{\rm disc} = 0.1 M_{\rm star}$, $R_0 = 200$au, $\alpha = 0.01$ and $\mathrm{Re} = 10^{14}$. We selected this disc as it presents both the features that theory is failing to explainn: observational data indeed show the presence of millimeter and centimeter sized particles in the outer part of the disc, and the existence of a double peaked grains population.

4.3.2. The simulations

We perform four simulations with the Brauer model. The first one, the reference model, reproduces the model presented in (Brauer et al., 2008). The second and third simulations implement the Brauer model with a bouncing regime (for two different values for the fragmenting velocity). Lastly, the fourth simulation presents the Brauer model with mass transfer. We assume $v_c = 30$ m/s, the same value as Brauer's study (Brauer et al., 2008), in order to be able to make a comparison with their results. The results for the grain size evolution are presented in figure 4.6.

We perform four simulations with different versions of the Tail model. In the simplest configuration T, there is no bouncing nor second coagulation regime. Simulations $\mathrm{T_{b1}}$ and $\mathrm{T_{b2}}$ introduce the bouncing regime by sequentially increasing the critical fragmenting velocity. Last, simulation $\mathrm{T_{mt}}$ implement the mass transfer. The results are shown in figure 4.6.

4.3.3. Discussion

The results for the Brauer model simulations are in agreement with what has been found in Brauer's work (Brauer et al., 2008): the size distribution reaches an equilibrium state rather quickly (in our case, less than 10^4 yrs), with a maximum size that can't be overcome with a value which is two orders of magnitude smaller than the millimeter-size.

The introduction of a probabilistic description of the collisional velocity changes the outcome of the grain size distribution significantly. The first effect of this new model is that it is possible to overcome Brauer's maximum size. This is due to the tail in the coagulation efficiency, which makes growth possible even for high velocity collisions, leading to the formation of larger grains, up to 0.5 mm. A second result is that the time to reach equilibrium in the Tail model is longer then in the Brauer model.

Adding a narrow bouncing region has no effect in both Tail and Brauer models, but if we expand it (simulations $\mathrm{Br_{b2}}$ and $\mathrm{T_{b2}}$) it is possible to see that this helps deplete the reservoir of small particles (sizes less than 0.001 cm) in favour of the formation of larger particles. This is a non linear effect; what is supposed to happen is that the presence of the bouncing stops the

medium-size particles from growing, giving more time to the small ones to be swept up by the former, in agreement with the results in the work by Windmark et al. (Windmark et al., 2012a). Lastly, the inclusion of the mass transfer does not play any role in the Brauer scenario, as the particles don't grow enough to get into the mass transfer regime. On the other hand, in the Tail model with mass transfer (simulation $\mathrm{T_{mt}}$), the net outcome of the implementation of this mechanism is that the small grains are helped to coagulate, as they don't cause fragmentation anymore when they encounter a large grain.

Therefore, we conclude that out coagulation-fragmentation solver is able to reproduce standard tests and previous results. It is therefore a solid code. We can also conclude that the idea of including a probability description of the collisional velocity leads to an increase in the maximal size of grains that theoretical models predict. This result points towards a solution of the meter (and millimiter) size problem for Core Accretion. Nevertheless, in our simulations (which are performed for the outer part of the disc) we do not form centimeter or even millimiter sized grains, which are expected from observational data. Improvements in the models are therefore still needed.

The following section presents some improvements and studies that have been successively published / submitted. A more correct mathematical treatment for the collisional velocity pdf, which distinguishes between deterministic and stochastic velocities, has been implemented. The model has been applied over different radii in the disc, and for different disc models. The results of those studies show how this simple idea has a large impact on the final grain size distribution, and can potentially lead to the solution of two of the long standing problems of CA: meter (and millimiter) problem at 1 (100) au and the existence of two-sized grain particles.

4.4. Successive studies

A new probability distribution function

In the work by Garaud et al. (Garaud et al., 2013) an improvement of the Tail model is proposed.

If we take into account the five mechanisms that generate collisions, we can divide them into two categories: radial, azimuthal and settling velocities are deterministic and act on three directions perpendicular to each other, while brownian motion and turbulence are stochastic and random mechanisms. This difference has to be taken into account when building the pdf for the collisional velocity. Therefore, we build the 3D pdf as the convolution of three 1D gaussians, each of them peaked at the deterministic velocity typical of that direction, and with the width given by the stochastic velocities. We refer to the publication Garaud et al. (2013) for the full mathematical procedure. Defining $\Delta v_{ij} = \sqrt{\Delta^2 v_R + \Delta^2 v_A + \Delta^2 v_S}$ and $\sigma_{ij}^2 = \pi \left(\Delta^2 v_B + \Delta^2 v_T\right)/8$, the new 3D pdf is

$$p(v) = \frac{1}{\sqrt{2\pi}\sigma_{ij}} \frac{v}{\Delta v_{ij}} \left[\exp\left(-\frac{(v - \Delta v_{ij})^2}{2\sigma_{ij}^2} \right) - \exp\left(-\frac{(v + \Delta v_{ij})^2}{2\sigma_{ij}^2} \right) \right] \tag{4.28}$$

This new pdf reduces to a Maxwellian in the case that stochastic motions dominate over the deterministic ones $\sigma_{ij} >> \Delta v_{ij}$. In the opposite case, when the deterministic velocities are dominating, the first term of the pdf becomes negligible and therefore the pdf follows the equation of a gaussian multiplied by the velocity, which gives a significant tail for large collisional values.

Substituting the pdf 4.28 into the equation 4.24, the mean coagulation efficiency is given by

$$\bar{\epsilon}_{ij}^{c} = \frac{\Delta_{ij}^2 + \sigma_{ij}^2}{\Delta_{ij}^2}\left[2\mathrm{erf}\left(\frac{\Delta_{ij}}{\sqrt{2}\sigma_{ij}}\right) - A(v_c)\right] + \frac{\sigma_{ij}}{\sqrt{2\pi}\Delta_{ij}}\left[2\exp\left(-\frac{\Delta_{ij}^2}{2\sigma_{ij}^2}\right) - \frac{B(v_c)}{\Delta_{ij}}\right] \tag{4.29}$$

and, in a similar way, the mean fragmenting efficiency is

$$\bar{\epsilon}_{ij}^{f} = \frac{\Delta_{ij}^2 + \sigma_{ij}^2}{2\Delta_{ij}}A(v_f) + \frac{\sigma_{ij}}{\sqrt{2\pi}\Delta)ij^2}B(v_f) \tag{4.30}$$

with

$$A(v) = \mathrm{erf}\left(\frac{v + \Delta_{ij}}{\sqrt{2}\sigma_{ij}}\right) - \mathrm{erf}\left(\frac{v - \Delta_{ij}}{\sqrt{2}\sigma_{ij}}\right) \tag{4.31}$$

$$B(v) = (v + \Delta_{ij})\exp\left(-\frac{(v - \Delta_{ij})^2}{2\sigma_{ij}^2}\right) - (v - \Delta_{ij})\exp\left(-\frac{(v + \Delta_{ij})^2}{2\sigma_{ij}^2}\right) \tag{4.32}$$

Both the mean efficiencies have a tail, therefore fragmentation and coagulation are never completely suppressed. This feature has been shown to be present also in the implementation of the Maxwellian pdf, but it is more evident with this new model. The model implements also a mass transfer criteria. The variable that controls the mass ratio for collisions to lead to sticking is chosen to be 500. A parameter study of the value of this variable shows that orders of magnitude changes have small impact on the particle size distribution evolution.

The model is run for a T Tauri disc at different radii, comparing the size distribution with the ones obtained with the Tail and Brauer model. There are mainly three results with this new implementation:

- the maximal size at large radii is larger then the value obtained with the other models. We are indeed able to observe the formation of centimeter sized grains.
- Also the maximal size at small radii is larger then obtained with the other models, reaching the meter sized at 30 au.
- Implementing a pdf instead than a fixed value for the collisional velocity in general leads to the formation of a long standing (on the order of millions of years) reservoir of small particles, as observed in real discs.

Therefore, it looks like this model, which comes from a more physically motivated description of the collisional velocity, is promising for solving a number of long-lasting problems in the theory of grain growth. Nevertheless, it is important to point out that our implementation is missing an important factor: the grains are always retained at the same disc radius. Therefore, there is no real radial drift, and this can lead to an artificial accumulation of grains.

The Brown Dwarf case

In the work by Meru et al. (Meru et al.) we present a study of the evolution of grains in brown dwarf discs. Brown dwarfs have been recently shown to have evidence of millimeter sized grains (Bouy et al., 2008) (Ricci et al., 2012) (Ricci et al., 2013). Despite this, theory has been struggling in showing growth to such large sizes in a brown dwarf, as they are very small and light discs. A first study with positive results in this context has been recently presented by

Pinilla et al. (Pinilla et al., 2013), who hypothesizes the presence of gas pressure maxima, which trap the grain particles, locally enhancing their density (and therefore collisional probability) and partially suppressing radial drift. In our work (Meru et al.) we present a study of growth in the brown dwarf case, using the collisional pdf that has been previously presented (Garaud et al., 2013). Our approach is more general, as we don't need to hypothesize the existence of gas pressure maxima. On the other hand, as already pointed out, our model completely lasts a description of the radial drift, which is present in the model of Pinilla (Pinilla et al., 2013).

The result of our study shows that grains can actually quite easily growth up to millimeter size in brown dwarf discs, contrary to the previous theoretical results obtained with simpler models for the collisional velocity. Moreover it is shown that, as long as brown dwarves are considered as rescaled T Tauri discs in terms of the stellar mass, disc mass and disc radius (as has been pointed out by Apai et al. Apai et al. (2004)), for each radius in a brown dwarf there is a corresponding radius in T Tauri discs which show the same behaviour in the grain size evolution. This one-to-one correlation seems to be related to the similar stochastic and deterministic velocities of the grains, although the environment is different.

4.5. Conclusions and outlook

In this chapter we presented the results of a new model for the growth of grains in circumstellar discs. We tested our code for solving the coagulation fragmentation equation, being able to recover the analytics. We compared our results with those of previous models, finding consistence. We then improved the model, adding more complexity to the collisional velocity description. The collisional velocity is no longer considered to be a single value, but a pdf peaked at the most probable value. This first modification has a big impact on the results, naturally enforcing non-zero coagulation and fragmentation probabilities. As a consequence, the maximal size of grains is larger then previously obtained, and small size particles can be retained as well. A second step is the implementation of a more complex and physically motivated pdf for the collisional velocity, which distinguishes between the role of stochastic and deterministic velocities. This modification causes an even larger maximum grain size.

The model has been applied to a number of different environments (T Tauri discs at large and small radii, brown dwarf discs) and it has been consistently found that the results obtained with this model are comparable with observational results. This idea is therefore a big step towards a consistent model for the coagulation and fragmentation of particles in circumstellar discs, which represents the first stage in CA theory of planet formation.

Nevertheless, there are still some improvements that our model needs in order to be self consistent. A correct treatment of the radial drift is missing and has potentially a large impact on the grain evolution. Moreover, grain porosity due to fractal growth is missing as well, although it is not clear how much this will affect the results. The treatment of mass transfer is quite simple, and further development is needed.

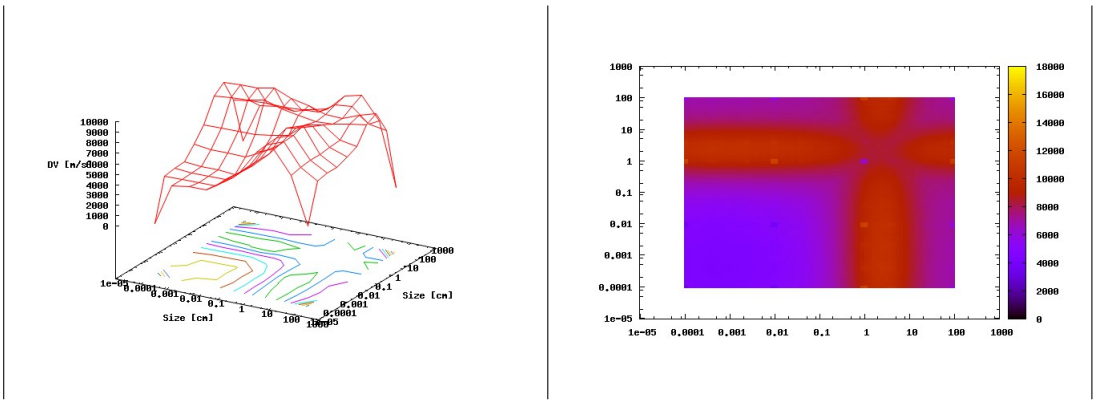

Figure 4.2.: Relative velocity as a function of the size of the colliding particles. On the left there is a 3D plot; on the right a 2D map. All the units are in cgs units.

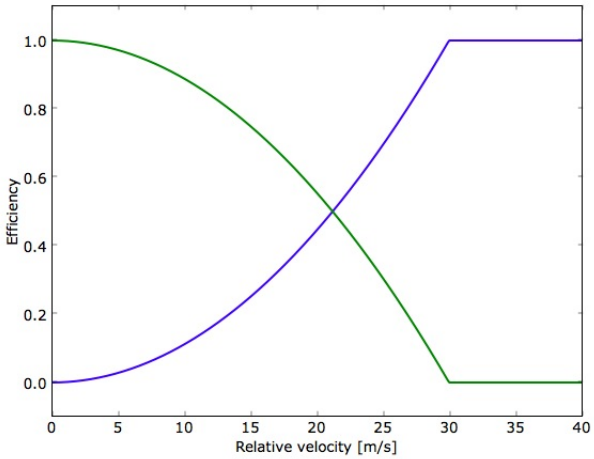

Figure 4.3.: Coagulation (in green) and fragmentation (in blue) efficiency as a function of relative velocity in the Brauer model, assuming $v_f = v_c = 30$ m/s.

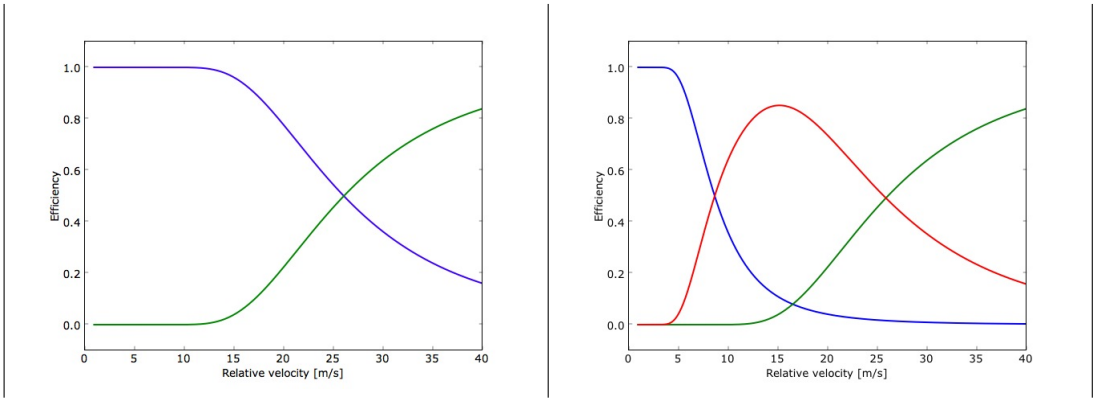

Figure 4.4.: Coagulation (in green) and fragmentation (in blue) efficiency as a function of relative velocity in the Tail model. On the left, the critical velocities are $v_f = v_c = 30$ m/s; on the right, $v_c = 10$ m/s and $v_f = 30$ m/s. The probability of the bouncing region is given by the red line.

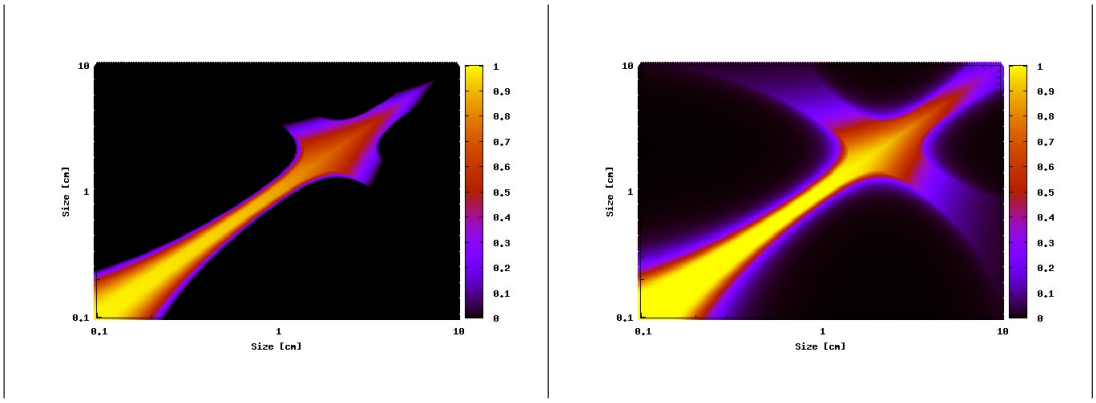

Figure 4.5.: Colour code coagulation efficiency map for the Brauer (on the left) and Tail (on the right) model as a function of the particle size (in cm).

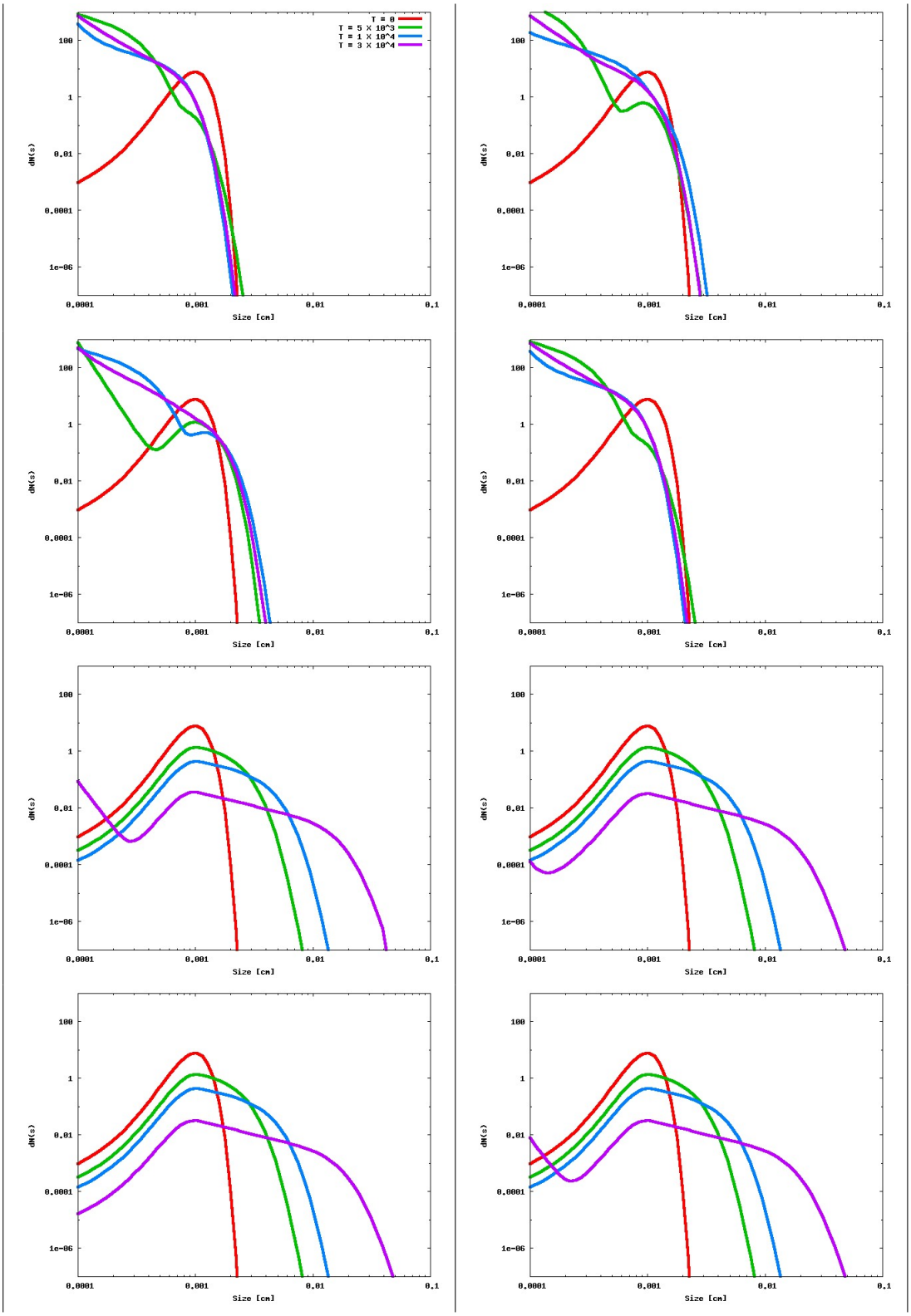

Figure 4.6.: Evolution of the grain size distribution. dN(s) is the number of particle inside a box of radius $a = 0.001$ au. From top to bottom, from left to right: simulation Br, Br_{b1}, Br_{b2}, Br_{mt}, T, T_{b1}, T_{b2}, T_{mt}. Legend (time corresponding to each colour line) is shown in the first graph.

A. Equation of state

In this Appendix we derive the equation of state for a mixture of atomic and diatomic hydrogen. We define the dissociation fraction a as

$$a = \frac{N_{\rm H}}{N_p}, \tag{A.1}$$

with $N_{\rm H}$ number of atoms and N_p total number of protons.

The atomic and molecular parts are assumed to be in chemical equilibrium. Within the molecular part, however, the two nuclear-spin configurations (ortho and para hydrogen) are not in equilibrium, but taken to be frozen at ortho : para = 3 : 1, as there is no efficient mechanism to convert them into each other in dusty clumps (Boley et al., 2007).

Atomic component

We now derive the thermodynamic functions for the atomic component. The partition function will be made up of only the translational component q_t per particle

$$q_t = \frac{V}{\Lambda_{\rm at}^3}, \tag{A.2}$$

where V is the volume and $\Lambda_{\rm at} = h/\sqrt{(2\pi m_{\rm H} k_B T)}$, with h being Planck's constant, $m_{\rm H}$ the atomic mass of hydrogen, k_B Boltzmann's constant and T the temperature. From that we can calculate $\log Q_{\rm H}$:

$$\log Q_{\rm H} = \log(q_t^{N_{\rm H}}) \simeq N_{\rm H} \log \frac{Ve}{N_{\rm H}\Lambda_{\rm at}^3} = N_{\rm H} \log \frac{e}{n_{\rm H}\Lambda_{\rm at}^3}, \tag{A.3}$$

where $n_{\rm H}$ is the number density. Now we can apply the definitions for the Helmholtz energy $A_{\rm H}$, internal energy $E_{\rm H}$, pressure $P_{\rm H}$ and entropy $S_{\rm H}$ to derive

$$A_{\rm H} = -k_B T \log Q_{\rm H} = -k_B T N_{\rm H} \log \frac{e}{n\Lambda_{\rm at}^3} \tag{A.4}$$

$$E_{\rm H} = k_B T^2 \frac{\partial \log Q_{\rm H}}{\partial T}\bigg|_{N_{\rm H},V} = \frac{3}{2} k_B N_{\rm H} T \tag{A.5}$$

$$P_{\rm H} = k_B T \frac{\partial \log Q_{\rm H}}{\partial V}\bigg|_{N_{\rm H},T} = \frac{N_{\rm H} T k_B}{V} = \frac{k_B \rho T}{m_{\rm H}} \tag{A.6}$$

$$S_{\rm H} = \frac{E_{\rm H} - A_{\rm H}}{T} = N_{\rm H} k_B \left(\frac{3}{2} + \log \frac{e}{n_{\rm H}\Lambda_{\rm at}^3} \right). \tag{A.7}$$

Diatomic component

In the diatomic case, the partition function has a rotational component q_r and a vibrational component q_v.

$$
\begin{aligned}
q_t &= \frac{V}{\Lambda_{\rm mol}^3} && \text{(A.8)}\\
q_r &= q_p^{1/4} \times q_o^{3/4} = \mathcal{S}_E^{1/4}\mathcal{S}_O^{3/4}\left(\exp\left(2\Theta_r/T\right)\right)^{3/4} && \text{(A.9)}\\
q_v &= 1/\left(1-\exp\left(-\Theta_v/T\right)\right), && \text{(A.10)}
\end{aligned}
$$

where $\Lambda_{\rm mol} = h/\sqrt{(4\pi m_{\rm H} k_B T)}$, $\Theta_r = 85K$ is the critical rotational temperature and $\Theta_v = 5987K$ critical vibrational temperature, and

$$
\begin{aligned}
\mathcal{S}_E &= \sum_{j\ \text{even}} (2j+1)\exp\left(-j(j+1)\Theta_r/T\right) && \text{(A.11)}\\
\mathcal{S}_O &= \sum_{j\ \text{odd}} 3(2j+1)\exp\left(-j(j+1)\Theta_r/T\right). && \text{(A.12)}
\end{aligned}
$$

From this we can derive $\log Q_{\rm H_2}$:

$$
\frac{\log Q_{\rm H_2}}{N_{\rm H_2}} \simeq \frac{1}{4}\log\left(\mathcal{S}_E\mathcal{S}_O^3\right) + \log\frac{e}{\Lambda_{\rm mol}^3 n_{\rm H_2}} - \log\left(1-\exp\left(-\Theta_v/T\right)\right) + \frac{3}{2}\frac{\Theta_r}{T} \qquad \text{(A.13)}
$$

We can now derive the thermodynamical functions for diatomic hydrogen:

$$
\begin{aligned}
A_{\rm H_2} &= = -k_B T N_{\rm H_2}\left[\frac{1}{4}\log\left(\mathcal{S}_E\left(\mathcal{S}_O\right)^3\right) + \frac{3}{2}\frac{\Theta_r}{T} + \log\frac{e}{\Lambda_{\rm mol}^3 n_{\rm H_2}} - \log\left(1-\exp\left(-\Theta_v/T\right)\right)\right]\\
E_{\rm H_2} &= k_B N_{\rm H_2} T\left[\frac{3}{2}\left(1-\frac{\Theta_r}{T}\right) + \frac{\Theta_v}{T}\frac{1}{\exp\Theta_v/T-1} + \frac{\Theta_r}{4T}\frac{\overline{\mathcal{S}_E}}{\mathcal{S}_E} + \frac{3\Theta_r}{4T}\frac{\overline{\mathcal{S}_O}}{\mathcal{S}_O}\right]\\
P_{\rm H_2} &= k_B T\frac{\partial \log Q_{\rm H_2}}{\partial V}|_{N_{\rm H_2},T} = \frac{N_{\rm H_2} T k_B}{V} = k_B T n_{\rm H_2}\\
S_{\rm H_2} &= N_{\rm H_2} k_B\left[\frac{3}{2} + \log\frac{e\mathcal{S}_E^{1/4}\mathcal{S}_O^{3/4}}{(1-e^{-\Theta_v/T})n_{\rm H_2}\Lambda_{\rm mol}^3} + \frac{\Theta_r}{4T}\left(\frac{\overline{\mathcal{S}_E}}{\mathcal{S}_E} + 3\frac{\overline{\mathcal{S}_O}}{\mathcal{S}_O}\right) + \frac{\Theta_v}{T}\frac{1}{e^{\Theta_v/T}-1}\right],
\end{aligned}
$$

where

$$
\begin{aligned}
\overline{\mathcal{S}_E} &= \sum_{j\ \text{even}} j(j+1)(2j+1)\exp\left(-j(j+1)\Theta_r/T\right)\\
\overline{\mathcal{S}_O} &= 3\sum_{j\ \text{odd}} j(j+1)(2j+1)\exp\left(-j(j+1)\Theta_r/T\right).
\end{aligned}
$$

Dissociation fraction from chemical equilibrium

We consider our system in chemical equilibrium, so that

$$
2H \leftrightharpoons H_2. \qquad \text{(A.14)}
$$

The value of the dissociation parameter a is determined by the equilibrium condition

$$\frac{[H]^2}{[H2]} = \frac{Q_{\rm H}^2({\rm int})}{\Lambda_{\rm at}^6} \frac{\Lambda_{\rm mol}^3}{Q_{\rm H_2}({\rm int})} \tag{A.15}$$

The left side of the equation corresponds to the ratio between the concentration of atomic / diatomic hydrogen:

$$\frac{[H]^2}{[H2]} = \frac{N_{\rm H}^2}{V^2} \frac{V}{N_{\rm H_2}} = \frac{N_p^2 a^2}{V^2} \frac{2V}{(1-a)N_p} = \frac{2a^2 N_p}{V(1-a)} = \frac{2a^2 n}{(1-a)}, \tag{A.16}$$

where n is the total number density. For the right side of the equation, we recall the functions used above, taking into account that $Q_i({\rm int})$ is the total internal partition function, which does not consider the translational term and instead has an extra term

$$\exp\left(-E_g/(k_B T)\right) \tag{A.17}$$

with E_g ground state energy. Putting everything together, we find that the equilibrium condition is

$$\frac{2a^2}{(1-a)} = \frac{F(T)}{n} \tag{A.18}$$

with

$$F(T) = \left(\frac{\sqrt{(\pi m_{\rm H} k_B T)}}{h}\right)^3 e^{(-T_{\rm dis}/(T))} \frac{1 - e^{(-\Theta_V/T)}}{\mathcal{S}_E^{1/4} \mathcal{S}_O^{3/4} \exp\left(3\Theta_r/(2T)\right)}, \tag{A.19}$$

where $E_{\rm dis}$ is the dissociation energy. The dissociation fraction as a function of temperature and number density is

$$a(T,n) = \frac{1}{4}\left(-\frac{F(T)}{n} + \sqrt{\frac{F(T)^2}{n^2} + 8\frac{F(T)}{n}}\right). \tag{A.20}$$

The equation of state

As we know that the pressure is additive, we can find the total pressure P as

$$P = P_{\rm H} + P_{\rm H_2} = \frac{N_{\rm H} T k_B}{V} + \frac{N_{\rm H_2} T k_B}{V} = \frac{k_B T}{V} a N_p \frac{(1-a)N_p}{2} = \frac{k_B T n (1+a)}{2}. \tag{A.21}$$

Internal energy per unit mass

The internal energy per unit mass is given by the sum of the internal energy of the atomic and diatomic component:

$$\begin{aligned} \epsilon &= (E_H + E_{H2})/(N_p m_H) = \\ &= \frac{k_B T}{2 m_H}\left[\frac{3}{2}(a+1) + (1-a)\left(\frac{\Theta_v}{T}\frac{1}{e^{\Theta_V/T}-1} + \frac{\Theta_r}{4T}\frac{\overline{\sum_E}}{\sum_E} + \frac{3\Theta_r}{4T}\frac{\overline{\sum_O}}{\sum_O} - \frac{3}{2}\frac{\Theta_r}{T}\right)\right] \end{aligned} \tag{A.22}$$

B. The clump evolution code

In this Appendix we present the code that has been written to study the evolution of a clump in isolation since its birth as a fragment of a spiral arm generated via GI until either its complete tidal disruption or the reaching of the Second Core Collapse (SCC here after). The syntax herein used is python's.

The circumstellar disc

A very important element in the evolution of the clumps is the circumstellar disc. Only its surface density profile and Toomre parameter are needed. We build them in a separate python file.

```
Mstar = 0.6*msol
T0 = 1500

def Omega(a):
    return pow(gc*Mstar*pow(a,-3), 0.5)

def T(a):
    temp = min(T0*pow(a/au, -5.0/4.0), T0)
    return max(temp, 30.0)

def Cs2(a):
    return pow(gam*kb*T(a)*pow(mu*mp,-1), 0.5)

def f3(s,r):
    nu0 = 5*pow(10,3)
    K = 3*pow(10,10)
    return K/(pow(r,2)*nu0) - 3*s/(2*r)

Ni = 500
ii_log = np.linspace(np.log10(0.001*au), np.log10(150.0*au), Ni)
ii = range(Ni)
for i in range(Ni):
    ii[i] = pow(10, ii_log[i])
result3 = integrate.odeint(f3, 0.0, ii)
sum = 0.0
for i in range(Ni):
    if(i ==0):
        sum += math.pi*result3[i]*pow(ii[i],2)/msol
    else:
        sum += math.pi*result3[i]*(pow(ii[i],2)-pow(ii[i-1],2))/msol
```

```
def Toomre(a, S):
    if(S == 0.0):
        return 0.0
    else:
        return Cs2(a)*Omega(a)*pow(math.pi*gc*S,-1)

M = sum/(Mstar*0.30/msol)
Si = range(Ni)
Ri = range(Ni)
Q = range(Ni)
sum2 = 0.0
for i in range(Ni):
    Ri[i] = ii[i]/au
    Q[i] = Toomre(ii[i], Si[i])
    if(i ==0):
        sum2 += math.pi*Si[i]*pow(ii[i],2)/msol
    else:
        sum2 += math.pi*Si[i]*(pow(ii[i],2)-pow(ii[i-1],2))/msol

file = open('Profili.txt', 'w')
mystr =  str(0.0) + '  ' + str(0.0) + '  ' + str(Q4[0]*100.0) + '\n'
file.write(mystr)

for i in range(len(Si)):
    mystr =  str(ii[i]) + '  ' + str(Si[i]) + '  ' + str(Q4[i]) + '\n'
    file.write(mystr)
file.close()
```

Function f3 reproduces $\partial\Sigma/\partial t$ which can be evaluated from eq. **??**. Once the table Profili.txt has been build, we import it into the evolution code:

```
cofP_r = []
cofP_s = []
cofP_q = []
fileP = open('Profili.txt')
for line in fileP:
    temp_last = line
    temp = temp_last.split(' ')
    cofP_r.append(float(temp[0]))
    cofP_s.append(float(temp[2]))
    cofP_q.append(float(temp[4]))
```

The initial condition

In order to build a clump, we need only three information: its initial mass, radius and semimajor axis. Those values are randomly selected into an interval which has been discussed in Chapter 3.

Once the clump has been characterized, we need to know its radius, inner density and inner temperature evolution. The first quantity will be used in the interaction between the clump and the circumstellar disc, while the latter two quantities are needed to determine the timescale for

reaching SCC. The behaviour of all those quantities is supposed to be similar to the one of the same quantities for the clumps studied at high resolution in Chapter 2, with the initial values rescaled.

Let us start with the dissociation parameter behaviour. We have that the inner density evolution follows the law $\rho(t) = a + b \times t + c \times t^2$ while the inner temperature evolves in a linear way $T(t) = d + e \times t$. The file CoefDiss is a table which contains those coefficients: the first row has (a, b, c) while the second raw is formed by $(e, f, 0.0)$. The first step is therefore to rescale a and d so that the same laws apply for this clump:

```
cofD = [[0 for col in range(3)] for row in range(2)]
file1 = open('CoefDiss')
for i in range(2):
    stri = file1.readline()
    tempor = stri.split(' ')
    for j in range(3):
        cofD[i][j] = float(tempor[j])
file1.close
factD = (M0/(mj*1.48))*pow(0.188*au/R0,3)
factT = (au*0.188/R0)*(M0/(mj*1.48))
cofD[0][0] = cofD[0][0]*factD
cofD[1][0] = cofD[1][0]*factT
```

$M0$ and $R0$ are the initial mass and radius of the clump; $1.48 M_J$ and $0.188 au$ are the mass and radius of the reference clump. Once we have rescaled the coefficients, we can find the timescale to reach SCC:

```
####---- Useful Constants --- ####
kb = 1.38e-16
mp = 1.67e-24
Thetar = 85.4
ThetaV = 5987.0
Tdis = 52327.23669
klimit = 20
year = 60*60*24*365.0
h = 6.62600755*pow(10, -34)*pow(10,7)


def SigmaE(x):
    return sum((2*(2*j)+1)*exp(-(2*j)*(2*j+1)*Thetar/x) for j in range(0,klimit))

def SigmaO(x):
    return 3.0*sum((4*j+3)*exp((2-(2*j+1)*((2*j+1)+1))*Thetar/x) for j in range(0,klimit))

def onlyt(T):
    return pow(pow(pi*mp*kb*T,0.5)/h, 3.0)*exp(-Tdis/T)*(1.0-exp(-ThetaV/T))
    /(pow(SigmaE(T)*pow(SigmaO(T),3),0.25))

def fun(T, Rho):
    kappa = mp*onlyt(T)/(Rho)
    if(kappa > pow(10, 13)):
```

```
        return 1.0
    return 0.25*(-kappa + pow(pow(kappa, 2) + 8.0*kappa,0.5))

def Dissoc(t_yr):
    t_sec = t_yr*year
    T = cofD[1][0]+cofD[1][1]*t_sec
    Rho = cofD[0][0]+cofD[0][1]*t_sec+cofD[0][2]*pow(t_sec,2)
    if(Rho<0.0 or T < 0.0):
        print('ERROR IN EXTRAPOLIATION:', Rho, T)
    return fun(T,Rho)

disso = []
i=0
t=0
while(i<3):
    disso.append(Dissoc(t))
    t += 1
    if(disso[t-1]>= 0.01):
        i = 4
    if(t > pow(10,5)):
        break
print('Time to reach SCC [yr]:', t)
```

In the previous part, SigmaE, SigmaO, onlyT are functions which are used to find the dissociation parameter (see Appendix A).

Radial Evolution in isolation

In a similar way as has been done for the dissociation time, it is possible to infer from the evolution of the reference clump the time evolution of the radius. From Chapter 2 we infer the evolution not only for the half mass radius, but for all the clump radii inside which there is im% of the total clump mass, where im goes from 2×10^4 to 1.0 with a step of 2×10^{-4}. For each of those radii, its time evolution is given by $r_{im} = r_{im} + A \times t$. The table is formed so that each row contains the elements (im, r_{im0}, A).

```
nR = 5000
fracIM = 0.5
cofR = [[0 for col in range(4)] for row in range(nR)]

file1 = open('CoefR')
for i in range(nR):
    stri = file1.readline()
    tempor = stri.split(' ')
    for j in range(4):
        cofR[i][j] = float(tempor[j])

ff = R0/(au*cofR[int(nR*fracIM)-1][1])
for i in range(nR):
    cofR[i][1] = cofR[i][1]*ff
```

```
file1.close
```

nR is the number of rows inside the radius table; fracIM is the mass fraction for the initial radius. cofR[][1] have now been rescaled to apply to the new clump.

The Evolution

In order to follow the evolution of the clump, we build the clump class:

```
class clump:
    def __init__(self, rag, mas, iq, io, ims, igo):
        self.r = rag
        self.m = mas
        self.im = iq
        self.im_old = io
        self.im_s = ims
self.ig = igo
    def addM(self, ics):
        self.m.append(ics)
    def addR(self, ics):
        self.r.append(ics)
    def addIM(self, ics):
        self.im_s.append(ics)
    def addG(self, ics):
        self.ig.append(ics)
```

There are four quantities whose temporal evolution is coupled to each other: the migration time, the semimajor axis a (initial value in the code: Rau), the clump radius and mass. From eq. 3.4 the migration time can be written as

$$\tau = K a^{3/2} Q \tag{B.1}$$

with K constant and therefore its time evolution is given by

$$\frac{d\tau}{da} = \frac{da}{dt}\left(\frac{3}{2}\frac{\tau}{a} + \frac{\tau}{a}\frac{da}{dt}\right) \tag{B.2}$$

Assuming that the semimajor axis evolves in time following the rule

$$a(t) = a_0 - \frac{a_0}{\tau} t \tag{B.3}$$

it is possible to derive

$$\frac{da}{dt} = -\frac{a_0}{\tau\left[1 - \frac{a_0 t}{\tau}\left(\frac{3}{2}\frac{1}{a} + \frac{1}{Q}\frac{dQ}{da}\right)\right]} \tag{B.4}$$

We already have the time evolution for the clump radius. The mass evolution is given by the mass accretion. As discussed in Chapter 3, the mass accretion is the minimum between the values given by the mass accretion from the disc (eq **??**) and the mass accretion allowed from the Kevin Helmoltz stability criteria. The time evolution of those four quantities is therefore implemented in the following way:

```
def Toomre(a,tt):
    for i in range(len(cofP_r)):
     if(cofP_r[i] - a >= 0.0):
    return cofP_q[i] + (cofP_q[i+1] - cofP_q[i])*(a - cofP_r[i])/(cofP_r[i+1] - cofP_r[i])

def Omega(a):
    return pow((gc*mstar)/pow(a,3),0.5)

def migrtime(M,a,tt):
    Torb = 2*pi/Omega(a)
    Q = Toomre(a, tt)
    q = M/mstar
    h_mgr = 0.1
    return Torb*5.6*pow(3.8-sig,-1)*gam*Q*(h_mgr*h_mgr*h_mgr/q)*pow(0.1/h_mgr,2)

def derivataTau(tt,tau,a,r,M):
    return 0.5*(cmp(a,0.011*au)+1)*(derivataR(tt,tau,a,r,M0)*(1.5*tau/a
    + tau*derivataQ(a)/Toomre(a, tt)))

def derivataR(tt,tau,a,r,M):
    tp = tt - tmin
    return 0.5*(cmp(a,0.011*au)+1)*(-initial_state[1]/(tau*(1-(tp*initial_state[1]/tau)*
    (1.5/a + derivataQ(a)/Toomre(a, tt)))))

def derRad(tt,a,r_old,M):
    return cofR[clp.im][2]*au + cofR[clp.im][3]*au*2*tt + r_old*derivataM(tt,a,r_old,M)/M

def derivataM(tt,a,r,M):
    dm = 1.0*pow(10,-7)*pow(3,np.log10((Sigm(a))/Sigm(100.0*au)))*pow(M/mj,2.0/3.0)*
    pow(mstar/msola,-1.0/6.0)*msola/year
    dmkh = 4*pi*sigmaSB*pow(r,3)*pow(Tmean(tt),4)/(gc*M)
    return 0.5*(cmp(a,0.011*au)+1)*(min(dm, dmkh))

def f(state, tt):
    return np.array([
            derivataTau(tt,state[0],state[1],state[2],state[3]),
            derivataR(tt,state[0],state[1],state[2],state[3]),
            derRad(tt, state[1], state[2], state[3]),
            derivataM(tt,state[1],state[2],state[3])
            ])

initial_state = np.array([
    migrtime(M0,Rau, 0.0),
    Rau,
    R0,
    M0
])

TMIN = 0.0*year
```

```
TMAX = 1.05*t*year
DT = 20.0*year
tstep = 40
tmin = TMIN
tmax = tmin+DT
tempo_tmp = np.linspace(tmin, tmax, tstep)
result, info = integrate.odeint(f, initial_state, tempo_tmp, full_output=True)
```

clp.im is a integer index which tells you the fraction of mass inside the radius you are considering. It is initialized to 0.5. While the clump gets tidally disrupted, this index decreases accordingly. If the clump mass gets lower that Neptune mass, the clump is considered to be tidally disrupted.

The prefactor $0.5 * (cmp(a, 0.011 * au) + 1)$ which appears in the functions for the time derivates of τ, a and M gives 0 if the semimajor axis is smaller that 0.011 au, which is the value we assume for the disc inner border.

The clump is not evolved until SCC at once; it is evolved only for $DT = 20$ years. After this evolution, the code checks if, at any timestep, the clump falls into one of the special categories: its radius is larger then the Hill radius / 3, the clump opens a gap, the clump radius is smaller the Jupiter radius. If one of these conditions applies, the clump is modified accordingly, and the integration is restarted.

Gap opening criteria

In a similar way as before, after a partial (in time) integration has been done, the code checks if at any timestep the clump is able to open a gap, according to the criteria described in Crida et al. (2006) and Kley and Nelson (2012). If this is the case, the new migration time is assumed to be the viscosity time.

```
#####---- Useful Constants ---####
alpha = 0.005

def temp(a):
    return T0*pow(a/au, -0.5)

def cs(a):
    Temp = max(T0*pow(a/au,-5.0/4.0),30.0)
    return pow(gam*kb*Temp/(mu*mp),0.5)

def Hdisk(a):
    return cs(a)*a*pow(gc*mstar/a,-0.5)    # Hydrostatic equilibrium

def Re(a): # Reynold number
    nu = alpha*pow(Hdisk(a),2)*Omega(a)
    return a*a*Omega(a)/nu

def tauvis(a):
    return pow(a,2)/(alpha*pow(Hdisk(a),2)*Omega(a))

def GderivataTau(tt,tau,a,r,M):
```

```
    return 0.5*(cmp(a,0.011*au)+1)*(GderivataR(tt,tau,a,r,M0)*(7.0/4.0)*
    CoefTau*pow(a,3.0/4.0))

def derRad(tt,a,r_old,M):
    return cofR[clp.im][2]*au + cofR[clp.im][3]*au*2*tt + r_old*derivataM(tt,a,r_old,M)/M

def GderivataM(tt,a,r,M):
    dm = 1.0*pow(10,-7)*pow(3,np.log10((0.1*Sigm(a))/Sigm(100.0*au)))*
    pow(M/mj,2.0/3.0)*pow(mstar/
      msola,-1.0/6.0)*msola/year
    dmkh = 4*pi*sigmaSB*pow(r,3)*pow(Tmean(tt),4)/(gc*M)
    return (0.5*(cmp(a,0.011*au)+1)*(min(dm, dmkh)))

def f4(state, tt):
    return np.array([
            GderivataTau(tt,state[0],state[1],state[2],state[3]),
            GderivataR(tt,state[0],state[1],state[2],state[3]),
            GderRad(tt, state[1], state[2], state[3]),
            GderivataM(tt,state[1],state[2],state[3])
            ])
```

The mass accretion can either be described as showed above, where the local Σ has been decreased by a factor of 10 due to the gap opening, or it can be set to 0, accordingly with the implemented model.

The three conditions and saving the result

As the integration is not done all at once, but at small steps and sometimes re-started, it is necessary to be cautious about how and when to save the results.

Once the integration has been done, the code checks for each timestep

- if the clump is still inside its Hill radius / 3;
- if the clump respects the condition for the gap opening and, if yes, if the gap has been open in that timestep or it was already open;
- if the clump radius is smaller then Jupiter radius.

In the first case, the radius and mass of the clump are reduced accordingly until it fits inside the sphere formed by the Hill radius /3, and then the integration is restarted. In the second case, if the clump opens a gap for the first time, the integration is restarted with the migration time given by the viscosity time; if it had already opened a gap, nothing happens. Last, if the clump radius is smaller that Jupiter radius, the simulation is restarted and the new function $dR/dt = 0$.

The integration of the clump evolution continues until either the clump has been disrupted by the tidal interaction with the central star, or the integrated time Tmax equals 1.05× SCC timescale. In both cases, the results are saved into two separated tables: one for the evolution of the clump, and one for the evolution of the dissociation parameter.

```
clp = clump([], [], [], [], [], [])
clp.im = (int(nR*fracIM) - 1)
```

```
HillF = 3

def rhill(M, a):
    if(a <= 0.1*au):
        a = 0.1*au
    return a*pow(M/(3*mstar),1.0/3.0)

def Gap(a,r,M):
    q = M/mstar
    if((3.0*Hdisk(a)/(4.0*rhill(M,a)) + 50/(q*Re(a))) <= 1.0 ):
return 1.0
    else:
return 0.0

while(tmax <= TMAX):
###### ---- INTEGRATION PART ---- ######
    for i in range(tstep):
        if(result[i,2]>rhill(result[i,3],result[i,1])/HillF): # Clump tidally destroyed
    emme = result[i,3]
    new_erre = result[i,2]
    if(clp.im > 1):
     DeltaR = new_erre/clp.im
            while(new_erre>rhill(result[i,3],result[i,1])/HillF):
                emme = result[i,3] - DeltaM
                if(clp.im>1):
                    clp.im = clp.im - 1
                    new_erre = new_erre - DeltaR
                else:
                    new_erre = new_erre - DeltaR
            initial_state = np.array([
                result[i,0],
                result[i,1],
                new_erre,
                emme
                ])
            tmin = tempo_tmp[i]
            tmax = tmin + DT
            tempo_tmp = np.linspace(tmin,tmax,tstep)
            break
elif(Gap(result[i,1], result[i,2], result[i,3]) > 0.5):  # The clump opens a gap
   if(i>1):
        if(Gap(result[i-1,1], result[i-1,2], result[i-1,3]) < 0.5):
      tmin = tempo_tmp[i]
                tmax = tmin + DT
         tempo_tmp = np.linspace(tmin,tmax,tstep)
                initial_state = np.array([
                       tauvis(result[i,1]),
                       result[i,1],
                       result[i,2],
```

```
                        result[i,3]
                        ])
    break
           else:
               tempo.append(tempo_tmp[i]/year)
               dm.append(derivataM(tempo_tmp[i], result[i,1],
               result[i,2], result[i,3]))
       cri.append(Criteria(tmin,initial_state[1],
       initial_state[2], initial_state[3]))
       tm.append(Tmean(tempo_tmp[i]))
       clm.append(clp.im)
       ti.append(Tinn(tempo_tmp[i]))
               erre.append(result[i,1]/au)
               clp.addR(result[i,2]/au)
       clp.addG(Gap(initial_state[1], initial_state[2], initial_state[3]))
               tau.append(result[i,0]/year)
               clp.addM(result[i,3]/mj)
               rh.append(rhill(result[i,3],result[i,1])/HillF/au)
elif(result[i,2]<=rj*0.9):
#            print('RJ')
            tmin = tempo_tmp[i]
            tmax = tmin + DT
            tempo_tmp = np.linspace(tmin,tmax,tstep)
            initial_state = np.array([
                result[i,0],
                result[i,1],
                rj,
                result[i,3]
                ])
    print('rj break')
    break
        else:
            tempo.append(tempo_tmp[i]/year)
            dm.append(derivataM(tempo_tmp[i], result[i,1], result[i,2], result[i,3]))
    cri.append(Criteria(tmin,initial_state[1], initial_state[2], initial_state[3]))
    tm.append(Tmean(tempo_tmp[i]))
    clm.append(clp.im)
    ti.append(Tinn(tempo_tmp[i]))
            erre.append(result[i,1]/au)
            clp.addR(result[i,2]/au)
    clp.addG(Gap(initial_state[1], initial_state[2], initial_state[3]))
            tau.append(result[i,0]/year)
            clp.addM(result[i,3]/mj)
            rh.append(rhill(result[i,3],result[i,1])/HillF/au)
    if(i==(tstep-1)):
#     print('NORMALE')
    tmin = tmax
            tmax = tmax + DT
            tempo_tmp = np.linspace(tmin,tmax,tstep)
```

```
            initial_state = np.array([
                result[i,0],
                result[i,1],
                result[i,2],
                result[i,3]
                ])


file = open(myfile, 'w')
for i in range(int(len(tempo))):
    if(i == 0):
         mystr =  str(tempo[i]) + '  ' + str(tau[i]) + '  ' +
         str(erre[i])+ '  ' + str(clp.m[i]) + '  ' + str(clp.r[i]) + '  ' +
         str(rh[i]) + ' ' + str(dm[i]*year/mj) + ' ' + str(clm[i]) + '\n'
         file.write(mystr)
    else:
         if(int(tempo[i]) != int(tempo[i-1])):
                mystr =  str(tempo[i]) + '  ' + str(tau[i]) + '  ' +
                str(erre[i])+ '  ' + str(clp.m[i]) + '  ' + str(clp.r[i]) +
                '  ' + str(rh[i]) + ' ' + str(dm[i]*year/mj) +
                ' ' + str(clm[i]) + '\n'
                file.write(mystr)
file.close()

file = open(myfileD, 'w')
ti = range(len(disso))
for i in range(len(disso)):
    mystr =  str(ti[i]) + '  ' + str(disso[i]) + '\n'
    file.write(mystr)
file.close()
```

Bibliography

O. Agertz, B. Moore, J. Stadel, D. Potter, F. Miniati, J. Read, L. Mayer, A. Gawryszczak, A. Kravtsov, Å. Nordlund, F. Pearce, V. Quilis, D. Rudd, V. Springel, J. Stone, E. Tasker, R. Teyssier, J. Wadsley, and R. Walder. Fundamental differences between SPH and grid methods. *MNRAS*, 380:963–978, September 2007. doi: 10.1111/j.1365-2966.2007.12183.x.

Y. Alibert, C. Mordasini, W. Benz, and C. Winisdoerffer. Models of giant planet formation with migration and disc evolution. *A & A*, 434:343–353, April 2005. doi: 10.1051/0004-6361:20042032.

D. Apai, I. Pascucci, M. F. Sterzik, N. van der Bliek, J. Bouwman, C. P. Dullemond, and T. Henning. Grain growth and dust settling in a brown dwarf disk. Gemini/T-ReCS observations of CFHT-BD-Tau 4. *A & A*, 426:L53–L57, November 2004. doi: 10.1051/0004-6361:200400080.

P. J. Armitage. *Astrophysics of Planet Formation*. 2010.

P. J. Armitage and C. J. Clarke. Magnetic braking of T Tauri stars. *MNRAS*, 280:458–468, May 1996.

P. Artymowicz. On the Wave Excitation and a Generalized Torque Formula for Lindblad Resonances Excited by External Potential. *ApJ*, 419:155, December 1993. doi: 10.1086/173469.

M. et al. Auvergne. The CoRoT satellite in flight: description and performance. *A & A*, 506: 411–424, October 2009. doi: 10.1051/0004-6361/200810860.

B. A. Ayliffe and M. R. Bate. Circumplanetary disc properties obtained from radiation hydrodynamical simulations of gas accretion by protoplanets. *MNRAS*, 397:657–665, August 2009. doi: 10.1111/j.1365-2966.2009.15002.x.

P. Barge and J. Sommeria. Did planet formation begin inside persistent gaseous vortices? *A & A*, 295:L1–L4, March 1995.

J. Barnes and P. Hut. A hierarchical O(N log N) force-calculation algorithm. , 324:446–449, December 1986. doi: 10.1038/324446a0.

C. Baruteau, F. Meru, and S.-J. Paardekooper. Rapid inward migration of planets formed by gravitational instability. *MNRAS*, 416:1971–1982, September 2011. doi: 10.1111/j.1365-2966.2011.19172.x.

M. R. Bate, I. A. Bonnell, and V. Bromm. The formation of a star cluster: predicting the properties of stars and brown dwarfs. *MNRAS*, 339:577–599, March 2003. doi: 10.1046/j.1365-8711.2003.06210.x.

J.-P. et al. Beaulieu. "discovery of a cool planet of 5.5 earth masses through gravitational microlensing". , 439:437–440, January 2006. doi: 10.1038/nature04441.

T. Birnstiel. *The Evolution of Gas and Dust in Protoplanetary Accretion Disks*. PhD thesis, PhD Thesis, 2011, 2011.

T. Birnstiel, C. P. Dullemond, and F. Brauer. Gas- and dust evolution in protoplanetary disks. *A & A*, 513:A79, April 2010. doi: 10.1051/0004-6361/200913731.

J. Blum. Dust growth in protoplanetary disks - a comprehensive experimental/theoretical approach. *Research in Astronomy and Astrophysics*, 10:1199–1214, December 2010. doi: 10.1088/1674-4527/10/12/002.

J. Blum and G. Wurm. The Growth Mechanisms of Macroscopic Bodies in Protoplanetary Disks. , 46:21–56, September 2008. doi: 10.1146/annurev.astro.46.060407.145152.

A. C. Boley. The Two Modes of Gas Giant Planet Formation. *ApJL*, 695:L53–L57, April 2009. doi: 10.1088/0004-637X/695/1/L53.

A. C. Boley and R. H. Durisen. On the Possibility of Enrichment and Differentiation in Gas Giants During Birth by Disk Instability. *ApJ*, 724:618–639, November 2010. doi: 10.1088/0004-637X/724/1/618.

A. C. Boley, T. W. Hartquist, R. H. Durisen, and S. Michael. The Internal Energy for Molecular Hydrogen in Gravitationally Unstable Protoplanetary Disks. *ApJL*, 656:L89–L92, February 2007. doi: 10.1086/512235.

A. C. Boley, T. Hayfield, L. Mayer, and R. H. Durisen. Clumps in the outer disk by disk instability: Why they are initially gas giants and the legacy of disruption. *Icarus*, 207:509–516, June 2010. doi: 10.1016/j.icarus.2010.01.015.

M. Bonavita, R. Jayawardhana, M. Janson, and D. Lafrenière. Direct imaging and spectroscopy of planets and brown dwarfs in wide orbits. In A.Sozzetti, M.G.Lattanzi, & A.P.Boss, editor, *IAU Symposium*, volume 276 of *IAU Symposium*, pages 113–116, November 2011. doi: 10.1017/S1743921311020035.

W. J. Borucki, D. G. Koch, G. Basri, N. Batalha, A. Boss, T. M. Brown, and Caldwell. Characteristics of Kepler Planetary Candidates Based on the First Data Set. *ApJ*, 728:117, February 2011. doi: 10.1088/0004-637X/728/2/117.

W. J. et al. Borucki. Kepler Planet-Detection Mission: Introduction and First Results. *Science*, 327:977–, February 2010. doi: 10.1126/science.1185402.

A. P. Boss. Giant planet formation by gravitational instability. *Science*, 276:1836–1839, 1997. doi: 10.1126/science.276.5320.1836.

A. P. Boss. Formation of Giant Planets by Disk Instability on Wide Orbits Around Protostars with Varied Masses. *ApJ*, 731:74, April 2011. doi: 10.1088/0004-637X/731/1/74.

J. Bouvier, S. H. P. Alencar, T. J. Harries, C. M. Johns-Krull, and M. M. Romanova. Magnetospheric Accretion in Classical T Tauri Stars. *Protostars and Planets V*, pages 479–494, 2007.

H. Bouy, N. Huélamo, C. Pinte, J. Olofsson, D. Barrado Y Navascués, E. L. Martín, E. Pantin, J.-L. Monin, G. Basri, J.-C. Augereau, F. Ménard, G. Duvert, G. Duchêne, F. Marchis, A. Bayo, S. Bottinelli, B. Lefort, and S. Guieu. Structural and compositional properties of brown dwarf disks: the case of 2MASS J04442713+2512164. *A & A*, 486:877–890, August 2008. doi: 10.1051/0004-6361:20078866.

F. Brauer, C. P. Dullemond, and T. Henning. Coagulation, fragmentation and radial motion of solid particles in protoplanetary disks. *A & A*, 480:859–877, March 2008. doi: 10.1051/0004-6361:20077759.

D. Charbonneau, T. M. Brown, D. W. Latham, and M. Mayor. Detection of Planetary Transits Across a Sun-like Star. *ApJL*, 529:L45–L48, January 2000. doi: 10.1086/312457.

A. Collier Cameron and C. G. Campbell. Rotational evolution of magnetic T Tauri stars with accretion discs. *A & A*, 274:309, July 1993.

A. Crida, A. Morbidelli, and F. Masset. On the width and shape of gaps in protoplanetary disks. *Icarus*, 181:587–604, April 2006. doi: 10.1016/j.icarus.2005.10.007.

S. J. Desch. Mass Distribution and Planet Formation in the Solar Nebula. *ApJ*, 671:878–893, December 2007. doi: 10.1086/522825.

B. T. Draine and H. M. Lee. Optical properties of interstellar graphite and silicate grains. *ApJ*, 285:89–108, October 1984. doi: 10.1086/162480.

C. P. Dullemond and C. Dominik. Dust coagulation in protoplanetary disks: A rapid depletion of small grains. *A & A*, 434:971–986, May 2005. doi: 10.1051/0004-6361:20042080.

R. H. Durisen, R. A. Gingold, J. E. Tohline, and A. P. Boss. Dynamic fission instabilities in rapidly rotating N = 3/2 polytropes - A comparison of results from finite-difference and smoothed particle hydrodynamics codes. *ApJ*, 305:281–308, June 1986. doi: 10.1086/164248.

R. H. Durisen, A. P. Boss, L. Mayer, A. F. Nelson, T. Quinn, and W. K. M. Rice. Gravitational Instabilities in Gaseous Protoplanetary Disks and Implications for Giant Planet Formation. *Protostars and Planets V*, pages 607–622, 2007a.

R. H. Durisen, A. P. Boss, L. Mayer, A. F. Nelson, T. Quinn, and W. K. M. Rice. Gravitational Instabilities in Gaseous Protoplanetary Disks and Implications for Giant Planet Formation. *Protostars and Planets V*, pages 607–622, 2007b.

J. A. Eisner. Disk Masses at the End of the Main Accretion Phase: CARMA Observations and Multi-wavelength Modeling of Class I Protostars. *ApJ*, 755:23, August 2012. doi: 10.1088/0004-637X/755/1/23.

D. A. Fischer and J. Valenti. The Planet-Metallicity Correlation. *ApJ*, 622:1102–1117, April 2005. doi: 10.1086/428383.

D. Forgan and K. Rice. Towards a Population Synthesis Model of Objects formed by Self-Gravitating Disc Fragmentation and Tidal Downsizing. *ArXiv e-prints*, April 2013.

M. Y. Fujimoto. Dynamical stability of differentially rotating bodies to non-axisymmetric perturbations. *A & A*, 176:53–58, April 1987.

E. Furlan, D. M. Watson, M. K. McClure, P. Manoj, C. Espaillat, P. D'Alessio, N. Calvet, K. H. Kim, B. A. Sargent, W. J. Forrest, and L. Hartmann. Disk Evolution in the Three Nearby Star-forming Regions of Taurus, Chamaeleon, and Ophiuchus. *ApJ*, 703:1964–1983, October 2009. doi: 10.1088/0004-637X/703/2/1964.

M. Galvagni, P. Garaud, C. Olczak, and F. Meru. Improving the grain growth model in the outer part of circumstellar disks. In *New Horizons in Astronomy: Frank N. Bash Symposium*, ISIMA, 2011.

M. Galvagni, T. Hayfield, A. Boley, L. Mayer, R. Roškar, and P. Saha. The collapse of protoplanetary clumps formed through disc instability: 3D simulations of the pre-dissociation phase. *MNRAS*, 427:1725–1740, December 2012. doi: 10.1111/j.1365-2966.2012.22096.x.

C. F. Gammie. Nonlinear Outcome of Gravitational Instability in Cooling, Gaseous Disks. *ApJ*, 553:174–183, May 2001. doi: 10.1086/320631.

P. Garaud, F. Meru, M. Galvagni, and C. Olczak. From Dust to Planetesimals: An Improved Model for Collisional Growth in Protoplanetary Disks. *ApJ*, 764:146, February 2013. doi: 10.1088/0004-637X/764/2/146.

R. A. Gingold and J. J. Monaghan. Smoothed particle hydrodynamics - Theory and application to non-spherical stars. *MNRAS*, 181:375–389, November 1977.

R. A. Gingold and J. J. Monaghan. Kernel estimates as a basis for general particle methods in hydrodynamics. *Journal of Computational Physics*, 46:429–453, June 1982. doi: 10.1016/0021-9991(82)90025-0.

P. Goldreich and S. Tremaine. The excitation of density waves at the Lindblad and corotation resonances by an external potential. *ApJ*, 233:857–871, November 1979. doi: 10.1086/157448.

P. Goldreich and S. Tremaine. Disk-satellite interactions. *ApJ*, 241:425–441, October 1980. doi: 10.1086/158356.

K. E. Haisch, Jr., E. A. Lada, and C. J. Lada. Disk Frequencies and Lifetimes in Young Clusters. *ApJL*, 553:L153–L156, June 2001. doi: 10.1086/320685.

J. Hashimoto, M. Tamura, T. Muto, T. Kudo, M. Fukagawa, T. Fukue, M. Goto, C. A. Grady, T. Henning, K. Hodapp, M. Honda, S. Inutsuka, E. Kokubo, G. Knapp, and McElwain. Direct Imaging of Fine Structures in Giant Planet-forming Regions of the Protoplanetary Disk Around AB Aurigae. *ApJL*, 729:L17, March 2011. doi: 10.1088/2041-8205/729/2/L17.

T. Hayfield, L. Mayer, J. Wadsley, and A. C. Boley. The properties of pre-stellar discs in isolated and multiple pre-stellar systems. *MNRAS*, 417:1839–1852, November 2011. doi: 10.1111/j.1365-2966.2011.19371.x.

R. Helled and P. Bodenheimer. The effects of metallicity and grain growth and settling on the early evolution of gaseous protoplanets. *Icarus*, 211:939–947, February 2011. doi: 10.1016/j.icarus.2010.09.024.

R. Helled and G. Schubert. Core formation in giant gaseous protoplanets. *Icarus*, 198:156–162, November 2008. doi: 10.1016/j.icarus.2008.08.002.

R. Helled and G. Schubert. Heavy-element Enrichment of a Jupiter-mass Protoplanet as a Function of Orbital Location. *ApJ*, 697:1256–1262, June 2009. doi: 10.1088/0004-637X/697/2/1256.

R. Helled, M. Podolak, and A. Kovetz. Planetesimal capture in the disk instability model. *Icarus*, 185:64–71, November 2006. doi: 10.1016/j.icarus.2006.06.011.

P. F. Hopkins and J. L. Christiansen. Turbulent Disks are Never Stable: Fragmentation and Turbulence-Promoted Planet Formation. *ArXiv e-prints*, January 2013.

S.-i. Inutsuka, M. N. Machida, and T. Matsumoto. Emergence of Protoplanetary Disks and Successive Formation of Gaseous Planets by Gravitational Instability. *ApJL*, 718:L58–L62, August 2010. doi: 10.1088/2041-8205/718/2/L58.

P. Kalas, J. R. Graham, E. Chiang, M. P. Fitzgerald, M. Clampin, E. S. Kite, K. Stapelfeldt, C. Marois, and J. Krist. Optical Images of an Exosolar Planet 25 Light-Years from Earth. *Science*, 322:1345–, November 2008. doi: 10.1126/science.1166609.

J. E. Kessler-Silacci. Probing Chemistry During Star and Planet Formation. In S. J. Kannappan, S. Redfield, J. E. Kessler-Silacci, M. Landriau, and N. Drory, editors, *New Horizons in Astronomy: Frank N. Bash Symposium*, volume 352 of *Astronomical Society of the Pacific Conference Series*, page 47, September 2006.

H. H. Klahr and P. Bodenheimer. Turbulence in Accretion Disks: Vorticity Generation and Angular Momentum Transport via the Global Baroclinic Instability. *ApJ*, 582:869–892, January 2003. doi: 10.1086/344743.

W. Kley and R. P. Nelson. Planet-Disk Interaction and Orbital Evolution. *A & A*, 50:211–249, September 2012. doi: 10.1146/annurev-astro-081811-125523.

A. Koenigl. Disk accretion onto magnetic T Tauri stars. *ApJL*, 370:L39–L43, March 1991. doi: 10.1086/185972.

G. P. Kuiper. On the Origin of the Solar System. *Proceedings of the National Academy of Science*, 37:1–14, January 1951a. doi: 10.1073/pnas.37.1.1.

G. P. Kuiper. On the Origin of the Solar System. *Proceedings of the National Academy of Science*, 37:1–14, January 1951b. doi: 10.1073/pnas.37.1.1.

D. Lafrenière, R. Jayawardhana, and M. H. van Kerkwijk. The Directly Imaged Planet Around the Young Solar Analog 1RXS J160929.1 - 210524: Confirmation of Common Proper Motion, Temperature, and Mass. *ApJ*, 719:497–504, August 2010. doi: 10.1088/0004-637X/719/1/497.

D. N. C. Lin and J. Papaloizou. On the structure and evolution of the primordial solar nebula. *MNRAS*, 191:37–48, April 1980.

D. N. C. Lin and J. Papaloizou. On the tidal interaction between protoplanets and the protoplanetary disk. III - Orbital migration of protoplanets. *ApJ*, 309:846–857, October 1986. doi: 10.1086/164653.

D. N. C. Lin and J. E. Pringle. A viscosity prescription for a self-gravitating accretion disc. *MNRAS*, 225:607–613, April 1987.

D. N. C. Lin and J. E. Pringle. The formation and initial evolution of protostellar disks. *ApJ*, 358:515–524, August 1990. doi: 10.1086/169004.

G. Lodato and C. J. Clarke. Resolution requirements for smoothed particle hydrodynamics simulations of self-gravitating accretion discs. *MNRAS*, 413:2735–2740, June 2011. doi: 10.1111/j.1365-2966.2011.18344.x.

L. B. Lucy. A numerical approach to the testing of the fission hypothesis. , 82:1013–1024, December 1977. doi: 10.1086/112164.

D. Lynden-Bell and J. E. Pringle. The evolution of viscous discs and the origin of the nebular variables. *MNRAS*, 168:603–637, September 1974.

B. Ma and J. Ge. Statistical Properties of Brown Dwarf Companions: Implications for Different Formation Mechanisms. *ArXiv e-prints*, March 2013.

M. N. Machida, E. Kokubo, S.-i. Inutsuka, and T. Matsumoto. Angular Momentum Accretion onto a Gas Giant Planet. *ApJ*, 685:1220–1236, October 2008. doi: 10.1086/590421.

M. N. Machida, S.-i. Inutsuka, and T. Matsumoto. Formation Process of the Circumstellar Disk: Long-term Simulations in the Main Accretion Phase of Star Formation. *ApJ*, 724:1006–1020, December 2010. doi: 10.1088/0004-637X/724/2/1006.

C. Marois, B. Macintosh, T. Barman, B. Zuckerman, I. Song, J. Patience, D. Lafrenière, and R. Doyon. Direct Imaging of Multiple Planets Orbiting the Star HR 8799. *Science*, 322:1348–, November 2008. doi: 10.1126/science.1166585.

C. Marois, B. Zuckerman, Q. M. Konopacky, B. Macintosh, and T. Barman. Images of a fourth planet orbiting HR 8799. , 468:1080–1083, December 2010. doi: 10.1038/nature09684.

R. G. Martin and S. H. Lubow. Tidal truncation of circumplanetary discs. *MNRAS*, 413: 1447–1461, May 2011. doi: 10.1111/j.1365-2966.2011.18228.x.

H. Masunaga, S. M. Miyama, and S.-I. Inutsuka. A Radiation Hydrodynamic Model for Protostellar Collapse. I. The First Collapse. *ApJ*, 495:346, March 1998. doi: 10.1086/305281.

J. S. Mathis, W. Rumpl, and K. H. Nordsieck. The size distribution of interstellar grains. *ApJ*, 217:425–433, October 1977. doi: 10.1086/155591.

L. Mayer and A. J. Gawryszczak. Protoplanetary Disk Fragmentation with Varying Radiative Physics, Initial Conditions and Numerical Techniques. In D. Fischer, F. A. Rasio, S. E. Thorsett, and A. Wolszczan, editors, *Extreme Solar Systems*, volume 398 of *Astronomical Society of the Pacific Conference Series*, page 243, 2008.

L. Mayer, T. Quinn, J. Wadsley, and J. Stadel. Formation of Giant Planets by Fragmentation of Protoplanetary Disks. *Science*, 298:1756–1759, November 2002a. doi: 10.1126/science.1077635.

L. Mayer, T. Quinn, J. Wadsley, and J. Stadel. Formation of Giant Planets by Fragmentation of Protoplanetary Disks. *Science*, 298:1756–1759, November 2002b. doi: 10.1126/science.1077635.

L. Mayer, T. Quinn, J. Wadsley, and J. Stadel. The Evolution of Gravitationally Unstable Protoplanetary Disks: Fragmentation and Possible Giant Planet Formation. *ApJ*, 609: 1045–1064, July 2004. doi: 10.1086/421288.

L. Mayer, G. Lufkin, T. Quinn, and J. Wadsley. Fragmentation of Gravitationally Unstable Gaseous Protoplanetary Disks with Radiative Transfer. *ApJL*, 661:L77–L80, May 2007. doi: 10.1086/518433.

M. Mayor and D. Queloz. A Jupiter-mass companion to a solar-type star. , 378:355–359, November 1995. doi: 10.1038/378355a0.

B. E. McArthur, G. F. Benedict, R. Barnes, E. Martioli, S. Korzennik, E. Nelan, and R. P. Butler. New Observational Constraints on the Andromedae System with Data from the Hubble Space Telescope and Hobby-Eberly Telescope. *ApJ*, 715:1203–1220, June 2010. doi: 10.1088/0004-637X/715/2/1203.

F. Meru and M. R. Bate. Non-convergence of the critical cooling time-scale for fragmentation of self-gravitating discs. *MNRAS*, 411:L1–L5, February 2011a. doi: 10.1111/j.1745-3933.2010.00978.x.

F. Meru and M. R. Bate. On the fragmentation criteria of self-gravitating protoplanetary discs. *MNRAS*, 410:559–572, January 2011b. doi: 10.1111/j.1365-2966.2010.17465.x.

F. Meru, M. Galvagni, and C. Olczak. Growth of grains in brown dwarf discs. *accepted for publication in Ajl*.

S. Michael, R. H. Durisen, and A. C. Boley. Migration of Gas Giant Planets in Gravitationally Unstable Disks. *ApJL*, 737:L42, August 2011. doi: 10.1088/2041-8205/737/2/L42.

H. Mizuno. Formation of the Giant Planets. *Progress of Theoretical Physics*, 64:544–557, August 1980. doi: 10.1143/PTP.64.544.

S. Mohanty, B. Ercolano, and N. J. Turner. Dead, Undead, and Zombie Zones in Protostellar Disks as a Function of Stellar Mass. *ApJ*, 764:65, February 2013. doi: 10.1088/0004-637X/764/1/65.

C. Mordasini. Luminosity of young Jupiters revisited. Massive cores make hot planets. *ArXiv e-prints*, June 2013.

C. Mordasini, Y. Alibert, and W. Benz. Extrasolar planet population synthesis. I. Method, formation tracks, and mass-distance distribution. *A & A*, 501:1139–1160, July 2009. doi: 10.1051/0004-6361/200810301.

C. Mordasini, Y. Alibert, H. Klahr, and T. Henning. Characterization of exoplanets from their formation. I. Models of combined planet formation and evolution. *A & A*, 547:A111, November 2012. doi: 10.1051/0004-6361/201118457.

N. Movshovitz, P. Bodenheimer, M. Podolak, and J. J. Lissauer. Formation of Jupiter using opacities based on detailed grain physics. *Icarus*, 209:616–624, October 2010. doi: 10.1016/j.icarus.2010.06.009.

T. Muto, C. A. Grady, J. Hashimoto, M. Fukagawa, J. B. Hornbeck, M. Sitko, R. Russell, C. Werren, M. Curé, and Currie. Discovery of Small-scale Spiral Structures in the Disk of SAO 206462 (HD 135344B): Implications for the Physical State of the Disk from Spiral Density Wave Theory. *ApJL*, 748:L22, April 2012. doi: 10.1088/2041-8205/748/2/L22.

Y. Nakagawa, M. Sekiya, and C. Hayashi. Settling and growth of dust particles in a laminar phase of a low-mass solar nebula. *Icarus*, 67:375–390, September 1986. doi: 10.1016/0019-1035(86)90121-1.

S. Nayakshin. Formation of planets by tidal downsizing of giant planet embryos. *MNRAS*, 408: L36–L40, October 2010. doi: 10.1111/j.1745-3933.2010.00923.x.

S. Nayakshin and S.-H. Cha. Radiative feedback from protoplanets in self-gravitating protoplanetary discs. *ArXiv e-prints*, June 2013.

S. Nayakshin and G. Lodato. Fu Ori outbursts and the planet-disc mass exchange. *MNRAS*, 426: 70–90, October 2012. doi: 10.1111/j.1365-2966.2012.21612.x.

R. P. Nelson and J. C. B. Papaloizou. The interaction of giant planets with a disc with MHD turbulence - IV. Migration rates of embedded protoplanets. *MNRAS*, 350:849–864, May 2004. doi: 10.1111/j.1365-2966.2004.07406.x.

E. L. Nielsen, M. C. Liu, Z. Wahhaj, B. A. Biller, M. Chun, L. M. Close, C. Ftaclas, T. L. Hayward, D. W. Toomey, and Gemini NICI Planet-Finding Campaign Team. The Gemini NICI Planet-Finding Campaign: Statistical Constraints on Planet Populations. *American Astronomical Society, ESS meeting*, 2:702, September 2011.

S. Okuzumi, H. Tanaka, T. Takeuchi, and M.-a. Sakagami. Electrostatic Barrier Against Dust Growth in Protoplanetary Disks. I. Classifying the Evolution of Size Distribution. *ApJ*, 731:95, April 2011. doi: 10.1088/0004-637X/731/2/95.

I. Oliveira, K. M. Pontoppidan, B. Merín, E. F. van Dishoeck, F. Lahuis, V. C. Geers, J. K. Jørgensen, J. Olofsson, J.-C. Augereau, and J. M. Brown. A Spitzer Survey of Protoplanetary Disk Dust in the Young Serpens Cloud: How do Dust Characteristics Evolve with Time? *ApJ*, 714:778–798, May 2010. doi: 10.1088/0004-637X/714/1/778.

C. W. Ormel. *The early stages of planet formation: how to grow from small to large*. PhD thesis, Kapteyn Astronomical Institute, University of Groningen, 2008.

C. W. Ormel and J. N. Cuzzi. Closed-form expressions for particle relative velocities induced by turbulence. *A & A*, 466:413–420, May 2007. doi: 10.1051/0004-6361:20066899.

J. E. Owen, C. J. Clarke, and B. Ercolano. On the theory of disc photoevaporation. *MNRAS*, 422:1880–1901, May 2012. doi: 10.1111/j.1365-2966.2011.20337.x.

S.-J. Paardekooper. Numerical convergence in self-gravitating shearing sheet simulations and the stochastic nature of disc fragmentation. *MNRAS*, 421:3286–3299, April 2012. doi: 10.1111/j.1365-2966.2012.20553.x.

J. Papaloizou and D. N. C. Lin. On the tidal interaction between protoplanets and the primordial solar nebula. I - Linear calculation of the role of angular momentum exchange. *ApJ*, 285:818–834, October 1984. doi: 10.1086/162561.

J. C. B. Papaloizou and C. Terquem. Dynamical relaxation and massive extrasolar planets. *MNRAS*, 325:221–230, July 2001. doi: 10.1046/j.1365-8711.2001.04386.x.

R. Perna, K. Menou, and E. Rauscher. Magnetic Drag on Hot Jupiter Atmospheric Winds. *ApJ*, 719:1421–1426, August 2010. doi: 10.1088/0004-637X/719/2/1421.

P. Pinilla, T. Birnstiel, L. Ricci, C. P. Dullemond, A. L. Uribe, L. Testi, and A. Natta. Trapping dust particles in the outer regions of protoplanetary disks. *A & A*, 538:A114, February 2012. doi: 10.1051/0004-6361/201118204.

P. Pinilla, T. Birnstiel, M. Benisty, L. Ricci, A. Natta, C. P. Dullemond, C. Dominik, and L. Testi. Explaining millimeter-sized particles in brown dwarf disks. *ArXiv e-prints*, April 2013.

M. Podolak, L. Mayer, and T. Quinn. Evolution of Coated Grains in Spiral Shocks of Self-gravitating Protoplanetary Disks. *ApJ*, 734:56, June 2011. doi: 10.1088/0004-637X/734/1/56.

J. B. Pollack, O. Hubickyj, P. Bodenheimer, J. J. Lissauer, M. Podolak, and Y. Greenzweig. Formation of the Giant Planets by Concurrent Accretion of Solids and Gas. *Icarus*, 124:62–85, November 1996. doi: 10.1006/icar.1996.0190.

D. J. Price. Smoothed Particle Hydrodynamics: Things I Wish My Mother Taught Me. In R. Capuzzo-Dolcetta, M. Limongi, and A. Tornambè, editors, *Advances in Computational Astrophysics: Methods, Tools, and Outcome*, volume 453 of *Astronomical Society of the Pacific Conference Series*, page 249, July 2012.

S. P. Quanz, D. Lafreniere, M. R. Meyer, M. M. Reggiani, and E. Buenzli. Direct imaging constraints on planet populations detected by microlensing. *ArXiv e-prints*, March 2012.

R. R. Rafikov. Properties of Gravitoturbulent Accretion Disks. *ApJ*, 704:281–291, October 2009. doi: 10.1088/0004-637X/704/1/281.

R. R. Rafikov. Constraint on the Giant Planet Production by Core Accretion. *ApJ*, 727:86, February 2011. doi: 10.1088/0004-637X/727/2/86.

D. Ragozzine and Kepler Team. The Very Compact Five Exoplanet System KOI-500: Mass Constraints from TTVs, Resonances, and Implications. In *AAS/Division for Planetary Sciences Meeting Abstracts*, volume 44 of *AAS/Division for Planetary Sciences Meeting Abstracts*, page 200.04, October 2012.

L. M. Rebull, J. R. Stauffer, S. T. Megeath, J. L. Hora, and L. Hartmann. A Correlation between Pre-Main-Sequence Stellar Rotation Rates and IRAC Excesses in Orion. *ApJ*, 646:297–303, July 2006. doi: 10.1086/504865.

L. Ricci, L. Testi, A. Natta, A. Scholz, and I. de Gregorio-Monsalvo. ALMA Observations of ρ-Oph 102: Grain Growth and Molecular Gas in the Disk around a Young Brown Dwarf. *ApJL*, 761:L20, December 2012. doi: 10.1088/2041-8205/761/2/L20.

L. Ricci, A. Isella, J. M. Carpenter, and L. Testi. CARMA Interferometric Observations of 2MASS J044427+2512: The First Spatially Resolved Observations of Thermal Emission of a Brown Dwarf Disk. *ApJL*, 764:L27, February 2013. doi: 10.1088/2041-8205/764/2/L27.

W. K. M. Rice, G. Lodato, and P. J. Armitage. Investigating fragmentation conditions in self-gravitating accretion discs. *MNRAS*, 364:L56–L60, November 2005. doi: 10.1111/j.1745-3933.2005.00105.x.

P. D. Rogers and J. Wadsley. The importance of photosphere cooling in simulations of gravitational instability in the inner regions of protostellar discs. *MNRAS*, 414:913–929, June 2011. doi: 10.1111/j.1365-2966.2011.18523.x.

P. D. Rogers and J. Wadsley. The fragmentation of protostellar discs: the Hill criterion for spiral arms. *MNRAS*, page 2995, May 2012. doi: 10.1111/j.1365-2966.2012.21014.x.

V. S. Safronov. *Evolution of the protoplanetary cloud and formation of the earth and planets.* 1972.

M. Shabram and A. C. Boley. The Evolution of Circumplanetary Disks around Planets in Wide Orbits: Implications for Formation Theory, Observations, and Moon Systems. *ApJ*, 767:63, April 2013. doi: 10.1088/0004-637X/767/1/63.

I. Shlosman and M. C. Begelman. Evolution of self-gravitating accretion disks in active galactic nuclei. *ApJ*, 341:685–691, June 1989. doi: 10.1086/167526.

M. V. Smoluchowski. Drei Vortrage uber Diffusion, Brownsche Bewegung und Koagulation von Kolloidteilchen. *Zeitschrift fur Physik*, 17:557–585, 1916.

D. S. Spiegel and A. Burrows. Spectral and Photometric Diagnostics of Giant Planet Formation Scenarios. *ApJ*, 745:174, February 2012. doi: 10.1088/0004-637X/745/2/174.

V. Springel. Smoothed Particle Hydrodynamics in Astrophysics. , 48:391–430, September 2010. doi: 10.1146/annurev-astro-081309-130914.

J. G. Stadel. *Cosmological N-body simulations and their analysis*. PhD thesis, University of Washington, 2001.

D. Stamatellos, A. P. Whitworth, T. Bisbas, and S. Goodwin. Radiative transfer and the energy equation in SPH simulations of star formation. *A & A*, 475:37–49, November 2007. doi: 10.1051/0004-6361:20077373.

T. Sumi, MOA, and OGLE Collaboration. Recent results from gravitational microlensing. *American Astronomical Society, ESS meeting*, 2:103, September 2011.

T. Takata and D. J. Stevenson. Despin Mechanism for Protogiant Planets and Ionization State of Protogiant Planetary Disks. *Icarus*, 123:404–421, October 1996. doi: 10.1006/icar.1996.0167.

H. Tanaka, T. Takeuchi, and W. R. Ward. Three-Dimensional Interaction between a Planet and an Isothermal Gaseous Disk. I. Corotation and Lindblad Torques and Planet Migration. *ApJ*, 565:1257–1274, February 2002. doi: 10.1086/324713.

H. Tanaka, Y. Himeno, and S. Ida. Dust Growth and Settling in Protoplanetary Disks and Disk Spectral Energy Distributions. I. Laminar Disks. *ApJ*, 625:414–426, May 2005. doi: 10.1086/429658.

A. Toomre. On the gravitational stability of a disk of stars. *ApJ*, 139:1217–1238, May 1964. doi: 10.1086/147861.

A. Vazan and R. Helled. On the Evolution and Survival of Protoplanets Embedded in a Protoplanetary Disk. *ApJ*, 756:90, September 2012. doi: 10.1088/0004-637X/756/1/90.

E. I. Vorobyov. Formation of giant planets and brown dwarfs on wide orbits. *A & A*, 552:A129, April 2013. doi: 10.1051/0004-6361/201220601.

E. I. Vorobyov and S. Basu. Secular evolution of viscous and self-gravitating circumstellar discs. *MNRAS*, 393:822–837, March 2009a. doi: 10.1111/j.1365-2966.2008.14376.x.

E. I. Vorobyov and S. Basu. The Bimodality of Accretion in T Tauri Stars and Brown Dwarfs. *ApJ*, 703:922–929, September 2009b. doi: 10.1088/0004-637X/703/1/922.

J. W. Wadsley, J. Stadel, and T. Quinn. Gasoline: a flexible, parallel implementation of TreeSPH. *Nature*, 9:137–158, February 2004. doi: 10.1016/j.newast.2003.08.004.

S. J. Weidenschilling. Aerodynamics of solid bodies in the solar nebula. *MNRAS*, 180:57–70, July 1977.

F. L. Whipple. On certain aerodynamic processes for asteroids and comets. In A. Elvius, editor, *From Plasma to Planet*, page 211, 1972.

S. C. Whitehouse and M. R. Bate. Smoothed particle hydrodynamics with radiative transfer in the flux-limited diffusion approximation. *MNRAS*, 353:1078–1094, October 2004. doi: 10.1111/j.1365-2966.2004.08131.x.

S. C. Whitehouse, M. R. Bate, and J. J. Monaghan. A faster algorithm for smoothed particle hydrodynamics with radiative transfer in the flux-limited diffusion approximation. *MNRAS*, 364:1367–1377, December 2005. doi: 10.1111/j.1365-2966.2005.09683.x.

D. J. Wilner, P. D'Alessio, N. Calvet, M. J. Claussen, and L. Hartmann. Toward Planetesimals in the Disk around TW Hydrae: 3.5 Centimeter Dust Emission. *ApJL*, 626:L109–L112, June 2005. doi: 10.1086/431757.

F. Windmark, T. Birnstiel, C. Güttler, J. Blum, C. P. Dullemond, and T. Henning. Planetesimal formation by sweep-up: how the bouncing barrier can be beneficial to growth. *A & A*, 540: A73, April 2012a. doi: 10.1051/0004-6361/201118475.

F. Windmark, T. Birnstiel, C. W. Ormel, and C. P. Dullemond. Breaking through: The effects of a velocity distribution on barriers to dust growth. *A & A*, 544:L16, August 2012b. doi: 10.1051/0004-6361/201220004.

A. Wolszczan and D. A. Frail. A planetary system around the millisecond pulsar PSR1257 + 12. , 355:145–147, January 1992. doi: 10.1038/355145a0.

J. T. Wright, G. W. Marcy, A. W. Howard, J. A. Johnson, T. Morton, and D. A. Fischer. The Frequency of Hot Jupiters Orbiting Nearby Solar-Type Stars. *ArXiv e-prints*, May 2012.

A. N. Youdin and E. I. Chiang. Particle Pileups and Planetesimal Formation. *ApJ*, 601: 1109–1119, February 2004. doi: 10.1086/379368.

Z. Zhu, L. Hartmann, R. P. Nelson, and C. F. Gammie. Challenges in Forming Planets by Gravitational Instability: Disk Irradiation and Clump Migration, Accretion, and Tidal Destruction. *ApJ*, 746:110, February 2012. doi: 10.1088/0004-637X/746/1/110.